Faculty of Engineering

Surface Roughness Prediction in End-Milling Process

A THESIS

Submitted in Partial Fulfillment of the

Requirements for the Degree of

MASTER OF SCIENCE

Department of Mechanical Engineering,

ASSIUT UNIVERSITY

By

Eng. Ibrahem Maher Abdel-Rahem Soltan

Mechanical Engineering - Assiut University

May 2008

Assiut University

Faculty of Engineering

Surface Roughness Prediction in End-Milling Process

By

Eng. Ibrahem Maher Abdel-Rahem Soltan

B. Sc., Mechanical Engineering, Assiut University, 2002

A THESIS

Submitted in partial fulfillment of the

requirements for the degree

MASTER OF SCIENCE

Department of Mechanical Engineering,

ASSIUT UNIVERSITY

Assiut-Egypt

2008

Supervision Committee:

Prof. Dr. R. M. El-Zahry
(Faculty of eng.- Assiut Univ.-Egypt)
Dr. Mohamed E. H. Eltaib
(Faculty of eng.- Assiut Univ.-Egypt)

Discussion Committee:

Prof. Dr.T. T. El-Midany
(Faculty of eng.- Mansoura Univ.-Egypt)
Prof. Dr. Ahmed A. Abo-Ismail
(Faculty of eng.- Assiut Univ.-Egypt)
Prof. Dr. R. M. El-Zahry

DEDICATION

To my parents,

For supporting me in every step of my life

My wife,

For her love and patience

And my adorable son

ACKNOWLEDGMENTS

First of all; my gratitude and thanks to **ALLAH**, The Most Gracious and The Most Merciful.

The author wishes to express his sincere gratitude to **Prof. Dr. R. M. El-zahry**, for suggesting the research point, valuable guidance, help and encouragement which made this research possible.

The author would like to express his deep thanks and sincere gratitude to **Dr. M. E. H. Eltaib**, for supplying me with his experience and for valuable discussions through out the stages of this work.

All thanks are for every one helped me through out the work in this thesis.

ABSTRACT

Surface roughness prediction for the end-milling process, which is one of the major cutting processes, is a very important economical consideration in order to increase machine operation and decrease production cost in an automated manufacturing environment.

In this study; prediction of surface roughness (Ra) for Brass (60/40) material based on cutting parameters: cutting speed, feed rate, and depth of cut; was studied.

Adaptive neuro-fuzzy inference system (ANFIS) was used to predict the surface roughness in the end milling process. Surface roughness was used as dependant variable while cutting speed of range (750 - 1750rpm), feed rate of range (50 - 250mm/min) and depth of cut of range (0.3 - 0.7mm) were used as predictor variables. Normal and feed forces were used as predictor variables to verify the ANFIS model. Different membership functions were adopted during the training process of ANFIS.

Surface roughness was measured in an off line manner using stylus based profile-meter (surtronic 3+). The normal and feed forces were measured in an on-line manner using two components dynamometer.

The effects of cutting parameters on the normal force, feed force and surface roughness were discussed. Experimental test data were used to examine the ANFIS model by defining the reliability and percentage error of the model. Experimental results demonstrate the effectiveness of the proposed model. While the predicted surface roughness was compared with measured data; the mean square error has been found equal to 8.5 % hence the achieved accuracy is equal to 91.5 %.

Although this work focuses on prediction of surface roughness for end-milling operation, the concepts introduced are general; ie., prediction of surface roughness using ANFIS can be applied to many other cutting and machining processes.

TABLE OF CONTENTS

Chapter **Page**

LIST OF FIGURES

Figure **Page**

LIST OF TABLES

Tables

NOMENCLATURE

ANFIS	Adaptive neuro-fuzzy inference system
Ra	Surface roughness (μm)
Fx	Feed force (N)
Fy	Normal force (N)
BUE	Built-up edge
n	Spindle speed (rpm)
f	Feed rate (mm/min)
t	Depth of cut (mm)
trimf	Triangular memberships function
trapmf	Trapezoidal memberships function
gbellmf	Generalized bell memberships function
gaussmf	Gaussian memberships function
pimf	pi-shaped memberships function
dsigmf	Difference between two sigmoid memberships function
psigmf	Product of two sigmoid memberships function
C_e	End-cutting edge angel
C_s	Side-cutting edge angle
Rt	Peak-to-valley value
t_r	Tool nose radius
ANN	Artificial neural network
Ft	Tangential force
Fr	Radial force

ψ	Helix angel
z	Number of tooth
K	Dynamometer ring constant (N/mm),
m	Dynamometer mass (kg),
f_d	Dynamometer natural frequency (rev./s).
f_m	The machine tool's vibration frequency
Vx	Output volt in mv
Ra_i	Measured Ra of sample number. i.
$\hat{R}a_i$	Predicted Ra generated by ANFIS model
E_i	Percentage error of sample number i.
E_{av}	Average percentage error of m sample data

CHAPTER ONE

INTRODUCTION

1.1 Motivation and background

The CNC end milling machine is widely used in industry because of its flexibility and efficiency. Applications of the end milling process can be found in almost every industry ranging from large aerospace industry to small tool and die makers. One reason for the popularity of the end milling process is that it can be used for both rough and finish machining of components.

The major problem which may result from the end milling process is the generation of a finished part surface which does not satisfy product design specifications. A finished part surface might be too rough or poor dimension accuracy. An undesirable part surface may require additional machining, thus lowering productivity and increasing the cost of the production.

In order to produce parts which conform to design specifications, proper machining conditions (spindle speed, feed rate, depth of cut, cutter diameter, number of cutting flutes, and tool geometry) must be selected.

In order to perform a manufacturing process at high productivity and low cost conditions and to produce high quality parts, the production of unacceptable part surfaces must be avoided. This problem is typically due to selection of machining conditions for the process which results in one or more of the followings:

excessive deflection of the work piece, excessive deflection of the end mill, tool wear and system instability (chatter vibration).

Chatter vibration is a phenomenon investigative of an unstable system, where the displacement of the tool relative to the work piece increases until the tool moves away from the work piece **[1 and 2].**

Traditionally, machining conditions have been selected based on empirical models, past experience or by trial and error.

Rather than using data based empirical models to select machining conditions; it would be more popular to perform the selection based on mathematical models that are derived from the mechanics of the end milling process. Such mechanistically based models are more difficult to develop than the empirical models because this requires the process modeler to understand the physics of the process and make appropriate assumptions when necessary.

1.2 Scope of the present work

The aim of this work is to develop ANFIS model to predict the surface roughness for end-milling process. The study consists of five main parts.

In the first part, studying and construction of adaptive neuro-fuzzy inference system (ANFIS) model using machining parameters (speed, feed rate and depth of cut) as input and the surface roughness (Ra) as an output.

The second part is focused on the design and manufacturing of a two axis milling dynamometer for measuring the force in the feed direction (Feed force) and the force normal to feed direction (Normal force).

The third part is focused on the construction of ANFIS model using measured milling force components (feed force and normal force) as input and Ra as output.

In the fourth part, the correlation between the cutting parameters and the predictor variables (feed force, normal force and surface roughness) was studied. In the fifth part, verification of ANFIS model was discussed.

In studying the surface roughness prediction, adaptive neuro-fuzzy inference system was used to predict the surface roughness in the end-milling process. Spindle speed, feed rate and depth of cut were used as predictor variables, and feed force and normal force were used as other predictor variables. Surface roughness was used as an independent variable. Different membership functions were adopted during the training process of ANFIS.

1.3 Thesis outline

There are seven chapters in this thesis.

Chapter two is a literature review of important research work in this area. It covers; surface roughness monitoring techniques and prediction of surface roughness using soft computing methods (regression, fuzzy logic, neural net work and ANFIS).

Chapter three presents studying for ANFIS model.

Chapter four covers measurements of surface roughness and milling force components.

Chapter five covers study of prediction of surface roughness (Ra) using feed force and normal force.

Chapter six presents results and discussion. This chapter also includes the verification of ANFIS model and the effect of speed, feed rate, and depth of cut on normal force, feed force and surface roughness.

Chapter seven presents a summary of this study as well as suggestions for future work in the area of the present research.

CHAPTER TWO

LITRATURE REVIEW

A review of the past research suggests that analysis of the end milling process can be divided into two main basic areas:

1 – Composition of Surface roughness Formed in Metal cutting.

2 - Methods for monitoring of the surface roughness.

The first area of research has been reviewed giving the composition of surface roughness formed by a set of process conditions (tool geometry, built-up edge, vibration, and tool wear). The second area has been mainly devoted to developing models based on fundamental theories. These models can be used to monitoring the surface roughness in an on-line and off-line manner.

2.1 Surface roughness

Surface Roughness is defined as a set of asperities of the real surface, conventionally described as deviations of the measured profile from a reference line within the limits of a length along which waviness is not taken into account **[3]**.

Surface roughness is one of the most important factors for evaluating surface quality during the finishing process. The quality of surface affects the functional characteristics of the work piece such as fatigue and fracture resistance and surface

friction. Furthermore, surface roughness in addition to tolerances imposes a critical constraint for cutting parameter selection in manufacturing process planning **[4]**.

The three-dimensional structure of the surface is made up of surface asperities, or peaks and valleys. These asperities are described by parameters of roughness and waviness, as well as flaws in the geometrical structure of the surface as shown in **Figures 2.1**. Therefore, they should be described in all three dimensions. However, practical difficulty with their measurements causes that the problem is reduced to a two-dimensional plane on which a roughness profile is traced.

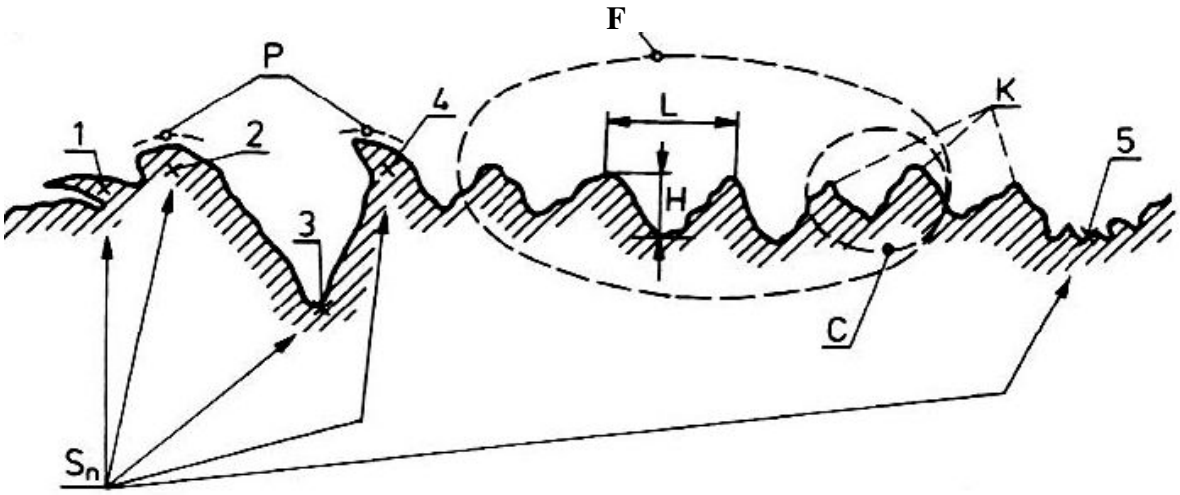

Figure 2.1 Profile of asperities on surface of a solid: H - peak to valley height; L - peak to peak distance; F - waviness; C - roughness; P - adhesion; K-orientation of asperities; Sn - asperity flaws; 1 - flaking; 2 - folding; 3 - scratch; 4 - burr; 5 - pit;

Table 2.1 Surface profile parameters

Parameter	Name	Standards	Related
Height Parameters			
Ra	Roughness Average (Ra)	ASME B46.1-1995	*Pa, Wa*
Rq	Root Mean Square (RMS) Roughness	ASME B46.1-1995	*Pq, Wq*
Rt	Maximum Height of the Profile	ASME B46.1-1995	*Pt, Wt*
Rv, Rm	Maximum Profile Valley Depth	ASME B46.1-1995	*Pv, Wv*
Rp	Maximum Profile Peak Height	ASME B46.1-1995	*Pp, Wp*
Rpm	Average Maximum Profile Peak Height	ASME B46.1-1995	
Rz	Average Maximum Height of the Profile	ASME B46.1-1995	*Pz, Wz, Rtm*
Rmax	Maximum Roughness Depth	ASME B46.1-1995	*Ry, Rymax, Rti,Rz*
Rc	Mean Height of Profile Irregularities	ISO 4287/1-1997	*Pc, Wc*
Rz(iso)	Roughness Height	ISO 4287/1-1997	
Ry	Maximum Height of the Profile	ISO 4287/1-1997	
Wt, W	Waviness Height	ASME B46.1-1995	*Rt,Pt*
Spacing Parameters			
S	Mean Spacing of Local Peaks of the Profile	ISO 4287/1-1997	
Sm, RSm	Mean Spacing of Profile Irregularities	ASME B46.1-1995	*PSm, WSm*
D	Profile Peak Density	ISO 4287/1-1997	*Sm*
Pc	Peak Count (Peak Density)	ASME B46.1-1995	
HSC	Hight Spot Count		
λa	Average Wavelength of the Profile	ISO 4287/1-1997	
λ q	Root Mean Square (RMS) Wavelength of the Profile	ISO 4287/1-1997	
Hybrid Parameters			
Δa	Average Absolute Slope	ASME B46.1-1995	*P Δ a, W Δ a*
Δ q	Root Mean Square (RMS) Slope	ASME B46.1-1995	*P Δ q, W Δ q*
Lo	Developed Profile Length	ISO 4287/1-1997	*lr*
lr	Profile Length Ratio	ISO 4287/1-1997	*Lo*
ADF and BAC Parameters			
Rsk,Sk	Skewness	ASME B46.1-1995	*Psk, Wsk*
Rku	Kurtosis	ASME B46.1-1995	*Pku, Wku*
tp, Rmr(c)	Profile Bearing Length Ratio (Material Ratio of the Profile)	ASME B46.1-1995	*Pmr(c), Wmr(c), Pmr, Rmr, Wmr*
Htp, Rδc	Profile Section Height Difference	ASME B46.1-1995	
H	Swedish Height		*Htp, Rt*
Rk	Core Roughness Depth	ISO 13565-1996	
Rpk	Reduced Peak Height	ISO 13565-1996	*Rpk**
Rvk	Reduced Valley Depth	ISO 13565-1996	*Rvk**
Mr1	Material Portion	ISO 13565-1996	*Rmr(c), tp*
Mr2	Material Portion	ISO 13565-1996	*Rmr(c), tp*
Vo	"Oil-Retention" Volume		
Rpq, Rvq, Rmq	Material Probability Curve Parameters		

The terms surface finish and surface roughness are used very widely in industry and are generally used to quantify the smoothness of a surface finish. Many of the concepts of surface metrology and terminology are given in **Table 2.1** and discussed as given in **Appendix-A [3]**.

The most common measures of primary roughness is known as arithmetic averages (Ra) and the total roughness (R_t) or the vertical distance from the deepest valley to the highest peak, which describes the deviation of the surface roughness from a mean line or center line as shown in **Figure 2.2** and is defined by **Equations (2.1)** and **(2.2)**.

$$Ra = \frac{1}{L}\int_0^L |y(x)|dx \quad \text{..... (2.1)}$$

$$R_t = R_{max} \quad \text{.....(2.2)}$$

Where L is the sampling length, $y's$ are the deviations from the mean line at location along the x direction.

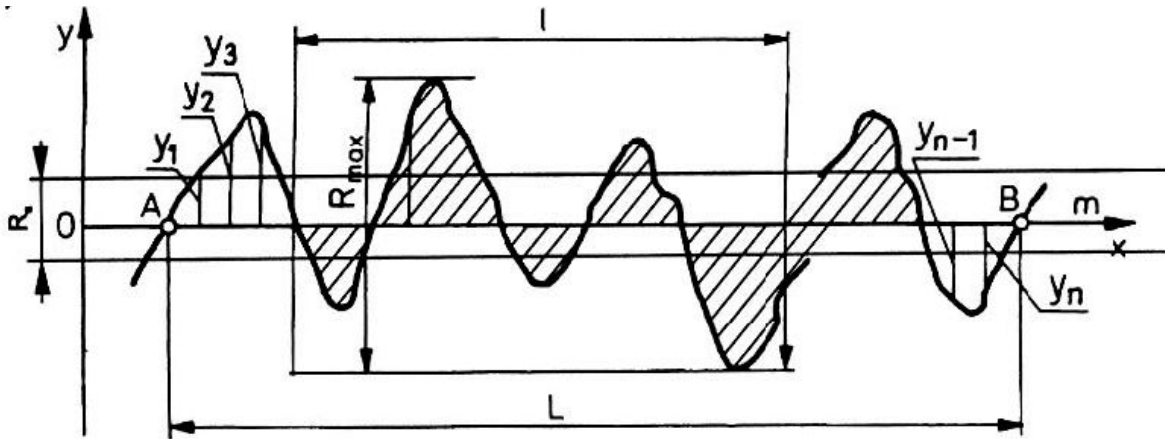

Figure 2.2 Evaluation of surface roughness average (Ra).

2.2 Composition of surface roughness formed in metal cutting

Based on the previous study of surface roughness formed in metal cutting, a machined surface is generally formed due to the following sources **[5 and 6]**.

- The geometry of cutting tool and cutting parameter setting,
- Built-up edge effect,
- Vibration or chattering of the cutting tool structure, and
- Tool- wear effect.

2.2.1 Geometrical effect on surface roughness

In a cutting operation, the component of surface roughness due to tool nose geometry and cutting parameters, such as speed, feed and depth of cut, may be readily calculated. **Figure 2.3** shows a plan view of a conventional turning operation with feed marks left behind on the finished surface **[5]**.

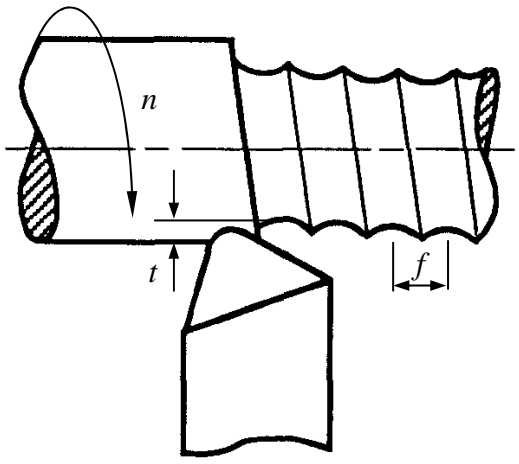

Figure 2.3 plan view of a conventional turning process with feed marks

Two simple geometries that show up on real cutting edge will be considered. The first type of cutting edge geometry considered is like that shown in **Figure 2.4**. This geometry generates a triangular cross section with base *f*, with one side inclined at angle C_e measured from the direction of *f* and with the other side inclined at C_s measured from the normal to *f*. From the geometry in **Figure 2.4** and the definition of R_t, it is easy to determine the maximum peak-to-valley roughness **[7]**.

$$R_t = \frac{f}{\cot(C_e) + \tan(C_s)} \quad \text{.....(3.1)}$$

The roughness (Ra) is referenced to the height center line ($R_t/2$), and then the portion below the center line is rectified, resulting in two triangles of height ($R_t/2$) and base ($f/2$). These triangular areas are divided by the *f* or

$$Ra = \frac{f}{4(\cot(C_e) + \tan(C_s))} \quad \text{.....(3.2)}$$

Where: C_e is the End-cutting edge angel, and C_s is the Side-cutting edge angle or lead angel.

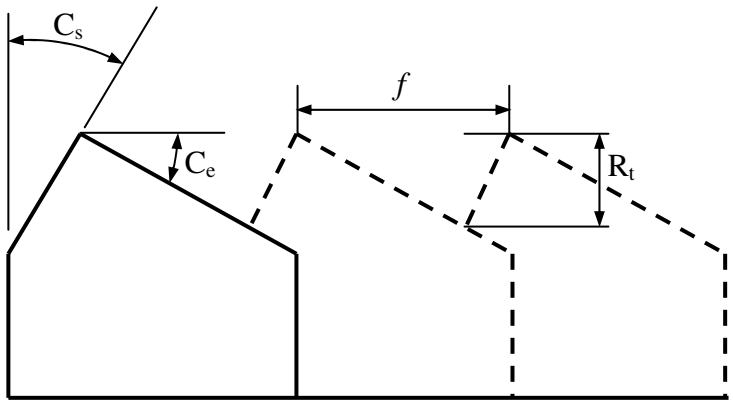

Figure 2.4 Geometric surface profiles with sharp nose edge.

A radius t_r, is more common on the nose or corner of a cutting edge. This produces a smoother finish as shown in **Figure 2.5.**

If the tool nose radius is large compared with the feed, the surface will be generated by the nose radius alone (**Case I in Figure 2.5**). Most of the finish machining operations falls into this case. From the geometry it is obvious that the ideal peak-to-valley value in this case is **[5].**

$$R_t = \overline{OT} - \overline{OU} = t_r^2 - (t_r^2 - f^2/4)^{\frac{1}{2}} = \frac{f^2}{8t_r} \qquad \text{if} \quad f < 2t_r sinC_e \text{ .....(3.3)}$$

Where tool nose radius (t_r = OT),

The general expression for the roughness (Ra) is quite complicated, but for finishing it is approximately

$$Ra \approx \frac{f^2}{18\ t_r \sqrt{3}} \qquad \text{.....(3.4)}$$

If the feed is larger than $2t_r sinC_e$ (**Case II in Figure 2.5**), the ideal peak-to-valley value will be

$$R_t = t_r(1 - \cos C_e + F \cos C_e - \sin C_e \sqrt{2F - F^2}) \text{ .....(3.5)}$$

Where $F = f \sin C_e / t_r$

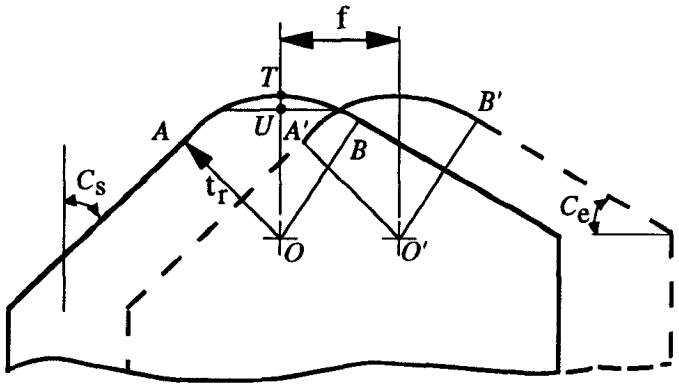

$$f < 2\,t_r \sin C_e$$

Case I: Two Noses Intersect

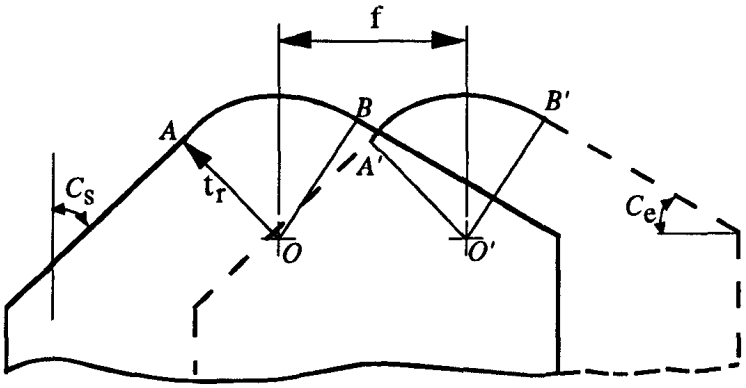

$$2\,t_r \sin C_e < f < t_r\left[\sin C_e + \cos C_s + (\cos C_e - \sin C_s)\cot C_e\right]$$

Case II: Tool Nose Intersects a Cutting Edge

Figure 2.5 Evaluation of the theoretical peak-to-valley value

Equation (3.3) shows that the ideal surface roughness decreases with a decrease in the feed rate or increase in the tool nose radius and is independent of the depth of cut and cutting speed.

The theoretical roughness for the work piece surface in end milling can be estimated using **Equations (3.1) and (3.2)**. If the corner radius t_r=0, the syrface

roughness depends only on the concavity angle (ψ) and the feed per tooth (f_z) and helix angle α=0 as shown in **Figure 2.6 [7]**.

$$R_t = \frac{f_z}{\cot(\psi)} \quad \text{.....(3.6)}$$

$$Ra = \frac{f_z}{4\cot(\psi)} \quad \text{.....(3.7)}$$

If the corner radius $t_r \neq 0$ on the cutting edge the surface roughness are:

$$R_t = [1-\cos(\psi)]t_r + f_z \sin(\psi)\cos(\psi) - \sqrt{2 f_z t_r \sin^3(\psi) - f_z^2 \sin^4(\psi)}$$

$$\approx \frac{f_z^2}{8 t_r} \qquad (f_z \leq 2t_r \sin(\psi)) \quad \text{.....(3.8)}$$

$$Ra = \frac{f_z^2}{t_r 18\sqrt{3}} \qquad (f_z \leq 2t_r \sin(\psi)) \quad \text{.....(3.9)}$$

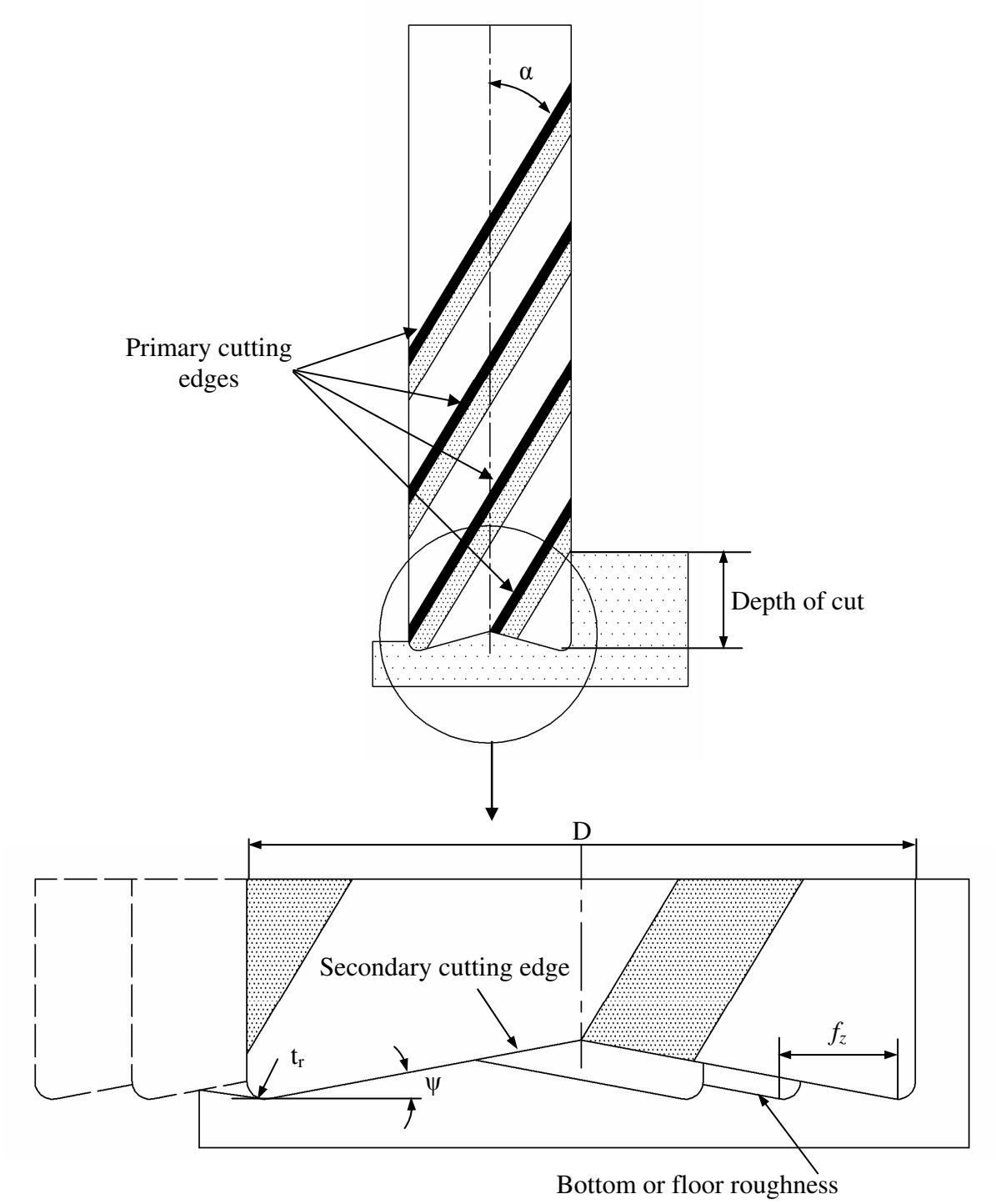

Figure 2.6 Geometry of the surface produced in an end-milling process.

A real machined surface roughness produced by end-milling will usually exceed the radial roughness due to other effects such as built-up edge, tool vibration and tool wear. These effects will be discussed in the following sections.

2.2.2 Effect of built-up edge on surface finish

A built-up edge (BUE) forms on the tool face at a relative low cutting speed when cutting such common materials as steel and aluminum. There is no built-up edge at very low cutting speed (say V=0.3 m/min) since the temperature on the face of the chip is not sufficient to cause the chip surface to behave in a ductile manner. With an increase in cutting speed the chip metal in contact with the chip face becomes ductile and the resulting plastic flow on the chip face causes strain hardening and a further increase in the force tending to fix the chip to the tool. When the bonding force between chip and tool exceeds the shear strength of the metal in the material body of the chip, at some particularly weak point near the tool face, the BUE forms. It causes poor surface finish **[5-7]**.

The BUE causes an increase in the rake angel which in turn causes a decrease in the magnitude of the resultant force on the tool as shown in **Figure 2.7.** As the BUE grows forward it will usually grow downward too, causing the surface to be damage. When the BUE becomes large the resultant force loads the BUE as a cantilever and finally the moment at the base of the BUE becomes sufficient to pry it loose. The BUE then passes off partly with the chip and partly on the finished surface. The growth and rapid breakage of the BUE cause a rough surface on the machined part, which is the characteristic of the BUE component of the surface roughness.

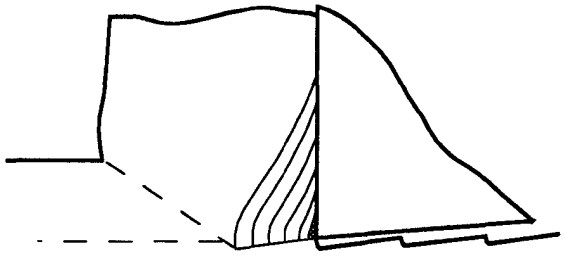

Figure 2.7 Formation of the Built-up edge

Based on the observation from cutting tests, there is a critical cutting speed for disappearance of the BUE. The critical cutting speed can be summarized under various conditions **[5]**:

1 - The critical cutting speed remains unchanged with varying depth of cut except at very small depths of cut where the critical cutting speed is slightly larger.

2 – The tool material has little effect on the critical cutting speed.

3 – With an increase in the feed rate, the critical cutting speed is reduced.

4 – With an increase in the rake angel of tool, the critical cutting speed is reduced.

5 – When cutting several kinds of steel, a lower critical speed is obtained for harder materials. In other words, brittle metals do not form BUE.

In general, the size of the BUE can be controlled by increasing the cutting speed to a value higher than the critical cutting speed. Therefore, high cutting speed is chosen for all of the cutting tests in this research to reduce the effect of BUE on the evaluation of machined surfaces.

2.2.3 Effect of tool vibration on surface finish

The dynamic displacement of parts of machine tool structure (vibration) is a problem that is natural in metal cutting processes. The displacement of the cutting tool relative to the work piece may harmfully affect surface finish, dimensional accuracy, tool life and machine life **[6-9]**.

Vibration in end milling process may arise due to internal sources such as the movement of rotating parts, work piece in-homogeneities, the feed mechanism of the machine tool and the varying cutting force. External sources as neighboring vibration machine tools may excite the floor and induce vibration into the machine tool structure. Milling processes are recognized for their characteristically large levels of vibration resulting from the cyclic nature of the chip loading mechanics and the cyclic nature of the cutting force system produced by a multi tooth cutter.

In general, the level of forced displacement present in machining system depends on the characteristics of the exciting force system as well as the dynamic properties of the structure **[6]**.

Study of tool vibration has extensive, and mathematical models to analyze the dynamic response of machining operation are readily available **[5 and 10]**. However, little work has been done to develop an approach which can link the surface texture generation and cutting dynamics together. Especially, the random vibrations of the cutting tool during machining have been observed and become a major difficulty in establishing the relationship between surface finish and cutting conditions.

One form of vibration which is widely recognized for its harmful effect is chatter. Chatter is an unstable form of forced vibration in which displacement amplitudes increase with time until they are large enough to cause the cutting tool

to move away from the work piece. At some point this vibration amplitude stabilizes and the cutter is not in contact with the work piece for a part of the oscillatory cycle **[11]**.

In machining, the phenomenon of chatter is totally unacceptable because it indicates the presence of severe vibrations, corrupt surface finish and large amount of acoustical noise.

Process decision makers search for cutting conditions that avoid large levels of forced vibration and chatter. This is an easy task since machine tool structures have low damping which is partly responsible for large levels of forced vibration in machine tool structure. Also the vibration can be eliminated by using a stable CNC end milling machine, homogeneous work piece and properly selrcted machining conditions.

2.2.4 Effect of tool wear on surface finish

Tool wear is an important factor that influences the real surface roughness. Tool wear is a result of mechanical and chemical interaction between the cutting tool and work piece as a result of removal of small parts of the cut material from the edge of the tool.

It has been observed that Ra versus cutting time curve has the same general shape as the conventional wear land versus cutting time **[12]**. In other words, as tool wear proceeds, the peak value of roughness increases due to vibration.

The increase of the roughness is due to the concentrated groove wear formed at the irregular edge of the tool. In finish cutting, small grooves develop along the feed direction on the cutting edge of tools which have small end cutting edge

angles **[13]**. On the other hand, when the tool is damaged, its effect on the cutting force variation can sometimes cause break chattering during machining.

2.3 Types of monitoring systems

Actual surface roughness monitoring can be achieved either through intensive post-process inspection, an in-process inspection, or surface roughness prediction methods. **[14]**.

2.3.1 Intensive post-process inspection

Post process inspection is the easiest to implement. But it can not prevent the parts from being processed before a defective batch is discovered **[14]**.

2.3.2 An in-process inspection

Measuring surface roughness in-process requires sensitive sensors added to a hostile environment **[15-18]**.

Chang et al. [15] developed a method to predict surface roughness during cutting. Surface roughness, was predicted from the displacement signal of spindle motion. The spindle-tool system including; spindle and chuck holder; could be modeled as a cantilever beam and the first mode shape of the cantilever was assumed to be the main vibration to determine surface roughness. The spindle displacement was measured in real time using cylindrical capacitive displacement sensor, which was installed at the spindle housing end cover. The linear regression model was proposed and its effectiveness was verified from cutting tests. Results

showed that the developed surface roughness model could accurately predict the roughness of milled surface within a 5% error level.

Huang and Chen [16] developed a multiple regression model to predict in-process surface roughness in turning operation using vibration measurements by an accelerometer. Machining parameters, such as feed rate, spindle speeds, and depth of cut, were used as predictors. The collected vibration signals were used as another predictor. The prediction accuracy was found as high as above 90%.

Samhouri, and Surgenor [17] used ANFIS to monitor and identify the surface roughness of grinding operation during cutting. Power spectral density (PSD) of the spindle vibration signal related to grinding features and surface finish is used as an input to ANFIS, which in turn outputs a value for the on-line predicted surface roughness. The adoption of Bell-shaped membership function (gbellmf) in ANFIS gave a prediction accuracy of 91%.

Savage et al. [18] identified the significant effects of tool diameter on tool vibration and work piece surface roughness in end mill cutting. The data collected demonstrates that tool diameter has a significant effect on vibration generation and surface roughness. Work piece vibration and surface roughness were significantly affected by the feed rate of the cutting tool. The interaction between tool diameter and feed rate did have a significant effect on surface roughness and work piece vibrations. However, this effect was largely due to feed rate. Results of this study showed that tool diameter should be considered as a major contributing factor in the surface roughness recognition model.

2.3.3 Surface roughness prediction system

Surface roughness prediction system can be used to determine the surface roughness indirectly **[19 and 20]**.

Baek et al. [19] studied and analyzed the effects of the end-mill run out errors and the variation of the feed rate on the surface roughness and the dimensional accuracy in a face-milling operation using a surface roughness model. The validity of the developed model was proved through cutting experiments, and the model was used to predict the machined surface roughness from the information of run outs and the cutting parameters.

It was found that the surface roughness was highly nonlinear to the feed rate. Therefore, in order to predict the surface roughness exactly, the insert run out errors must be measured earlier. Second, the optimal feed rate was obtained by solving the objective function with a bisection method. The verification results confirm that the developed surface roughness model and the optimization scheme were good enough for controlling the machined surface roughness, while maximizing the material removal rate.

Colak et al. [20] used genetic expression programming method for predicting surface roughness of milling surface with relation to cutting parameters. At the end of the study; a linear equation is obtained for surface roughness related to experimental study at an accuracy of 91%.

2.4 Surface roughness prediction techniques

Several techniques including multiple regressions, fuzzy logic, artificial neural network (ANN) and adaptive neuro-fuzzy inference system (ANFIS) have been used to predict surface roughness of different cutting process **[4 and 14-31]**:

2.4.1 Multiple regression models

Multiple regressions are used to determine the correlation between a certain variable and a combination of predictor variables and may be used to analyze data and generate a model. From the multiple regression models, one can obtain the relationship between the criterion variable and the predictive variable **[32 and 33]**. There for, it was used to predict the surface roughness in different cutting operations **[4, 14 and 20]**.

Lou et al. [4] examined the relation between the surface roughness and cutting parameters using multiple regression models and found that:

1. The surface roughness (Ra) could be predicted effectively by applying spindle speed, feed rate, depth of cut, and their interactions in the multiple regression models.

2. The multiple regression models could predict the surface roughness (Ra) with average percentage deviation of 9.71% or 90.29% accuracy from training data set.

3. This multiple regression model could predict the surface roughness (Ra) from testing data set that was not included in the multiple regression analysis with average percentage deviation of 9.97 % or accuracy of 90.03%.

4. Feed rate was the most significant machining parameter used to predict the surface roughness in the multiple regression models.

Kirby et al. [14] developed a surface roughness prediction model for a turning operation. The study involved a basic factorial design, which includes three controlled factors and three responses variables. The response variables for this design include surface roughness, measured in micro inches and the vibration signals in the X (radial), Y (tangential) and Z (feed) axes, measured in volts. The controlled factors include the three main parameters controlled in a turning operation (spindle speed, feed rate and depth of cut). A single cutting parameter and vibration along three axes were used to develop a multiple regression model for an in-process surface roughness prediction system. A strong linear relationship among the parameters (feed rate and vibration measured in three axes) and the response (surface roughness) were found using multiple regression and analysis of variance (ANOVA). The effectiveness of this system was demonstrated using a validation run of different cutting parameter values. With the experimental design given, predictions were made with errors of 9.96% based on the experimental run and 10.77% based on the validation run. These results are reasonable, given the effective measurement accuracy of the stylus profilometer used. This also demonstrates that spindle speed and depth of cut do not necessarily have to be fixed for an effective surface roughness prediction model.

Senussi et al. [21] studied the effect of turning process parameters (cutting speed, feed rate, and depth of cut) and nose radius of the tool as input variables on the surface roughness (Ra) as response or output. Three experiments were conducted; they were used to investigate the surface roughness resulted by tool corner radii of the values: 0.4mm, 0.8mm, and 1.2mm.

Response surface methodology (R.S.M) was used to determine and present the cause and effect of the relationship between true mean response and input control variables influencing the response as a two or three dimensional hyper surface.

R.S.M has been used for designing a three factor with five level central composite rotatable factors design in order to construct statistical models capable of accurate prediction of responses.

The results obtained showed that the application of R.S.M can predict the effect of machining parameters on surface roughness. The five level factorial designs can be employed easily for developing statistical models to predict surface roughness by controllable machining parameters. The combined effect of cutting speed at its higher level, feed rate and depth of cut at their lower values, and large nose radius can result in better surface roughness.

From the results obtained and discussion, the following facts were concluded:

1- Good surface roughness was obtained at high cutting speed (200 m/min) and large corner radius (1.2 mm).

2- Rough surface roughness was obtained at high feed rate (0.2 mm/rev) and small corner radius (0.4 mm).

3- Surface roughness was better at small depth of cut (0.4 mm) and large corner radius (1.2 mm).

4- There is no significant interaction effect between cutting speed and depth of cut on surface roughness at this range of machining parameters [160-200 m/min and 0.4-2.0 mm] of Austenitic Stainless Steel 304.

5- No significant effect between feed rate and depth of cut on surface roughness at this range of machining parameters [0.04-0.20 mm/rev and 0.4-2.0 mm] of Austenitic Stainless Steel 304.

6- The interaction effect between cutting speed and feed rate on surface roughness is reported easily, so, surface is rough at high level of feed rate [0.20 mm/rev], but it is better when increasing in cutting speed [200 m/min].

2.4.2 Fuzzy logic

Fuzzy sets were introduced by **Zadeh [34-37]** as a means of representing and manipulating data that was not precise, but rather fuzzy. There is a strong relationship between Boolean logic and the concept of a subset, there is a similar strong relationship between fuzzy logic and fuzzy subset theory. It has been used to model complex systems that can be monitored, controlled and operated humans based on if-then rules that were develop over years of knowledge and experience.

It was used to predict the surface roughness in different cutting operations.

Abd El-Raaouf et al. [22] studied the applicability of the fuzzy technique in the field of machined surface quality. The document includes the operation of the fuzzy technique in combination with the parametric analysis for generating the different combinations of machining conditions that lead to high surface quality.

A mathematical model is developed to relate the four cutting parameters namely; cutting speed, un-deformed chip thickness, tool rake angle, and tool wear land length to both the total force and power consumption in addition to the surface roughness during orthogonal cutting.

The membership function is utilized to generate the fuzzy model. The non linear program is used throughout de-fuzzification process. The comparison of the results with respect to the reference crisp model proves the efficiency of the fuzzy technique in a wide class of engineering applications.

2.4.3 Artificial neural network (ANN)

Artificial neural system can be considered as simplified mathematical models of brain like systems and they function as parallel distributed computing network.

However, in contrast to conventional computers, which are programmed to perform specific task, most neural networks must be trained. They can learn new associations, new functional dependencies and new patterns. Although computers outperform both biological and artificial neural systems represent the promising new generation of information processing networks **[35-41]**.

It was used to predict the surface roughness in different cutting operations **[23 and 24]**.

Feng and Wang [23] focused on developing an empirical model for surface roughness prediction in finish turning. The model considers the following working parameters: work piece hardness (material), feed, cutter nose radius, spindle speed and depth of cut.

Two competing data mining techniques, nonlinear regression analysis and computational neural networks, are applied in developing the empirical models. The values of surface roughness predicted by these models are then compared with those from some of the representative models in the literature. Metal cutting experiments and tests of hypothesis demonstrate that the model developed in this research have a satisfactory goodness of fit.

It has also presented an accurate procedure for model validation and model comparison. The multiple regression models could predict the surface roughness with root mean square error (RMS) equal to 0.332 and for neural network equal to 0.32.

Ozel and Karpat [24] utilized neural network modeling to predict surface roughness and tool flank wear over the machining time for variety of cutting conditions in finish hard turning. Regressions models are also developed in order to capture process specific parameters.

A set of sparse experimental data for finish turning of hardened AISI 52100 steel obtained from literature and the experimental data obtained from performed experiments in finish turning of hardened AISI H-13 steel have been utilized. The data sets from measured surface roughness and tool flank wear were employed to train the neural network models.

Trained neural network models were used in predicting surface roughness and tool flank wear for other cutting conditions. A comparison of neural network models with regression models is also carried out. Predictive neural network models are found to be capable of better predictions for surface roughness and tool flank wear within the range that they had been trained.

Predictive neural network modeling is also extended to predict tool wear and surface roughness patterns seen in finish hard turning processes. Decrease in the feed rate resulted in better surface roughness but slightly faster tool wear development, and increasing cutting speed resulted in significant increase in tool wear development but resulted in better surface roughness. Increase in the workpiece hardness resultant in better surface roughness but higher tool wear.

The average root mean square error for neural networks of tool flank wear prediction for honed tools equal to 5.9, for tool flank wear prediction for chamfered tools equals to 2.1, for surface roughness prediction for honed tools equals to 5.4 and for surface roughness prediction for chamfered equals to 9.3.

2.4.4 Adaptive neuro-fuzzy inference system (ANFIS)

ANFIS is a fuzzy inference system implemented in the framework of an adaptive neural network. By using a hybrid learning procedure, ANFIS can be used to construct an input-output mapping based on both human-knowledge as

fuzzy if-then rules and predetermined input-output data pairs for neural networks training. It provides a means for fuzzy modeling to learn information about the data set, in order to compute the membership function parameters that best allow the associated fuzzy inference system to track the given input-output data **[39-41]**.

Recently, ANFIS was used to predict the work piece surface roughness in turning operation **[25-27]**. It was also used to predict surface roughness in end milling operation **[28-31]**.

Lee et al. [25] proposed a method using an adaptive neuro-fuzzy inference system (ANFIS) to establish the relationship between actual surface roughness and texture features of the surface image. The accurate modeling of surface roughness can effectively estimate surface roughness.

The input parameters of a training model are spatial frequency, arithmetic mean value, and standard deviation of gray levels from the surface image, without involving cutting parameters (cutting speed, feed rate, and depth of cut).

Experiments demonstrate the validity and effectiveness of fuzzy neural networks for modeling and estimating surface roughness. Experimental results show that the proposed ANFIS-based method outperforms the existing polynomial-network-based method in terms of training and test accuracy of surface roughness. To further verify the estimation accuracy, several experiments using unseen test images are performed and the results are shown that the errors are smaller than 7.14% and the mean error is only 4.12%.

Jiao et al. [26] used the recently developed fuzzy adaptive network (FAN) to model surface roughness in turning operations. The FAN network has both the learning ability of neural network and linguistic representation of complex, not well-understood, unclear phenomenon. Furthermore, it can continuously improve the initially obtained rough model based on the daily operating data. To illustrate

this approach, a model representing the influences of machining parameters on surface roughness is established and then the model is verified by the use of the results of direct experiments.

Finally, a comparison with the results based on statistical regression is provided. The proposed approach is much more powerful than the classical regression approach. First, this approach summarizes past data and there is no need to repeat the calculations of past data whenever new data become available, which is the case in the regression approach. Second, this approach has the learning ability of the neural network with the newly available daily operating data. And, finally, the FAN network can estimate many parameters and even tune the network structure and thus is much more powerful than the usual multiple variables regression analysis.

The disadvantage is that the resulting model is implicit and is represented by the network. However, this implicit model can be obtained or represented explicitly in equation forms by further manipulations or optimizations.

Ho et al. [27] proposed a method using an adaptive neuro-fuzzy inference system (ANFIS) to accurately establish the relationship between the features of surface image and the actual surface roughness, and consequently can effectively predict surface roughness using cutting parameters (cutting speed, feed rate, and depth of cut) and gray level of the surface image.

Experimental results show that the proposed ANFIS-based method outperforms the existing polynomial network-based method in terms of modeling and prediction accuracy. To further verify the prediction accuracy, several experiments using verification data are performed and the results show that the errors are smaller than 4.6%, and the mean error is only 0.38%. Compared with the mean

error 6.2% of the polynomial network-based method, the proposed ANFIS-based method is more useful to accurately predicted surface roughness.

Dweiri et al. [28] used the adaptive neuro fuzzy inference system to predict the effect of machining variables (spindle speed, feed rate, depth of cut, and number of flutes) on surface roughness of alumic-79 in down milling machining process in order to improve and increase its range of application.

Optimum surface roughness of 0.224 μm is achieved for four flutes at the spindle speed of 2000 rpm, feed rate of 0.06 mm/tooth, and depth of cut of 2 mm. Also it was found for the two flutes that the minimum surface roughness of 0.327 μm is achieved at the spindle speed of 2000 rpm, feed rate of 0.05 mm/tooth, and depth of cut of 2mm. Results show that the error is less than 5%.

Lo [29] used ANFIS to predict the work piece surface roughness after the end milling process and analyze the effect of three milling parameters, including spindle speed, feed rate and depth of cut, on the surface roughness. A total of 48 sets of experimental data are used for training in ANFIS. After the training is completed, another 24 sets of data are used as testing data.

The surface roughness values predicted by ANFIS are compared with the measurement values derived from the 24 data sets in order to determine the error of ANFIS. Besides, the 48 sets of experimental data are analyzed to verify the results obtained by ANFIS. The following conclusions can be drawn from the above analysis:

(1) The error of the surface roughness values predicted by ANFIS with the triangular membership function is only 4%, reaching accuracy as high as 96%. In contrast, the error by ANFIS with trapezoidal membership function is 6.7%, with an accuracy of 93.3%.

(2) Among the three end milling process parameters of spindle speed, feed rate and depth of cut, changes of the feed rate have the most impact on work piece surface roughness, followed by spindle speed and the depth of cut, which has the least impact.

Soltan, Eltaib, and El-Zahry [30] used multiple regression model and ANFIS model for prediction of surface roughness in end milling operation. The models were verified with test data where the average errors were 8% and 6% for multiple regression model and ANFIS respectively. These results indicate that ANFIS model with the generalized bell membership function (gbellmf) is more accurate than multiple regression models in prediction of surface roughness.

Hence, the aim of the second paper for the same authors is to predict the surface roughness in end milling operation using ANFIS and improve the ANFIS model to obtain the higher accuracy. The achieved accuracy has been found equal to 96% **[31]**.

CHAPTER THREE

SURFACE ROUGHNESS PREDICTION USING ANFIS MODEL BASED ON MACHINING PARAMETERS

3.1 Introduction

This chapter is focused on studying the prediction of surface roughness using the machining conditions (speed, feed rate and depth of cut), as input; and the surface roughness (Ra) as output.

The process under study can be represented by the model shown in **Figure 3.1**.

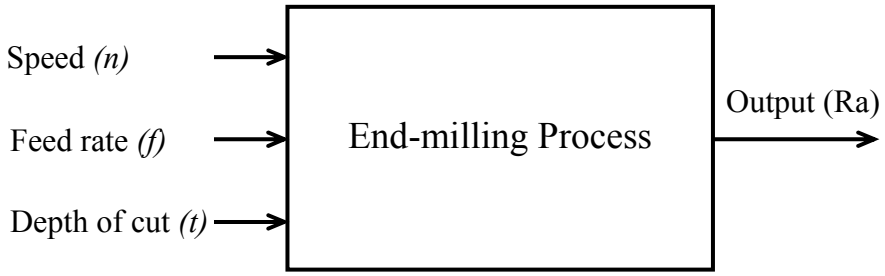

Figure 3.1 The End -Milling process model

3.2 ANFIS prediction model

While fuzzy logic provides an inference mechanism under cognitive uncertainty, computational neural networks offer exciting advantages, such as learning, adaptation, fault-tolerance, parallelism and generalization. To enable a system to deal with cognitive uncertainties in a manner more like humans, one may incorporate the concept of fuzzy logic into the neural networks. The computational process envisioned for fuzzy neural systems is as follows. It starts with the development of a fuzzy neuron based on the understanding of biological neuronal morphologies, followed by learning mechanisms as shown in **Figure 3.2**. This leads to the following three steps in a fuzzy neural computational process **[43]**.

- Development of fuzzy neural models motivated by biological neurons,
- Models of synaptic connections which incorporates fuzziness into neural network,
- Development of learning algorithms (that is the method of adjusting the synaptic weights)

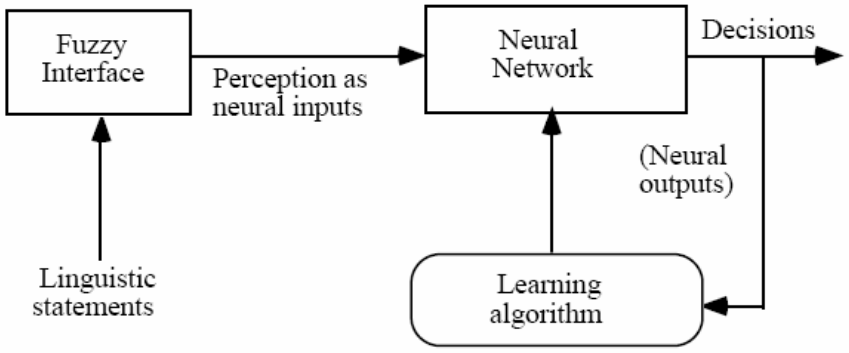

Figure 3.2 The model of fuzzy neural system.

ANFIS architecture is shown in **Figure 3.3**. Five network layers are used by ANFIS to perform the following fuzzy inference steps: (i) input fuzzification, (ii) fuzzy set database construction, (iii) fuzzy rule base construction, (iv) decision making, and (v) output de-fuzzification. ANFIS has been constructed through MATLAB software.

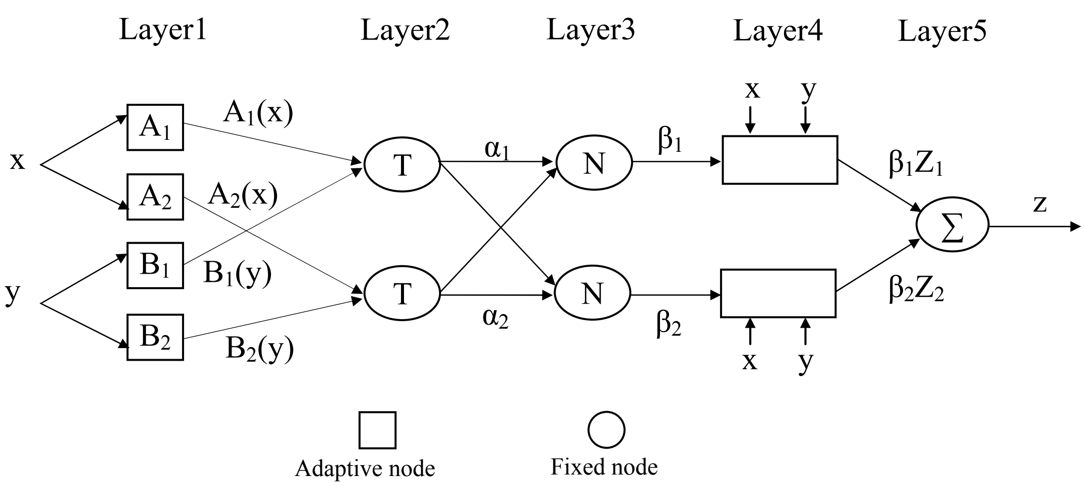

Figure 3.3 ANFIS architecture for a two-input Sugeno fuzzy model.

For explain this model simply, we have assumed only two rules, and two linguistic values for each input variable.

• **Layer 1** the output of the node is the degree to which the given input satisfies the linguistic label associated to this node. Usually, we choose bell-shaped membership functions to represent the linguistic terms.

$$A_i(u) = \exp\left[-\frac{1}{2}\left(\frac{u-a_{i1}}{b_{i1}}\right)^2\right], \quad \ldots\ldots(3.2)$$

$$B_i(v) = \exp\left[-\frac{1}{2}\left(\frac{v - a_{i2}}{b_{i2}}\right)^2\right], \quad \ldots\ldots\ldots\ldots\ldots\ldots\ldots\ldots\ldots\ldots\ldots\ldots\ldots\ldots\ldots\ldots\ldots\ldots\ldots\ldots\ldots\ldots\ldots\ldots\ldots\ldots\ldots\ldots(3.3)$$

Where

$\{a_{i1}, a_{i2}, b_{i1}, b_{i2}\}$ is the parameter set.

As the values of these parameters change, the bell-shaped functions vary accordingly, thus exhibiting various forms of membership functions on linguistic labels A_i and B_i. In fact, any continuous, such as trapezoidal and triangular-shaped membership functions are also quantified candidates for node functions in this layer. Parameters in this layer are referred to as principle parameters.

• **Layer 2** each node computes the firing strength of the associated rule. The output of top neuron is

$$\alpha_1 = A_1(x) \times B_1(y) \ldots\ldots\ldots\ldots\ldots\ldots\ldots\ldots\ldots\ldots\ldots\ldots\ldots\ldots\ldots\ldots\ldots\ldots\ldots\ldots\ldots\ldots\ldots\ldots\ldots\ldots(3.4)$$

and the output of the bottom neuron is

$$\alpha_2 = A_2(x) \times B_2(y) \ldots\ldots\ldots\ldots\ldots\ldots\ldots\ldots\ldots\ldots\ldots\ldots\ldots\ldots\ldots\ldots\ldots\ldots\ldots\ldots\ldots\ldots\ldots\ldots\ldots\ldots(3.5)$$

The nodes of this layer are called rule nodes.

• **Layer 3** every node in this layer is labeled by N to indicate the normalization of the firing levels.

The output of top neuron is the normalized (with respect to the sum of firing levels) firing level of the first rule

$$\beta_1 = \frac{\alpha_1}{\alpha_1 + \alpha_2} \;, \quad \ldots\ldots(3.6)$$

and the output of the bottom neuron is the normalized firing level of the second rule

$$\beta_2 = \frac{\alpha_2}{\alpha_1 + \alpha_2} \;, \quad \ldots\ldots(3.7)$$

• **Layer 4** the output of top neuron is the product of the normalized firing level and the individual rule output of the first rule

$$\beta_1 z_1 = \beta_1 (a_1 x + b_1 y), \quad \ldots\ldots(3.8)$$

The output of bottom neuron is the product of the normalized firing level and the individual rule output of the second rule

$$\beta_2 z_2 = \beta_2 (a_2 x + b_2 y), \quad \ldots\ldots(3.9)$$

• **Layer 5** the single node in this layer computes the overall system output as the sum of all incoming signals, i.e.

$$z = \beta_1 z_1 + \beta_2 z_2 \quad \ldots\ldots(3.10)$$

If a crisp training set $\{(x^k, y^k), k = 1, \ldots, K\}$ is given then the parameters of the hybrid neural net (which determine the shape of the membership functions of the

premises) can be learned by descent-type methods. This architecture and learning procedure is called ANFIS (adaptive-network-based fuzzy inference system).

The error function for pattern k can be given by

$$E_k = (y^k - o^k)^2 \quad \text{……(3.11)}$$

Where y^k is the desired output and o^k is the computed output by the hybrid neural net.

3.3 Construction of ANFIS model

1 - First of all the training data were determined and then this data loads on the ANFIS using graphical user interface in MATLAB program as shown in **Figure 3.4.**

Seventy five readings were used as training data set as shown in **Tables 3.1** and thirty two readings were used as testing data set as listed in **Table 3.2**.

The range selected of speed is 750, 1000, 1250, 1500 and 1750 rpm, for feed rate is 50, 100, 150, 200 and 250 mm/min, and for depth of cut is 0.3, 0.5 and 0.7 mm.

Every point in this data repeated three times and take the average value based the **Equation (3.1)**.

$$x_{av} = \frac{x_1 + x_2 + x_3}{3} \quad \text{……(3.1)}$$

Table 3.1 Measured Ra in microns (training data set)

***n* rpm**	**750**			**1000**			**1250**			**1500**			**1750**		
***t* mm** / ***f* mm/min**	**0.3**	**0.5**	**0.7**	**0.3**	**0.5**	**0.7**	**0.3**	**0.5**	**0.7**	**0.3**	**0.5**	**0.7**	**0.3**	**0.5**	**0.7**
50	1.1	1.36	1.9	0.96	1.12	1.36	1.18	1.6	1.08	0.6	0.82	1.02	0.84	0.82	1.54
100	1.28	2.06	2.22	1.02	1.44	1.78	1.18	1.3	1.14	0.86	1.02	1.24	0.98	1.16	1.22
150	1.42	2.63	2.96	1.54	1.54	2.24	1.24	1.34	1.22	1.32	1.36	1.38	1.1	1.26	1.62
200	1.54	3.5	3.52	1.16	2.28	2.64	1.26	1.5	1.44	1.56	1.56	1.4	1.32	1.62	1.6
250	1.82	2.5	5.5	1.58	2.96	3.14	1.66	1.38	1.62	1.32	1.26	1.42	1.48	1.74	1.56

Table 3.2 Measured Ra in microns (testing data set)

***n* rpm**	**875**		**1125**		**1375**		**1625**	
***t* mm** / ***f* mm/min**	**0.4**	**0.6**	**0.4**	**0.6**	**0.4**	**0.6**	**0.4**	**0.6**
75	1.42	1.86	1.02	1.36	1.02	1.18	0.76	1.22
125	1.96	2.36	1.28	1.62	1.14	1.33	1.16	1.32
175	2.42	2.66	1.36	1.92	1.22	1.32	1.22	1.38
225	2.06	2.88	1.56	1.96	1.26	1.52	1.3	1.44

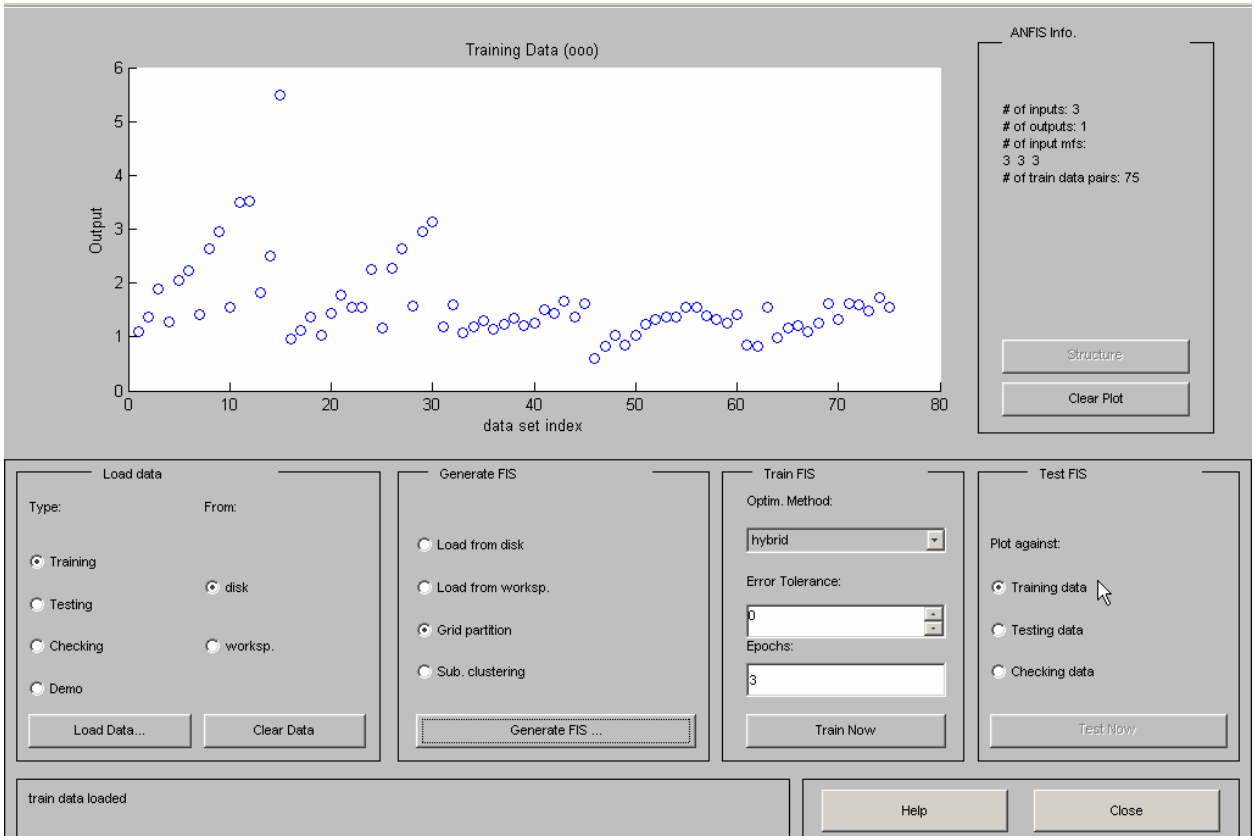

Figure 3.4 loading the training data set

2 - Fuzzy inference system (FIS) is generated by choosing the suitable type of input and output membership functions and determining the number of membership function in each input parameters as shown in **Figure 3.5**.

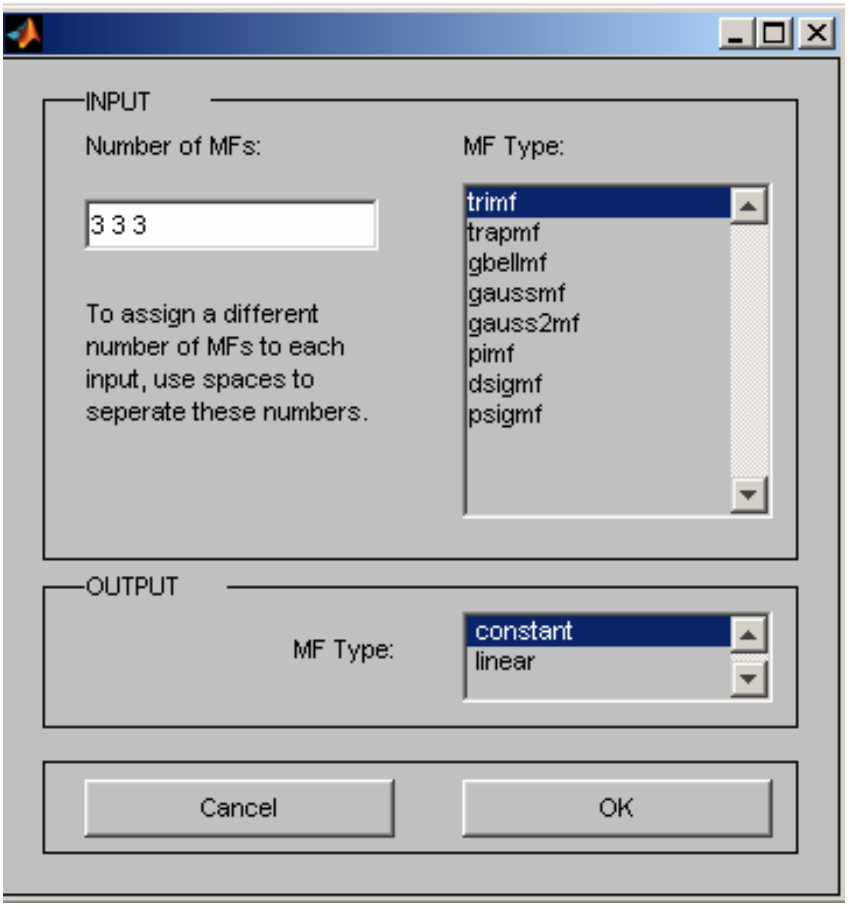

Figure 3.5 Generate fuzzy inference system

3 -The input and output parameters are lapelled and the fuzzy inference system type is determined as shown in **Figure 3.6**.

There are two types of fuzzy inference system can be implemented in the fuzzy logic toolbox: Mamadani-type and Sugeno-type inference systems. These two types of inference systems vary somewhat in the way outputs are determined. The main difference between Mamdani and Sugeno is that the Sugeno output membership functions are either linear or constant. So that, the Sugeno system lends itself to the use of adaptive techniques for constructing fuzzy models. These adaptive techniques can be used to customize the membership functions so that the fuzzy system best models the data.

A typical rule in a Sugeno fuzzy model has the form

If Input $1 = x$ and Input $2 = y$, then Output is $z = ax + by + c$

For a zero-order Sugeno model, the output level z is a constant ($a=b=0$).

The output level z_i of each rule is weighted by the firing strength w_i of the rule. For example, for an AND rule with Input $1 = x$ and Input $2 = y$, the firing strength is

$$w\text{i} = \text{And Method } (F1(x), F2(y)) \quad \ldots\ldots(3.14)$$

Where *F1(x) and F2(y)* are the membership functions for Inputs *1* and *2*. The final output of the system is the weighted average of all rule outputs, computed as

$$Final\ output = \frac{\sum_{i=1}^{N} w_i z_i}{\sum_{i=1}^{N} w_i} \quad \ldots\ldots(3.15)$$

Advantages of the Sugeno Method

- It is computationally efficient.
- It works well with linear techniques.
- It works well with optimization and adaptive techniques.
- It has guaranteed continuity of the output surface.
- It is well-suited to mathematical analysis.

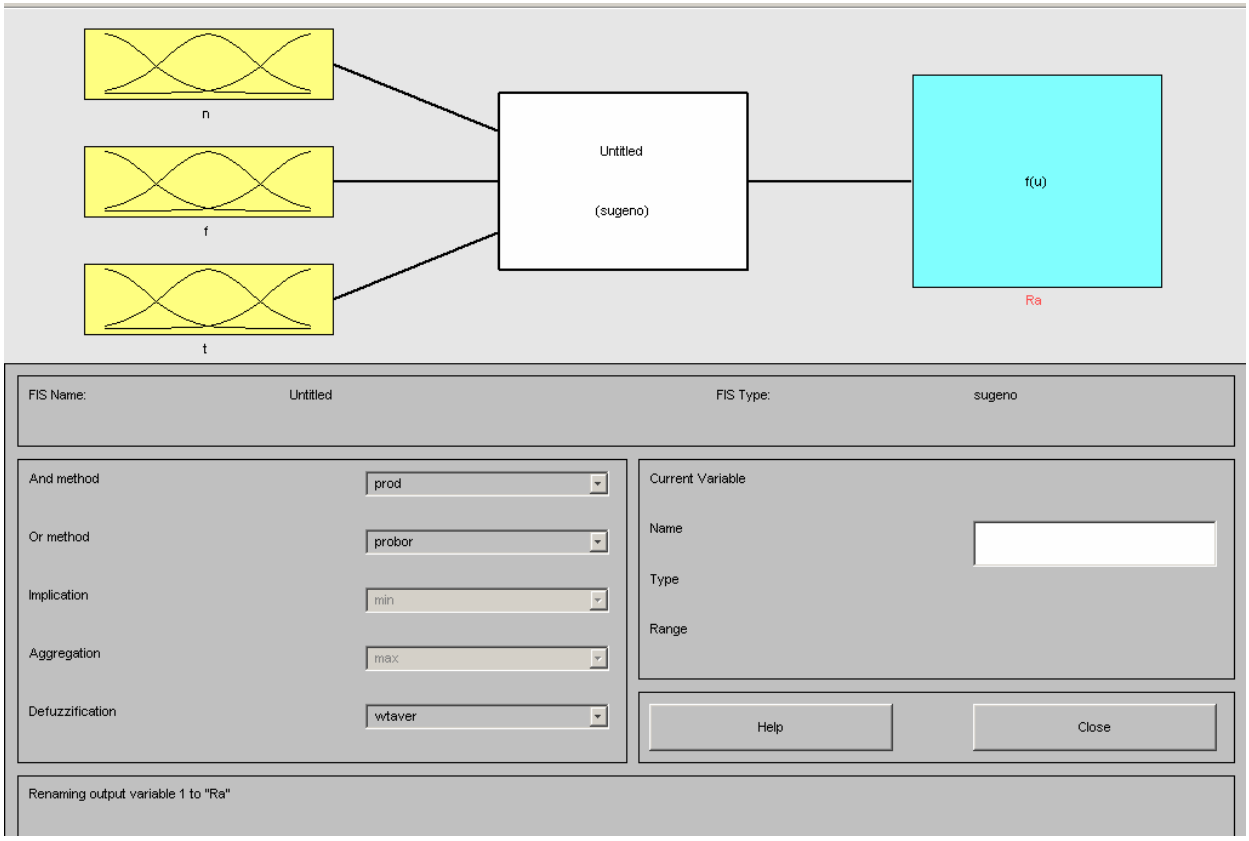

Figure 3.6 Fuzzy rule architecture

4 –The input and output membership functions are labeled and the range of the input variable is determined as shown in **Figure 3.7**.

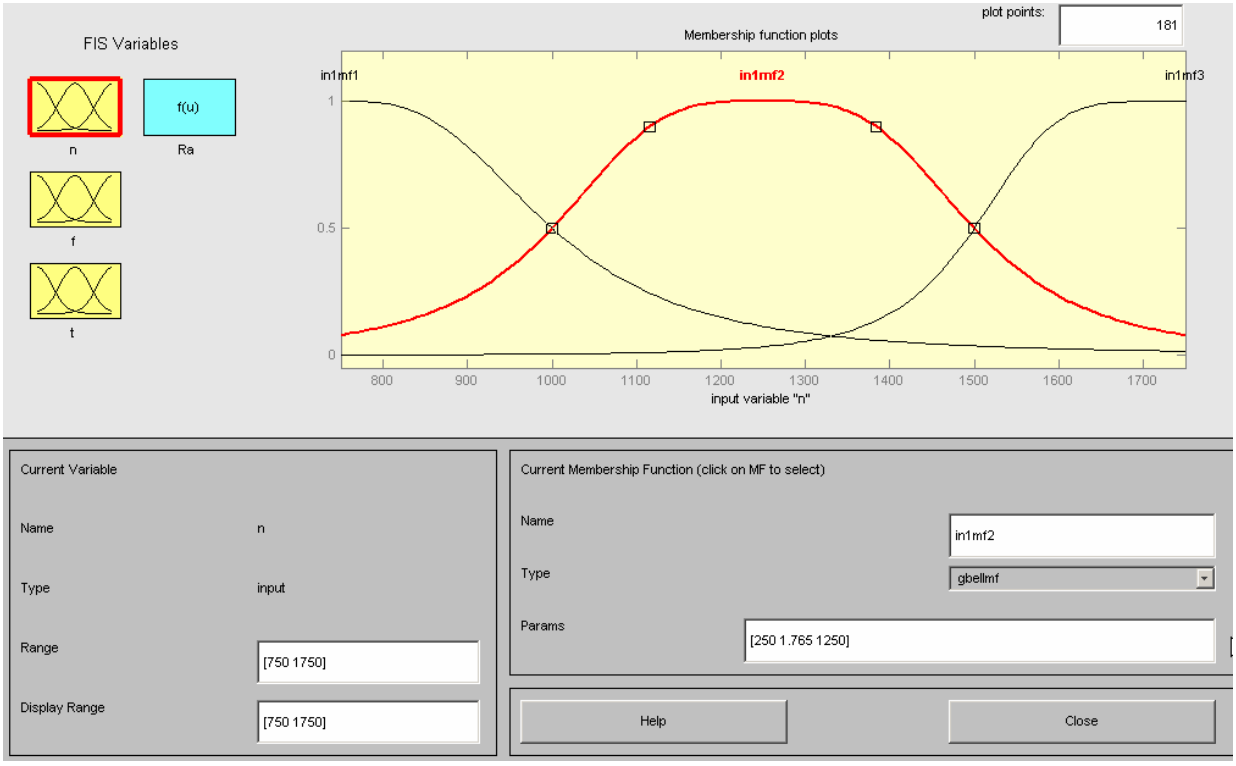

Figure 3.7 Fuzzy inference system properties

5 – The ANFIS rules are determined and used as shown in **Figure 3.8**.

For example:

If (speed) is (750rpm) and (feed rate) is (50mm/min) and (depth of cut) is (0.3mm) then (Ra) is (1.1µm)

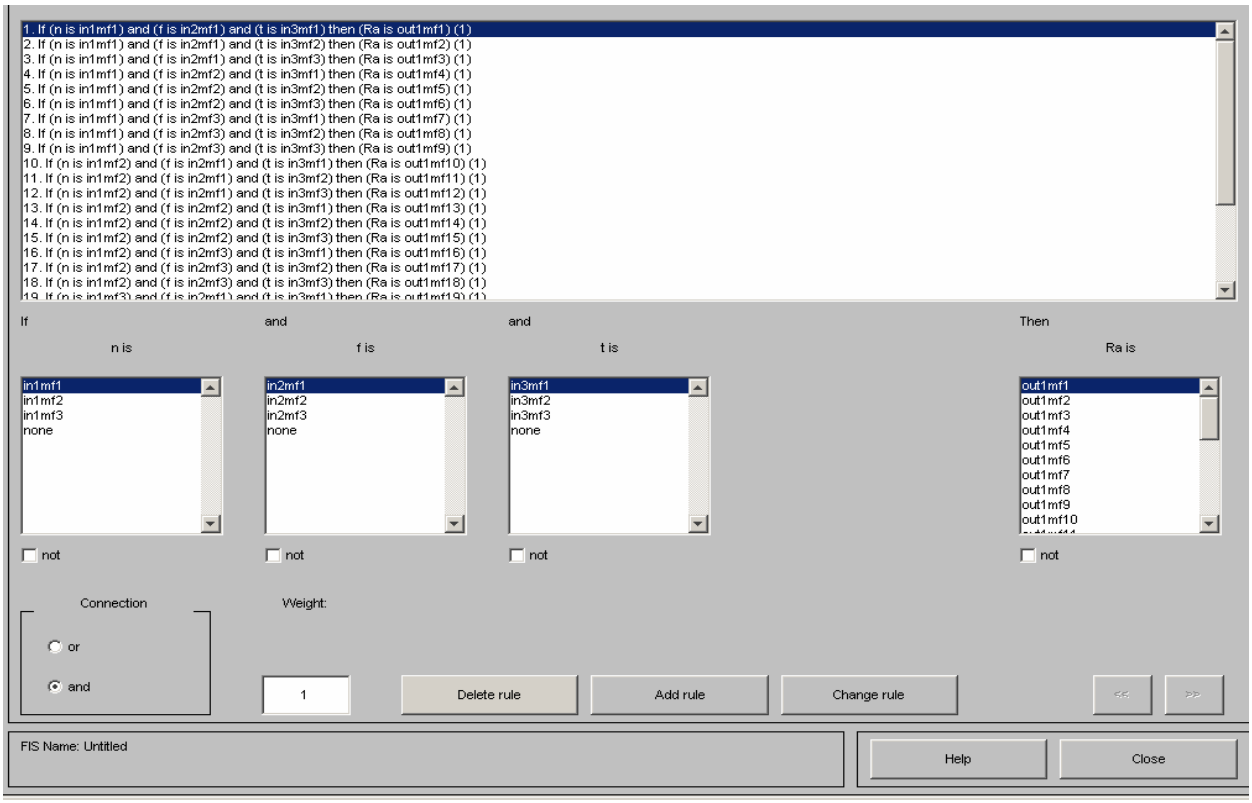

Figure 3.8 Fuzzy rules properties

6 - Learning algorithms are decided upon by determining the number of learning cycle (epochs) at which the error was steady and the obtained error is examined as shown in **Figure 3.9**.

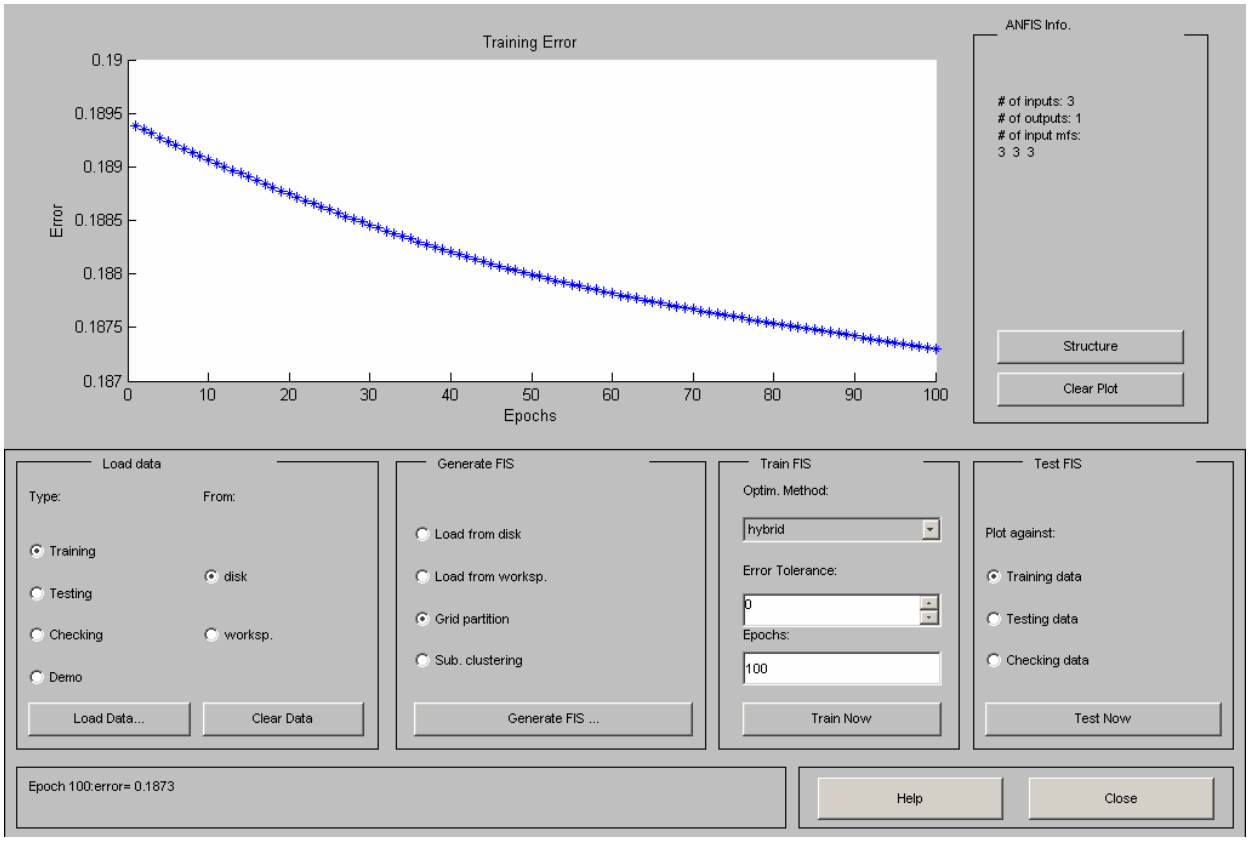

Figure 3.9 Development of learning algorithm

Different membership functions were used for training ANFIS to predict surface roughness. During the training the 75 Ra values (training data sets) were used to conduct 100 cycles of learning with average error as shown in **Figure 3.10-3.16**.

- The triangular memberships function (trimf) gives a training average error equals 0.19447.

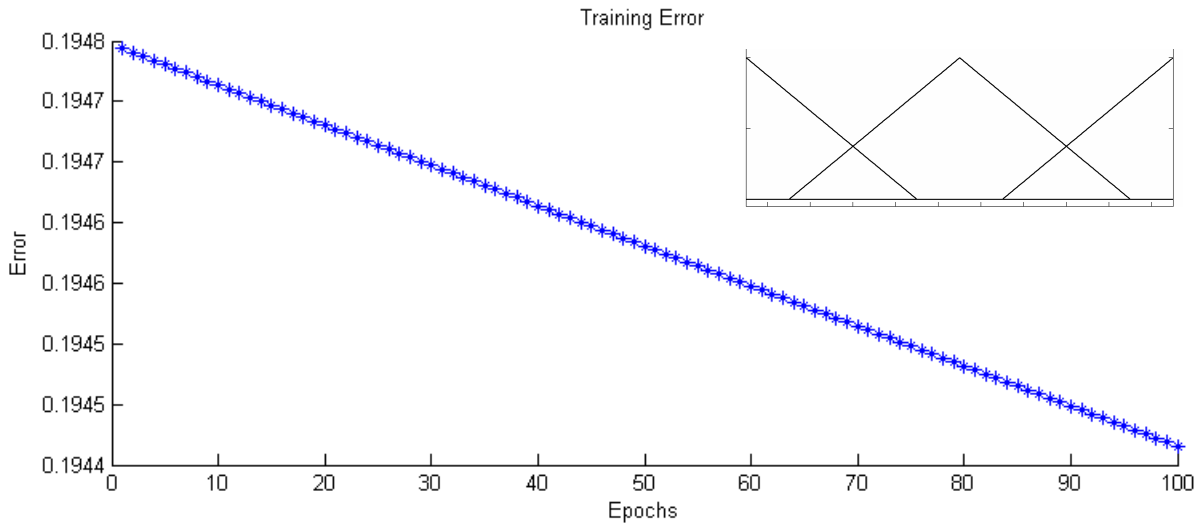

Figure 3.10 Training error curve of modeling Ra for trimf using 100 epochs.

- The trapezoidal memberships function (trapmf) gives a training average error equals 0.19443.

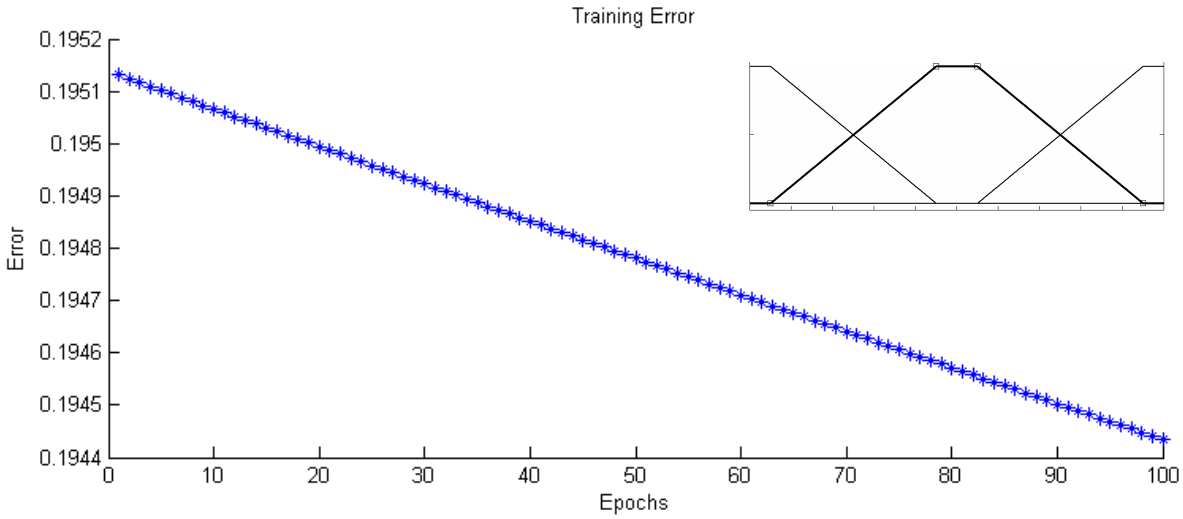

Figure 3.11 Training error curve of modeling Ra for trapmf using 100 epochs.

- The Generalized bell memberships function (gbellmf) gives a training average error equals 0.1873.

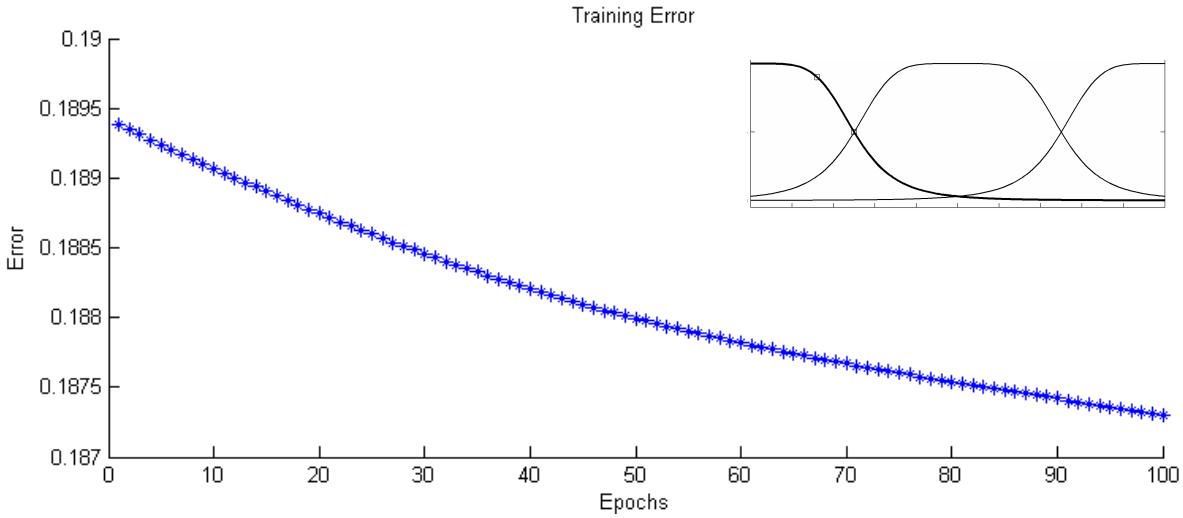

Figure 3.12 Training error curve of modeling Ra for gbellmf using 100 epochs.

- The Gaussian memberships function (gaussmf) gives a training average error equals 0.19176.

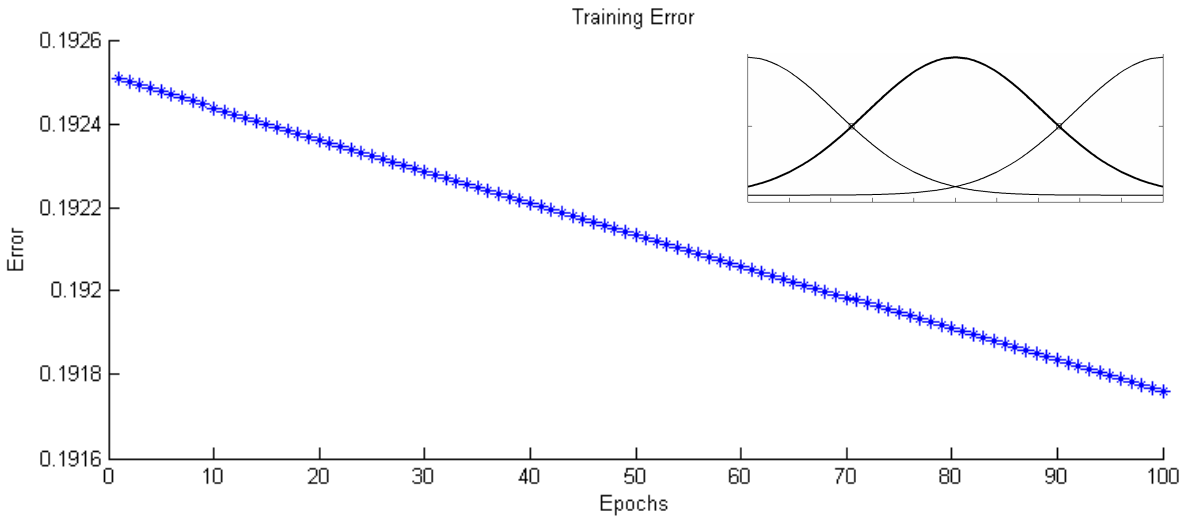

Figure 3.13 Training error curve of modeling Ra for gaussmf using 100 epochs.

- The pi-shaped memberships function (pimf) gives a training average error equals 0.19379.

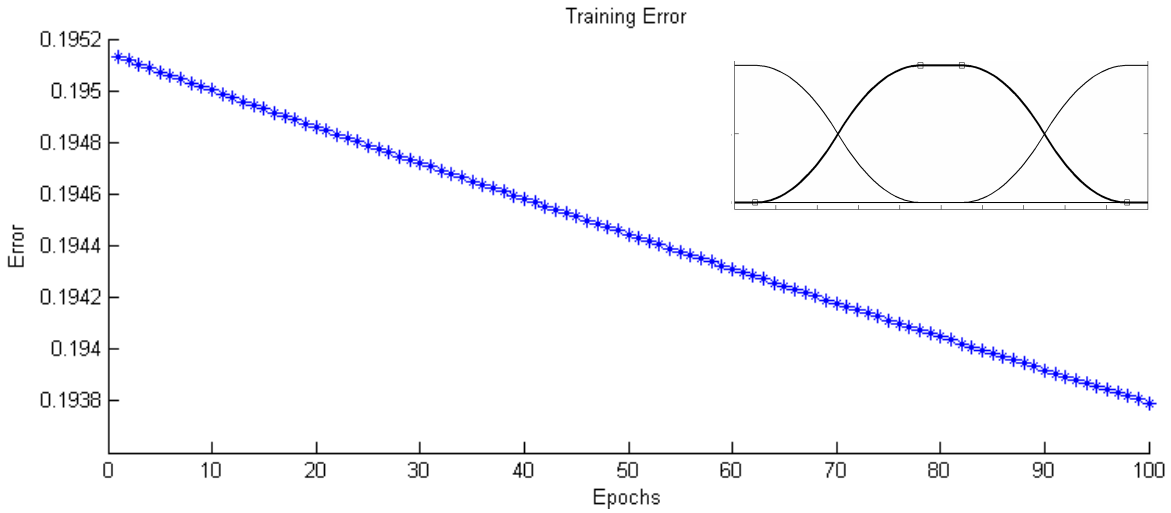

Figure 3.14 Training error curve of modeling Ra for pimf using 100 epochs.

- The difference between two sigmoid memberships function (dsigmf) gives a training average error equals 0.19369.

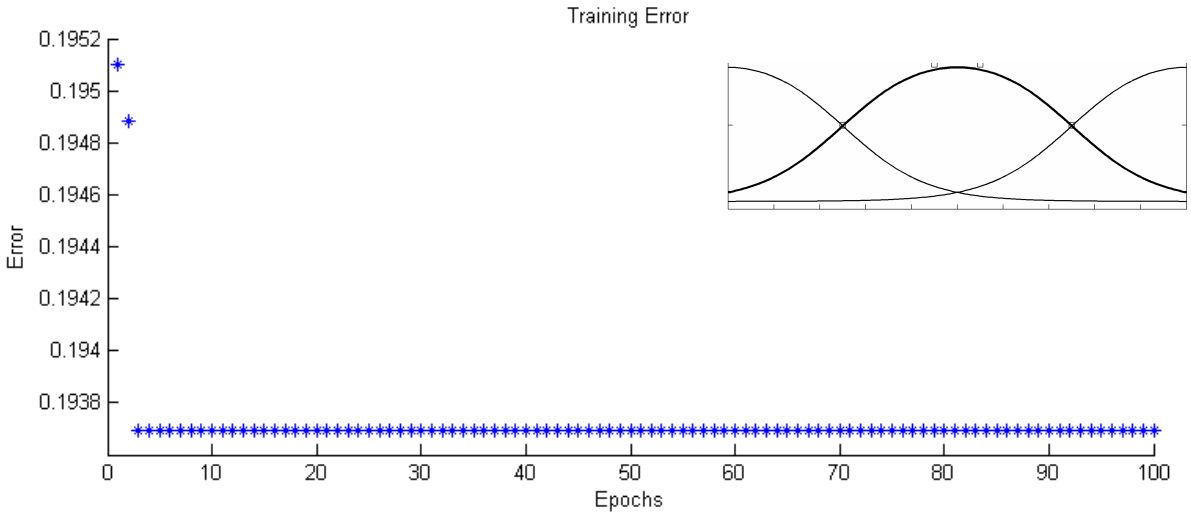

Figure 3.15 Training error curve of modeling Ra for dsigmf using 100 epochs.

- The product of two sigmoid memberships function (psigmf) gives a training average error equals 0.19369.

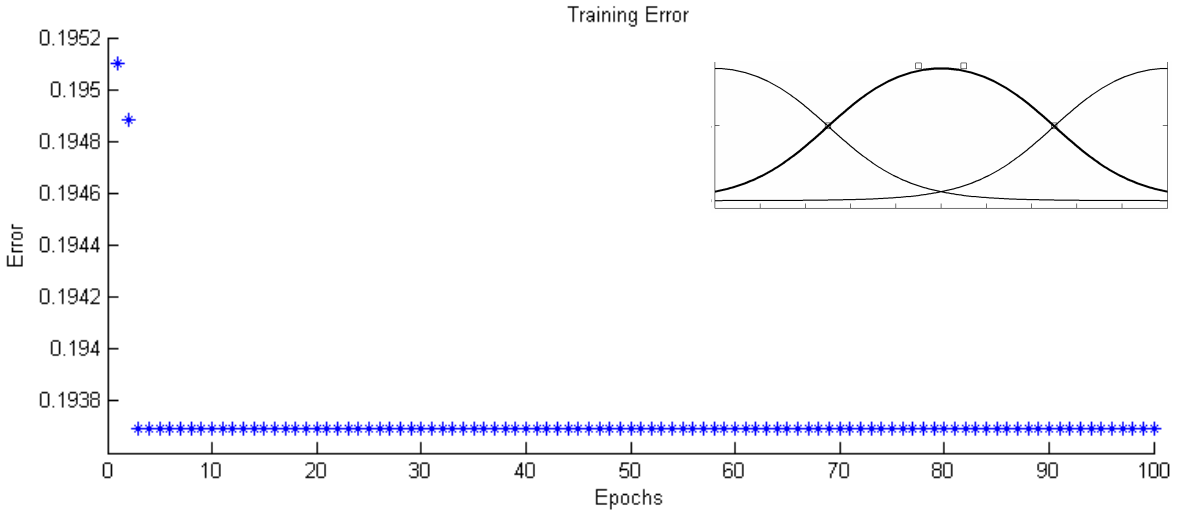

Figure 3.16 Training error curve of modeling Ra for psigmf using 100 epochs.

It is shown that; the generalized bell membership functions (gbellmf) give the lowest training error. Therefore, these functions were adopted during the training process of ANFIS in this study.

The membership functions of every input parameter within the architecture can be divided into three areas, i.e. small, medium and large areas. **Figures 3.17–3.19** show the initial and final membership functions of the three end milling parameters derived by training data via the gbellmf.

In **Figure 3.17** the initial membership function and the final membership function of the speed only experience small changes in the small and large areas, but slightly greater variation in the medium area. These changes indicate that all the range of speed has great effect on surface roughness.

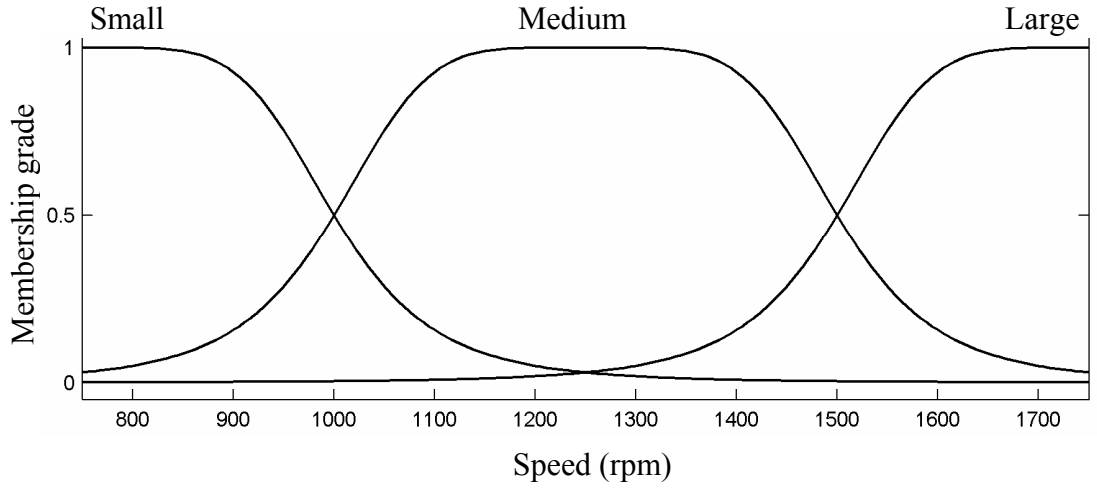

a) Initial membership functions

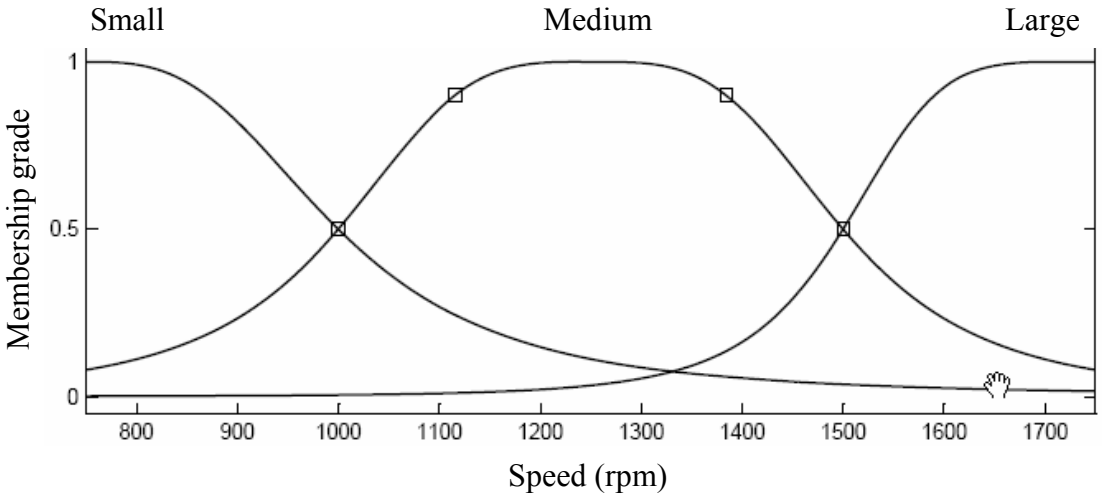

b) Final membership functions

Figure 3.17 Initial and final membership function of speed.

Figure 3.18 shows the initial and final membership functions of the feed rate. It is indicated that the final membership function after training experiences great variation in the small medium and large areas. These changes indicate that all the range of feed rate has great effect on surface roughness.

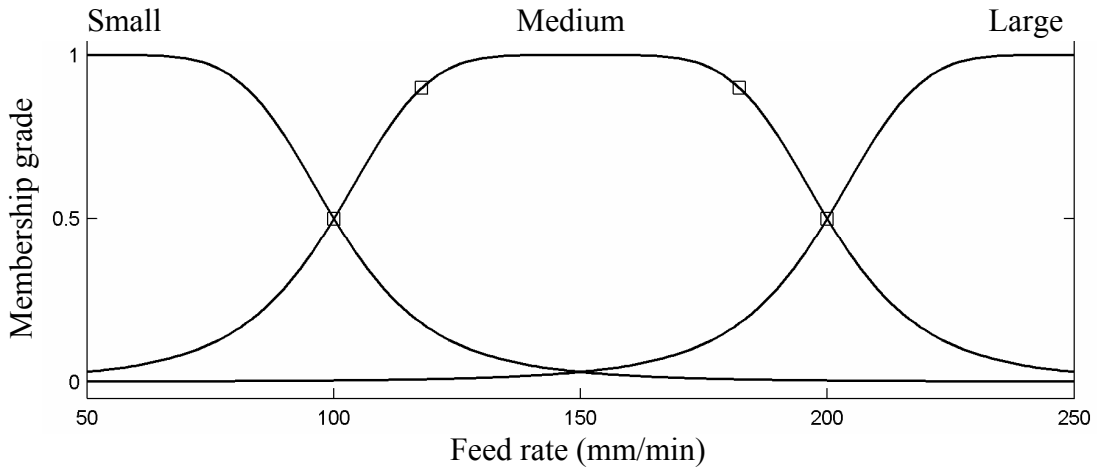

a) Initial membership functions

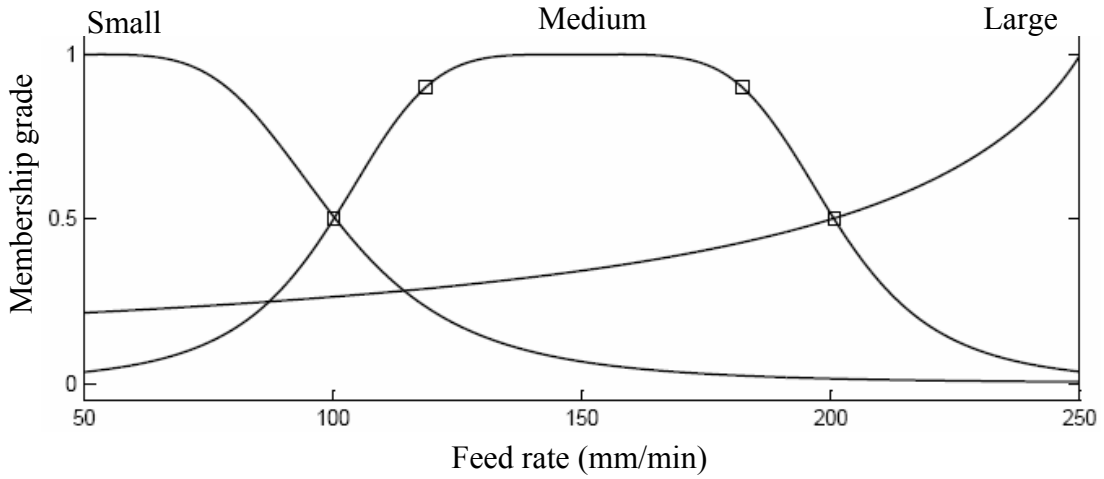

b) Final membership functions

Figure 3.18 Initial and final membership function of feed rate.

Figure 3.19 shows the initial and final membership functions of the depth of cut. There is obviously a small change in the final membership function shape after training in the small, medium and large areas. These changes indicate that the small, medium and large values of depth of cut have slightly effect on surface roughness.

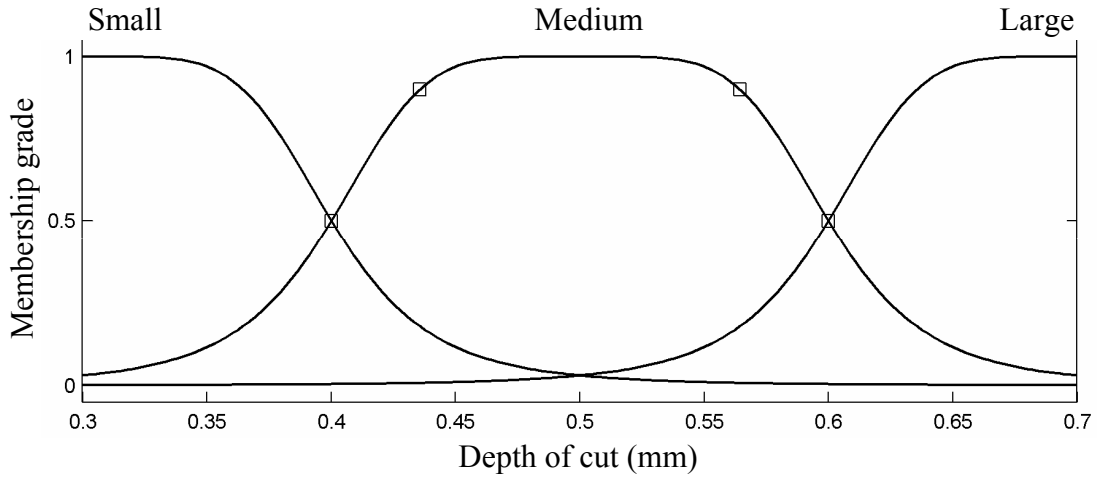

a) Initial membership functions

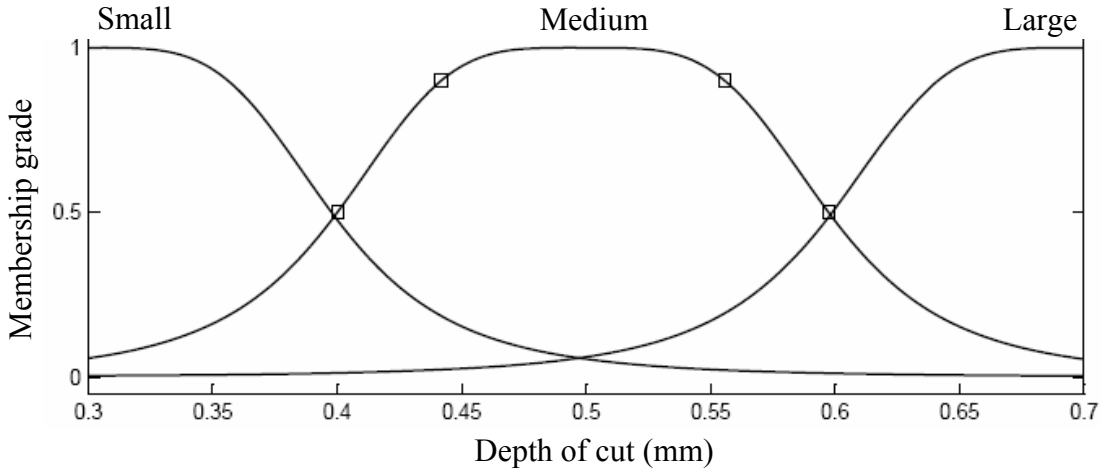

b) Final membership functions

Figure 3.19 Initial and final membership function of depth of cut.

The above analysis indicates that among the three end-milling parameters studied, speed has the most impact on surface roughness, followed by feed rate and finally by depth of cut, which was the least significant factor of all.

Figure 3.20 shows that comparison between the values of the measured Ra and predicted Ra by ANFIS model of the training data set using the gbellmf.

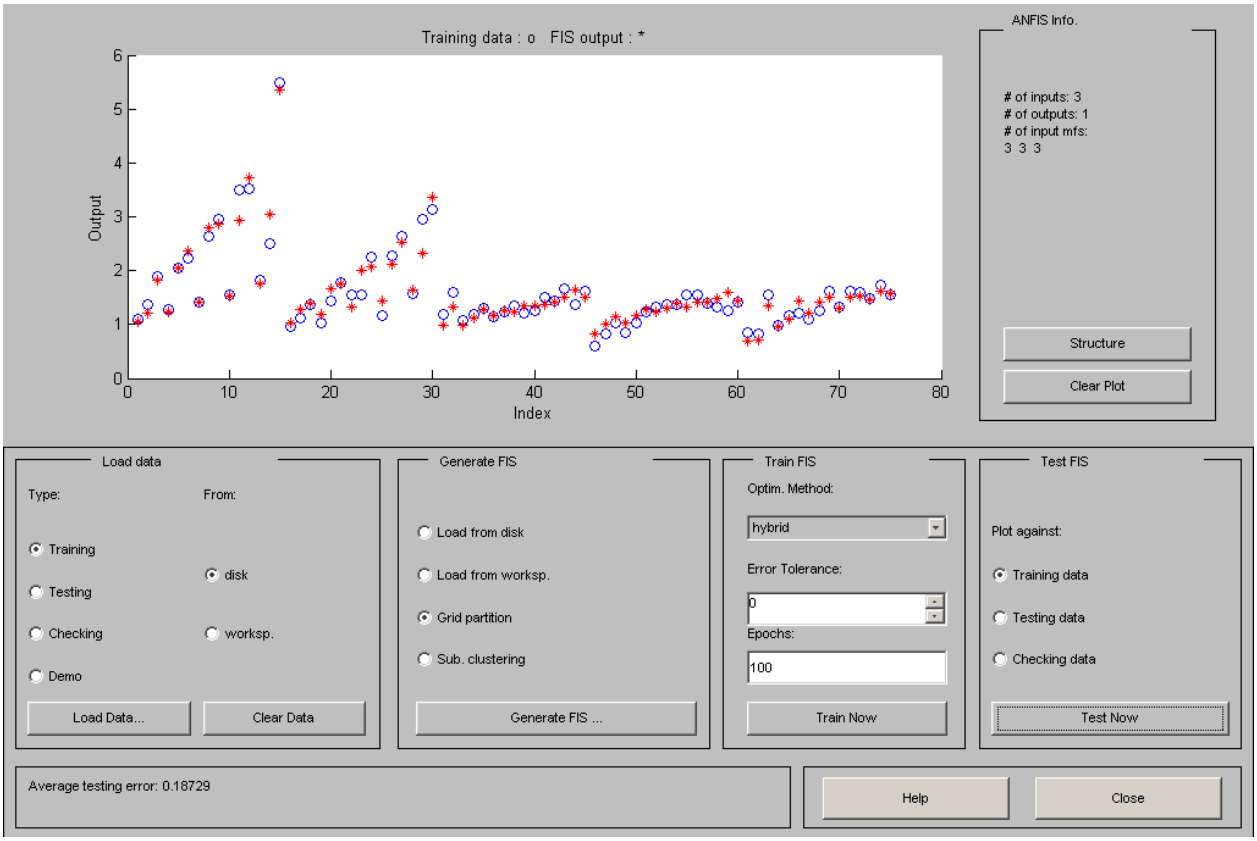

Figure 3.20 Measured Ra versus predicted Ra of the training data

7 - The fuzzy rule architecture of ANFIS when the gbellmf function is adopted consists of 27 fuzzy rules as shown in **Figure 3.21.** From this figure we can compute the value of Ra by put any values of speed, feed rate and depth of cut within the range of the training data.

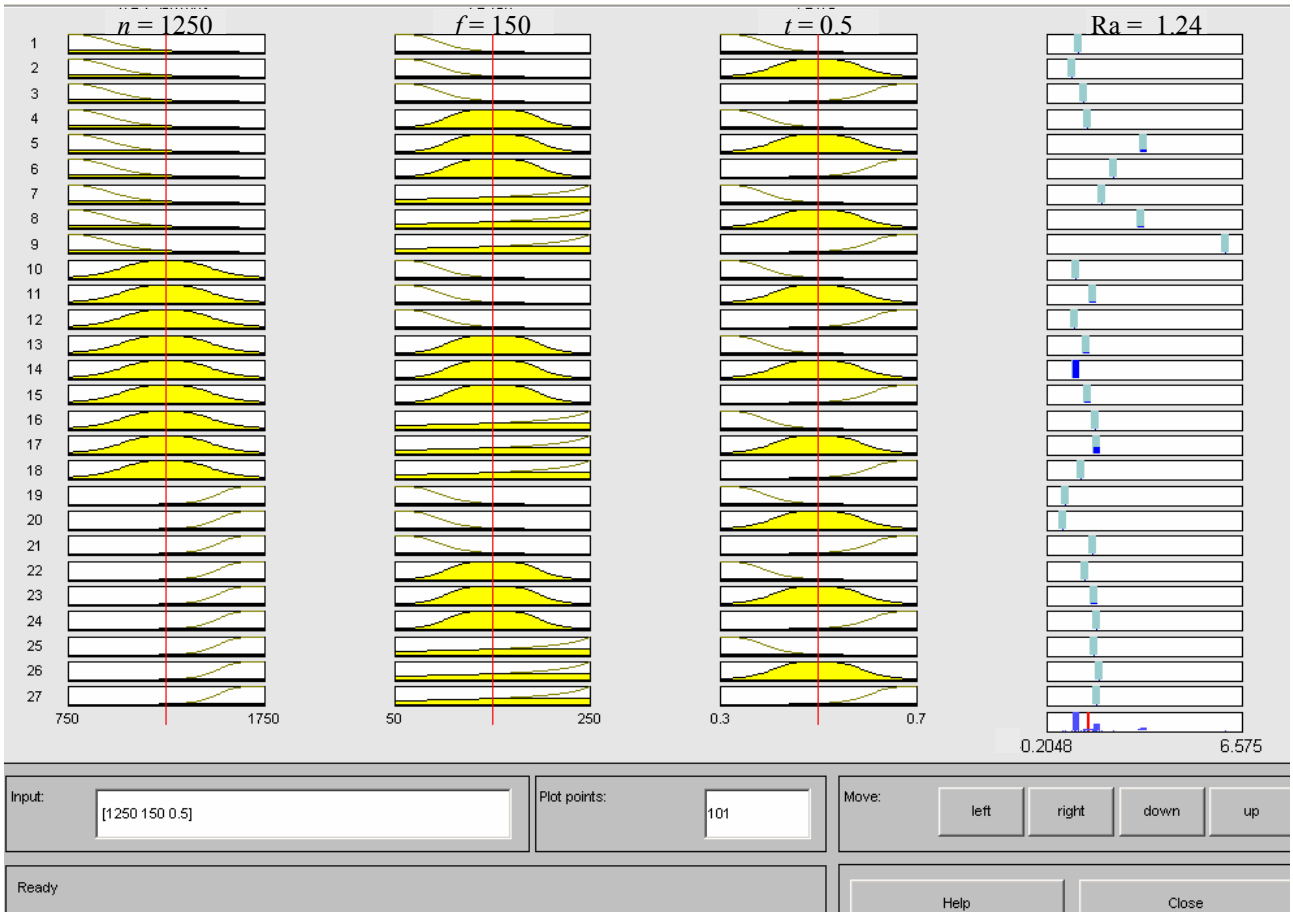

Figure 3.21 The rule viewer of fuzzy toolbox of Matlab program of modeling Ra.

3.4 Constraints of the ANFIS

ANFIS is much more complex than the fuzzy inference systems, and is not available for all of the fuzzy inference system options. Specifically, ANFIS only supports Sugeno-type systems, and these must have the following properties **[43]**.

- First or zero order Sugeno-type systems.
- Single output, obtained using weighted average de-fuzzification. All output membership functions must be the same type and either is linear or constant.
- No rule sharing. Different rules cannot share the same output membership function, namely the number of output membership functions must be equal to the number of rules.
- Have unit weight for each rule.

3.5 ANFIS model verification

The relationships between the cutting parameters in end milling and the produced surface roughness as obtained by ANFIS can be verified by the use of the cutting force signals induced during end milling process. The latter have long been used; in metal machining practice; as a technique for on-line assessment of the surface roughness. Therefore, a parallel line of research is adopted in the present study, by the measurement of cutting force components At the same cutting parameters used in the training and construction of the above ANFIS model.

CHAPTER FOUR

EXPERIMENTAL WORK

The experiments were performed using ProLight2000 CNC end milling machine, **Figure 4.1**. A high-speed steel four-flute end milling cutter with a diameter of (7/16 inch)11 mm was used for machining blocks of Brass (60/40) under specific machining conditions (Speed *n*, feed rate *f* and depth of cut *t*).

Figure 4.1 ProLight2000 CNC end milling machine.

4.1 Measurements of surface roughness

The surface roughness Ra was measured by a stylus-based profile-meter (Surtronic 3+, accuracy of 99%) as shown in **Figure 4.2**. The direction of measurement of the surface roughness is perpendicular to the direction of the lay. The measurement length of each specimen equals to 12.5 mm divided into five cuts; of length; 2.5 mm each.

Figure 4.2 Stylus-based profilometer.

4.2 The analysis and measurement of the forces in end milling

Direct measurement of forces *Ft* and *Fr* is difficult because they are oscillating rapidly during the cutting; and a suitable dynamometer can be recording the average force in the feed direction and the normal direction **[44]**.

Total forces acting on the cutter: Assuming that three teeth are in engagement with the work piece as shown in **Figure 4.3**. This figure illustrates these conditions and shows how the forces acting may be resolved to give the magnitude of the reactions of the cutter on the work piece **[44]**.

The feed force $(Fx) = fx_1 + fx_2 + fx_3$

The normal force $(Fy) = fy_1 + fy_2 + fy_3$

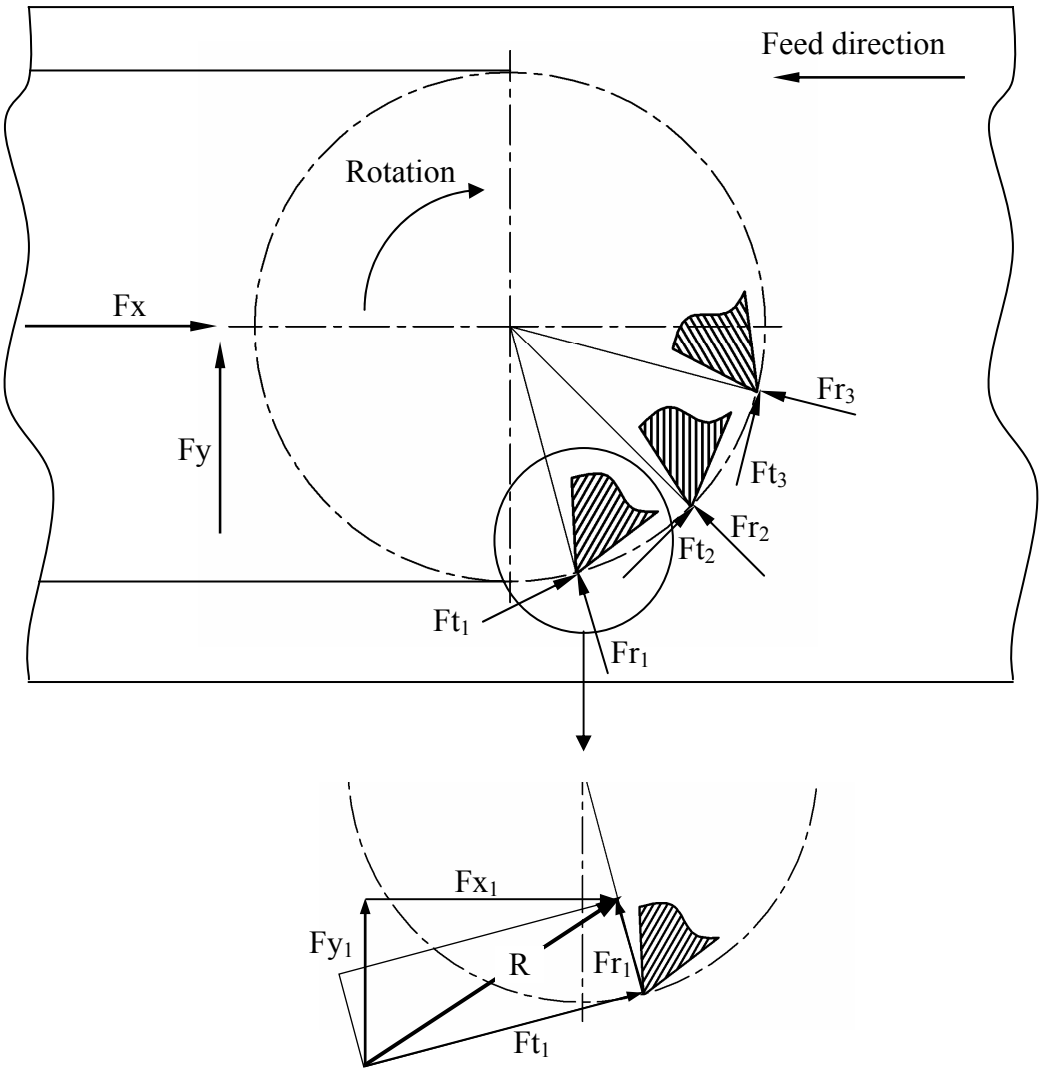

Figure 4.3 Forces acting on cutter tooth

4.3 Milling dynamometer

In this study, a Strain Gage based, two components, computer linked dynamometer was designed and manufactured to measure force components in end milling. The dynamometer can be used in static force measurements and also in dynamic force measurements in the two directions.

Strain gages were bonded on the circular rings for sensing of the force signals. The analogue force signals obtained from two-channels have been amplified and converted into digital signals via a data acquisition card and recorded via a computer. Although the dynamometer was developed primarily for milling operations, it can be used to measure forces during most of machining operations i.e. turning, grinding, drilling, etc.

Machining tests were performed at different cutting parameters and the results showed that the dynamometer could be used reliably to measure forces. The designed and constructed dynamometer is capable of measuring feed force (*Fx*) and normal force (*Fy*).

This dynamometer consists of four elastic circular rings on which strain gauges were mounted and necessary connections were made to form measuring bridges, as shown in **Figures 4.4** and **4.5**. These rings are fixed and held between two metal plates.

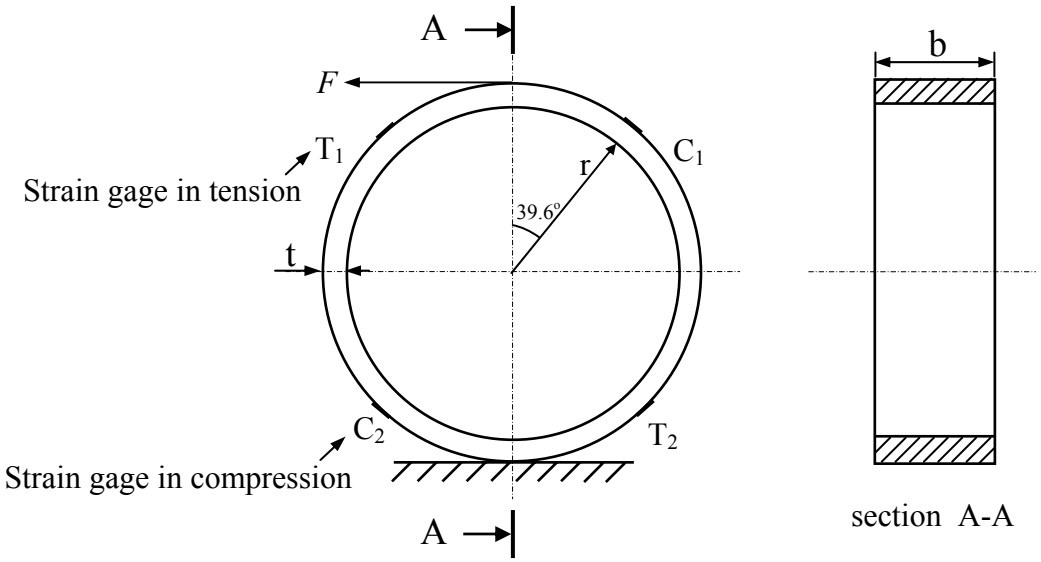

Figure 4.4 Loading conditions

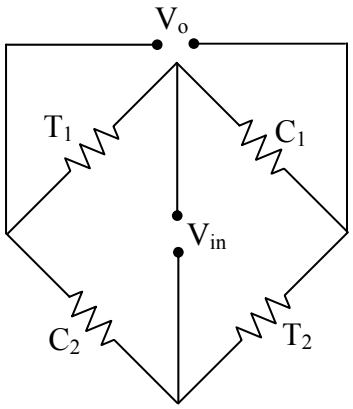

Figure 4.5 Strain gages configurations on sensing element

4.3.1 Dynamometer design and construction

In dynamometer design, factors such as sensitivity, rigidity, elasticity, accuracy and easy calibration should be taken into account. In addition, selection of rings material is also important as manufacturing of them could cause problems. In this study, all these factors were taken into consideration. Initially, design principles of the dynamometer were verified and then the construction was made according to the ring theory **[45-48]**. Four circular rings manufactured in workshop were placed between two plates and fixed with screws. The plates are used to house, position and increase the rigidity of the circular rings. Strain gauges were mounted on the circular rings. Normal and feed force components can be measured simultaneously during machining with the aid of 8 strain gauges mounted on the circular rings. The angle where the strain is being zero in case of radial loading and maximum in case of tangential loading has been calculated equal to 39.6 deg. for circular ring **[49]** and verified by finite element simulation as shown in **Figure 4.6**.

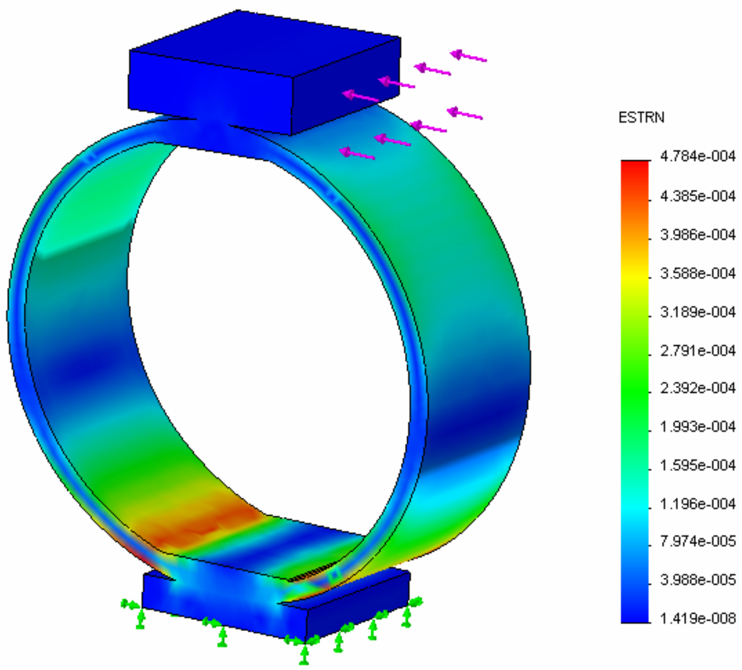

Figure 4.6 Strain distributions using finite element simulation

The maximum normal force during end milling process of the type shown in **Figure 4.7** and **4.8** can be calculated from the empirical **Equation (4.1)**, at minimum speed (750 rpm), maximum feed (250 mm/min) and maximum depth of cut (0.7 mm). The constants C, x and y have been provided by Prikryl and Musilkova **[6]**.

$$F_{max} = C.\ t^{y}.\ f^{x}.\ \Sigma \sin^{x}(\psi_i) \qquad (4.1)$$

Where: $f = 4$ *mm/sec* $= 250$ *mm/min* $= 0.333$ *mm/rev, at 750 rpm*

$t = 0.7$ *mm*

$C = 67,$ $x = 0.79,$ $y = 0.66,$

$\psi_0 = 360/z = 90^o$

$\psi_1 = 45^o$, $\psi_2 = \psi_0 + \psi_1$, $\psi_3 = \psi_0 + 2\psi_1$ etc.

$\Sigma sin^x(\psi_i) = 1.521457$

Where: ψ = helix angel, z = number of tooth, and C, x ,y = constants

$$F_{max} = 67 \times (0.7)^{0.66} \times (0.333)^{0.79} \times 1.521457 = 33\ kg = 330\ N$$

The thickness t, radius r, and width of the circular strain ring b are the three basic controllable parameters that affect the rigidity and sensitivity. Since there is no effect of ring width b and modulus of elasticity (E) on the strain per unit deflection **[48]**; b can be taken as 20mm to set up the rings securely.

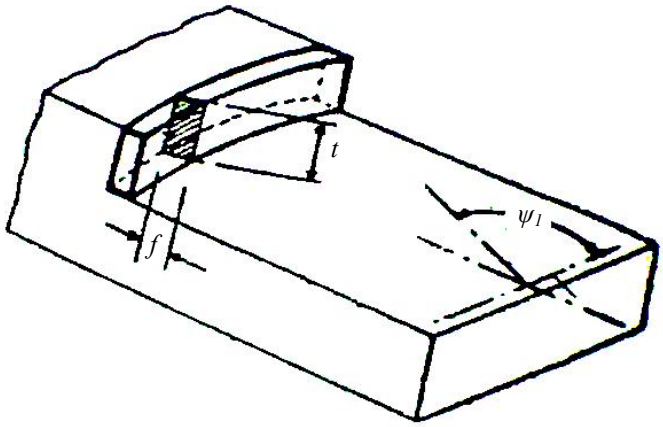

Figure 4.7 Area of cut during face milling process

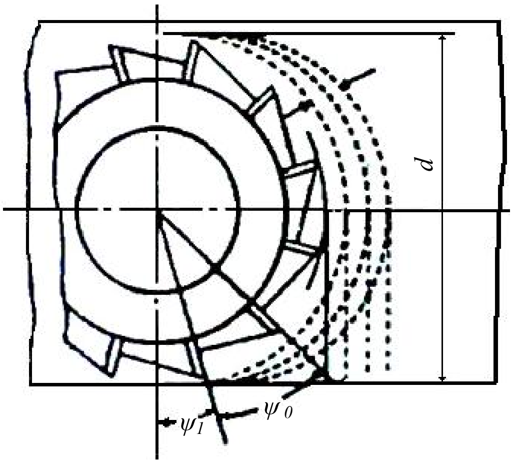

Figure 4.8 The multiple tooth action in face milling process

Normal force should be considered for the purpose of the ring design for maximization of sensitivity (e_z/F_z) and stiffness (F_z/δ_z). The strain gauges should be placed where the stress concentration has maximum value. The strain per unit deflection can be expressed as in **Equation (4.2) [45-48]**.

$$\frac{e_z}{\delta_z / r} = \frac{1.09\,t}{1.8\,r} = 0.61\,\frac{t}{r} \qquad \text{(4.2)}$$

Where δ_z is the deflection in a radial direction and e_z is the strain due to thrust force (F_z). It is clear that for maximum sensitivity and rigidity e_z/δ_z should be as large as possible. This requires that r should be as small as possible and t as large as possible. But small r brings some difficulties in mounting the internal strain gauges accurately. Therefore, for a given size of r and b, t should be large enough to be consistent with the desired sensitivity.

The octagonal ring is substantially stiffer than the circular ring when t/r less than or equals to 0.05, the difference in displacement of circular ring and octagonal

ring is <10% if t/r greater than or equals 0.25 **[47]**. In order to be consistent with this expression, the ring thickness and ring radius were taken as 2mm and 22mm, respectively. Thus, the rate of t/r (2/22= 0.1) provides corresponding sensitivity to stiffness ratio e/(δ/r) for the circular ring. A dynamometer essentially consists of a ring element or a measuring set-up containing a ring element.

As the ring element is an important part of a dynamometer, the following factors should be taken into account when selecting the ring materials:

– Rigidity,

– High natural frequency,

– High heat conductivity,

– Deformation under the load should conform to that of strain gauges.

In this study, steel 30, which meets the above requirements, was selected as the ring material. Some of the physical and mechanical properties of this material as follow:

Yield strength = 300 N/mm^2

Modulus of elasticity = 210000 N/mm^2

Carbon content = 0.30%

By using the above values, elastic strains e_z and e_y due to forces F_z and F_y are calculated according to ring theory by using the following equations as follows:

$$e_z = \pm \frac{1.09\,F_z r}{Ebt^2} = \frac{1.09 \times 82.5 \times 22}{210000 \times 20 \times 2^2} = 1.177 \times 10^{-4} \quad \text{……(4.3)}$$

$$e_y = \pm \frac{2.18\,F_y r}{Ebt^2} = \frac{2.18 \times 82.5 \times 22}{210000 \times 20 \times 2^2} = 2.355 \times 10^{-4} \quad \text{……(4.4)}$$

Similarly, the stresses occurring on the rings can be calculated by placing e_z and e_y values in **Equations (4.3)** and **(4.4)** as follows:

$$\sigma_y = Ee_y = 210000 \times 2.355 \times 10^{-4} = 50\ N/mm^2 \quad \ldots\ldots\ldots\ldots\ldots\ldots\ldots\ldots\ldots\ldots\ldots\ldots (4.5)$$

$$\sigma_z = Ee_z = 210000 \times 1.177 \times 10^{-4} = 25\ N/mm^2 \quad \ldots\ldots\ldots\ldots\ldots\ldots\ldots\ldots\ldots\ldots\ldots\ldots (4.6)$$

As steel 30 was used for manufacturing the ring and its yield strength is 300 N/mm^2, the calculated stress values occurring on the rings are within safety limits for this material. **Figures 4.9, 4.10** show the final design and assembly drawing of the milling dynamometer.

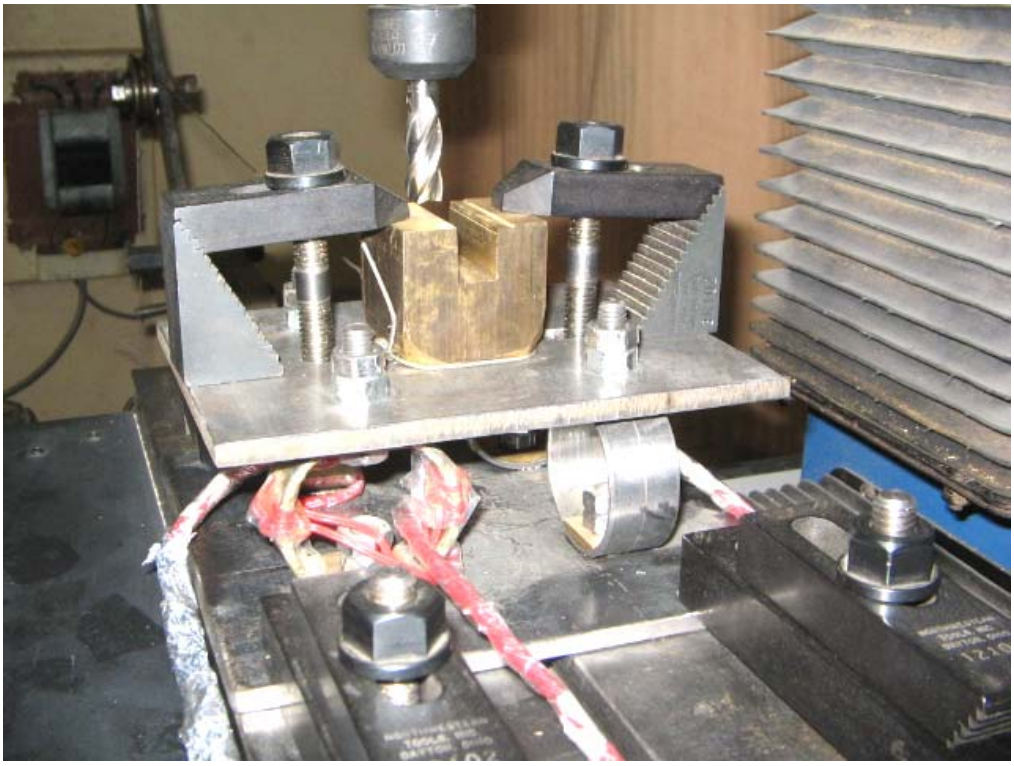

Figure 4.9 The end milling dynamometer

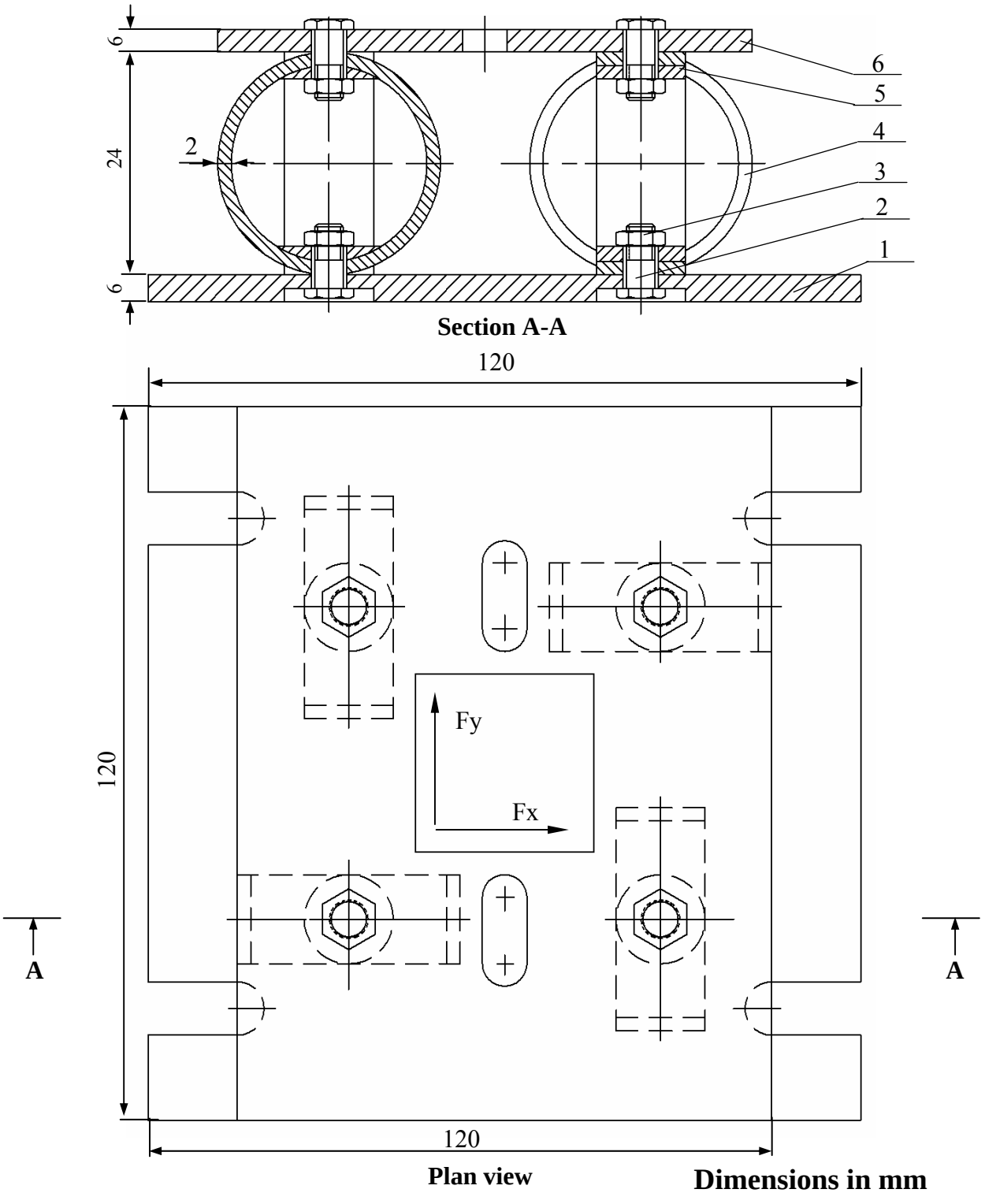

Figure 4.10 Assembly drawing of the milling dynamometer.

Table 4.1 parts list of the milling dynamometer.

6	1	Top plate	Steel
5	8	Seat	Brass
4	4	Circular ring	Steel
3	8	Nut	Steel
2	8	Bolt	Steel
1	1	Base plate	Steel
No.	No. Off	Description & Specifications	Material

4.3.2 Strain gages

The strain gage terminals were connected in a full Wheatstone bridge form as shown in **Figures 4.4** and **4.5**. Thus the voltage gain from each strain gage is multiplied four times to give the result bridge gain.

Temperature compensation, strain gage size, insulation, cleaning agent, Strain gage cement, cables, and protective agent were subjected to the following conditions:

1- The self-temperature-compensation gage was developed as the method of compensating temperature with a single gage. With the self-temperature-compensation gage, the temperature coefficient of resistance of the sensing element is controlled based on the linear expansion coefficient of the measuring object. Thus, the gage enables strain measurement without receiving any thermal effect if it is matched with the measuring object.

2- Strain gage with measuring grid length of 2 mm is suitable for the measurement of dynamic strain.

3- The effect of the insulation resistance has a lesser effect with low resistance strain gages. Therefore, strain gage type (KFG-2N-120-C1-11L1M2R) of the following technical data, were used, **Table 4.2.**

Table 4.2 Strain gage specifications

Temperature compensation for	Steel
Gage length	2 mm
Gage resistance (24°C,50%RH)	119.6 ± 0.4 Ω
Gage factor(24°C,50%RH)	2.11 ± 1.0 %
Adoptable thermal expansion	11.7 PPM/ °C
Transverse sensitivity(24°C,50%RH)	2.00 %
Application gage cement	CC-33A, EP-34

4- The measuring points were first cleaned using organic solvent (Acetone)

5- Adhesive material type is Cyano-Acrylate Base, which a cold adhesive was used. This type of adhesive gives good characteristics when used with the type selected above, such as, low hysteretic, high fatigue limit etc.

6- The connecting wires must be as short as possible and have a low resistance value.

7- Humidity, temperature, and other environmental factors affect the measurement point reliability. It is of great importance to cover the measurement point with a protective cover.

4.3.3 Dynamic properties of the dynamometer

The rigidity criterion is the natural frequency of the dynamometer. All machine tools are subjected to self excited and forced vibrations. In order that the measured force data not be influenced forces by any vibrating motion of the dynamometer during cutting. A dynamometer's natural frequency should be as high as possible. Vibration frequency of the machine tool to which the dynamometer is mounted for normal force measurement should conform to the natural frequency of the dynamometer. Vibration frequency of the machine tool is related to the spindle

speed of the machine tool. The dynamometer should have natural frequency of at least four times the frequency of the machine tool **[46-48]**. The machine tool's vibration frequency is obtained from the relation:

$f_m = n/60$ *rev./s.* ……(4.7)

Therefore, the dynamometer natural frequency should be given by:

$f_d \geq 4 \times n/60.$

If the dynamometer is considered a small mass supported by ring elements for analysis purposes, its natural frequency depending on the dynamometer mass and ring constant is then obtained from the relation **[46-48]**:

$$f_d = \frac{1}{2\pi}\sqrt{K/m} \quad \text{……(4.8)}$$

Where

K = dynamometer ring constant (N/mm),

m = dynamometer mass (kg),

f_d = dynamometer natural frequency (rev./s).

In order to determine the natural frequency of the dynamometer, the ring constant of the dynamometer should be determined first. Dynamometer ring constant (rigidity) is given by the following equation **[46-48]**:

$$K_z = \frac{F_z}{\delta_z} = \frac{Ebt^3}{1.8r^3} N/mm \quad \text{……(4.9)}$$

Where

F_z : Force applied to the dynamometer vertically (N)

δ_z : Deflection due to the radial force

E: Dynamometer's modulus of elasticity (N/mm^2)

t: Thickness of the circular ring (mm)

b: Width of the circular ring (mm)

r: Inner radius of the circular ring (mm)

$$K_z = \frac{Ebt^3}{1.8r^3} = \frac{210000 \times 20 \times 2^3}{1.8 \times 22^3} = 1753\ N/mm$$

$$f_d = \frac{1}{2\pi}\sqrt{\frac{1753 \times 1000}{3.5}} = 708\ rev./s.$$

If the maximum spindle speed of the machine tool is taken as 2000 rpm, then f_m:

$$f_m = n/60 = 1750/60 = 29\ rev./s.$$

It is found that 708 rev/s > 4×29. Therefore, the above requirement is fulfilled.
The radial force component is maximum 50 N and the rigidity of the dynamometer (K_z) is 1753 N/mm then maximum strain in z direction is given by:

$$K_z = F_z / \delta_z \quad \ldots\ldots\ldots\ldots\ldots\ldots\ldots\ldots\ldots\ldots\ldots\ldots\ldots\ldots\ldots\ldots\ldots\ldots\ldots\ldots\ldots\ldots\ldots (4.10)$$

$$\delta_z = F_z / K_z = 50/1753 = 0.028\ mm$$

The strain gauges used have 2% elongation limit on a 2 mm length. According to this value, 2×2% = 0.04 mm and as the maximum force 50 N results in elongation of 0.028 mm of the strain gauge and therefore 0.028 mm is lower than 0.04 mm elongation.

4.4 Data acquisition system

In order to read and store the feed and normal forces data automatically on a computer during metal cutting, a data acquisition system with the necessary hardware and software was also devised and connected to the developed dynamometer. For this purpose;

1 - The operational amplifier (OPAMP) was used to enlarge the electric signal of the strain gages and converts this signal from 0 to 5 volts according to value of deflection. The amplifier specifications as in **Appendix A**

2 - An analog-to-digital converter (ADC) was used to convert analogue data from instrumentation amplifier circuit to digital data to be interfaced with the computer. The ADC specifications as in **Appendix B**

3 - A personal computer was used to read and store the data coming from the ADC.

Feed and normal forces signals were captured and processed using a personal computer through OPAMP and ADC card. The stored feed and normal forces data can be retrieved and used for analysis purposes when required **[50 and 51]**.

4.5 Test rig components

The test rig components are shown in **Figure 4.11**. It consists of the dynamometer connected to an amplifier with power supply followed by A/D board and then personal computer.

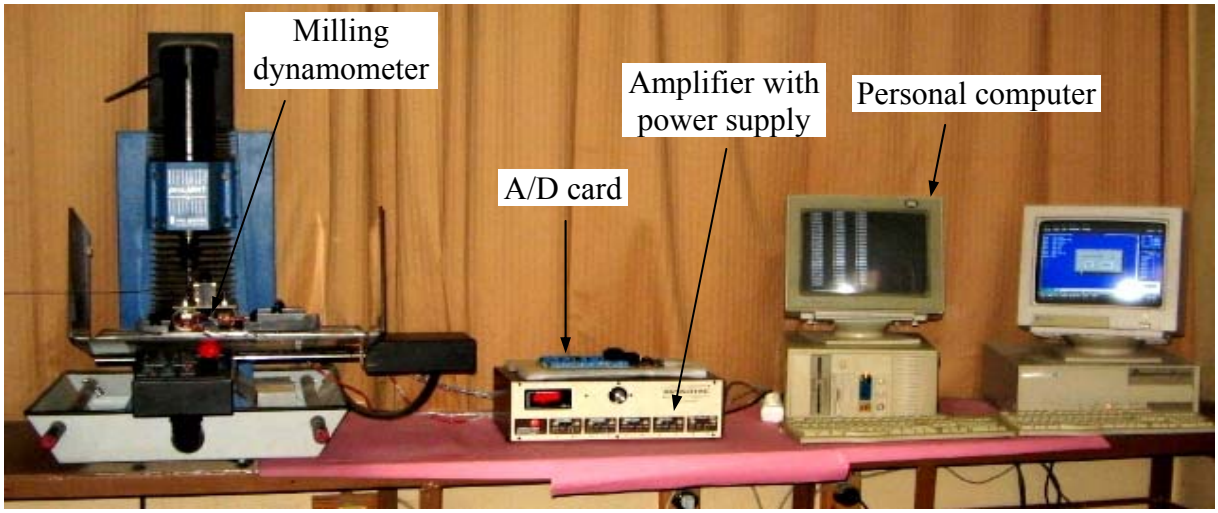

Figure 4.11 The experimental setup

4.6 Calibration test

The aim is to determine the elastic deflection of the ring components and consequently the output voltage under the applied load, and the cross sensitivity between the forces in x and y directions.

For the calibration, initially the load ring was positioned horizontally between the dynamometer and the milling machine and then loads of 10 N were applied up to 330 N (calibrated by digital meter), as shown in **Figure 4.12**. Similarly, after the application of each load the strain was recorded. For each direction, a calibration curve was obtained to convert the output readings into normal force values. **Figures 4.13** and **4.14** show calibration curves for the x and y forces respectively. All measurements were repeated three times to verify consistency and very close values were obtained**.**

Additionally, the effect of loading in one direction on the other force components was also examined and minor fluctuations were observed. Therefore, the effect of loading in one direction on the other force components can be ignored.

Using the regression analysis (Microsoft excel statistical software), the relation between the applied load in x-direction and output volt is found to be:

$$F_x = 1.5 + 0.65V_x \quad \text{………………………………………………………………(4.11)}$$

V_x = output volt in feed direction (mv)

Similarly, the relation between the applied load in y direction and output volt were obtained.

$$F_y = 4 + 0.5\ V_y \quad \text{…………………………………………………………………(4.12)}$$

V_y = output volt in normal direction (mv)

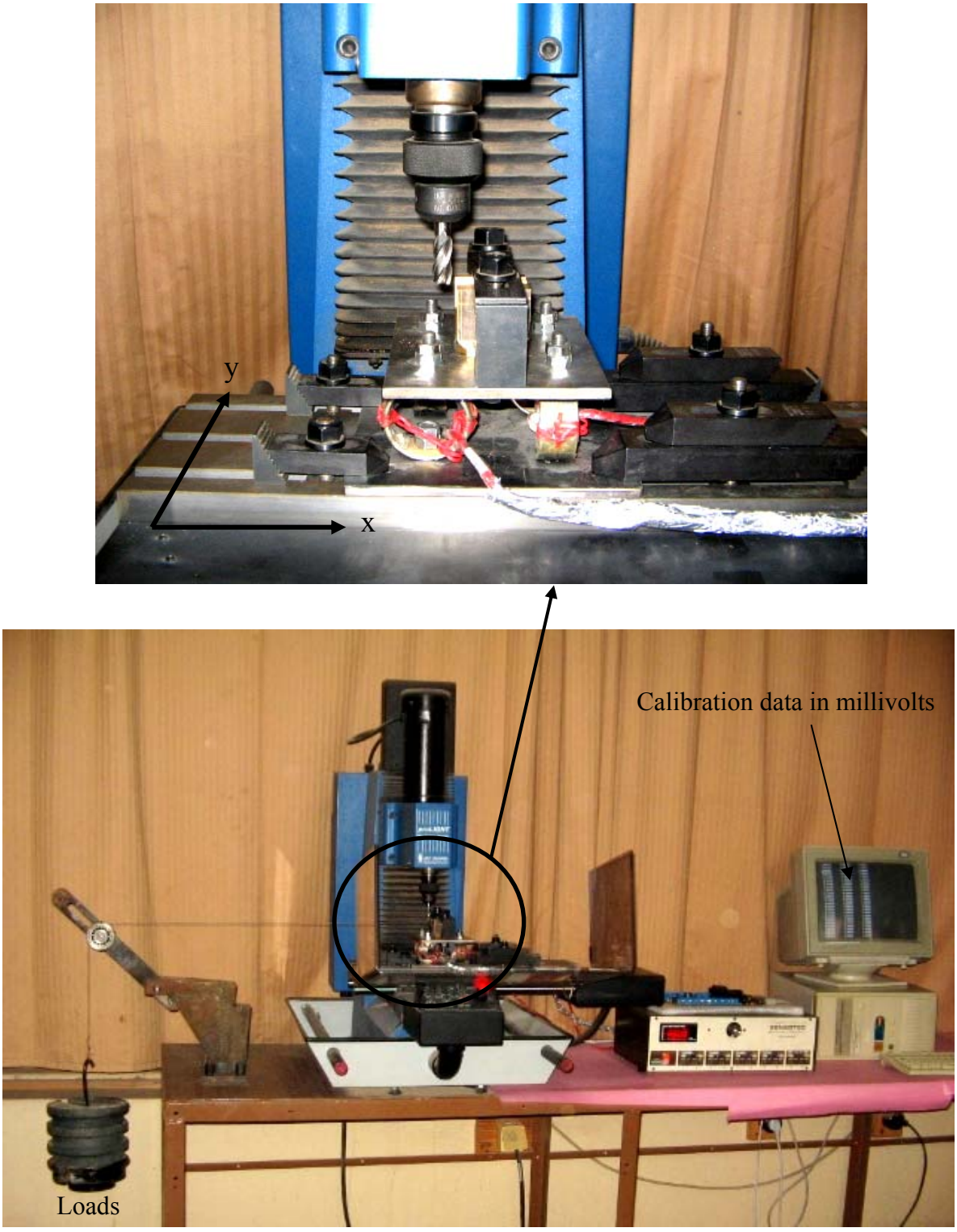

Figure 4.12 The calibration setup

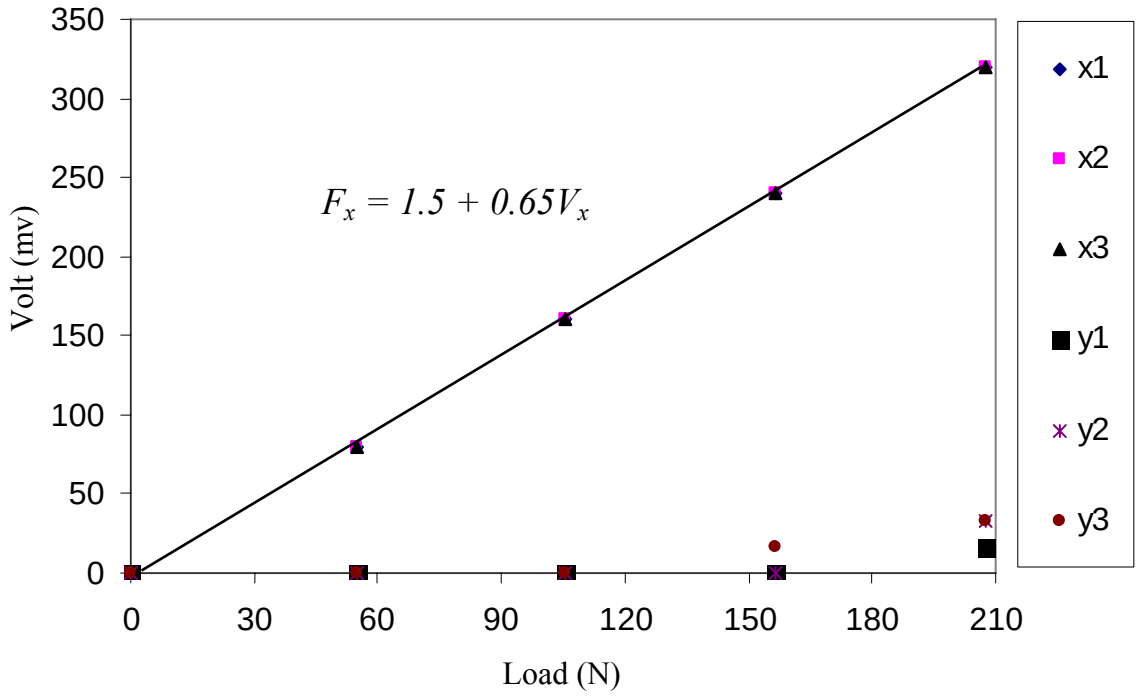

Figure 4.13 Calibration curve in x-direction

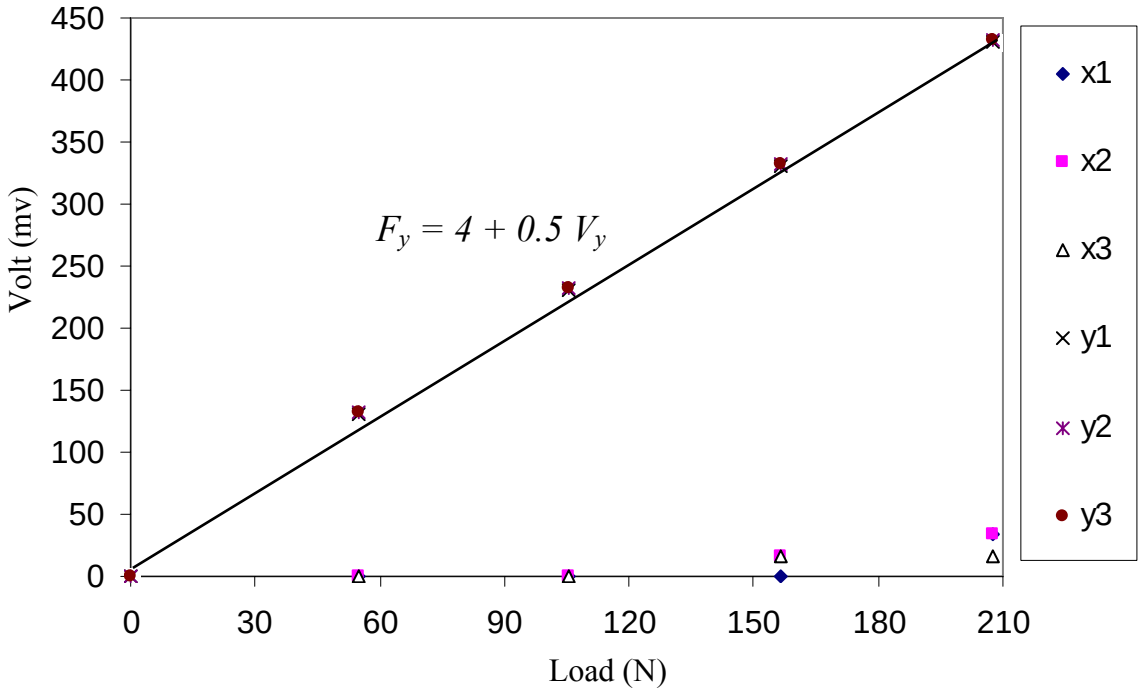

Figure 4.14 Calibration curve in y-direction

Table 4.3 Statistical analysis of load dynamometer output relationships in x-direction.

Regression Statistics	
Multiple R	0.999
R Square	0.998
Adjusted R Square	0.997
Standard Error	6.004
Observations	7

ANOVA					
	Df	SS	MS	F	Significance F
Regression	1	72894.99	72894.99	2021.864	1.027E-07
Residual	5	180.267	36.053		
Total	6	73075.257			

	Coefficients	Standard Error	t Stat	P-value	Lower 95%	Upper 95%
Intercept	1.5	4.040	1.321	0.244	-5.05	15.722
X Variable 1	0.65	0.014	44.965	1.027E-07	0.589	0.661

Table 4.4 Statistical analysis of load dynamometer output relationships in y-direction.

Regression Statistics	
Multiple R	0.999
R Square	0.996
Adjusted R Square	0.995
Standard Error	7.562
Observations	7

ANOVA					
	Df	SS	MS	F	Significance F
Regression	1	72789.355	72789.355	1272.977	3.255E-07
Residual	5	285.902	57.18		
Total	6	73075.257			

	Coefficients	Standard Error	t Stat	P-value	Lower 95%	Upper 95%
Intercept	4	5.4278	-1.656	0.159	-22.943	4.962
X Variable 1	0.5	0.014	35.679	3.255E-07	0.4718	0.545

Figures 4.13 and 4.14 and Tables 4.3 and 4.4 giving the statistical analysis of the obtained relations for all output, it can be seen that, linear relations between loads in the two directions and its output voltage exist.

CHAPTER FIVE

SURFACE ROUGHNESS PREDICTION USING ANFIS MODEL BASED ON FEED AND NORMAL FORCES

5.1 Introduction

This chapter is focused on studying the prediction of surface roughness using the feed and normal force components at the same machining parameters as input; and the surface roughness (Ra) as output.

The dynamometer was used to measure the force in the feed direction and normal direction. Seventy five readings were used as training data set as shown in **Tables 5.1** and thirty two readings were used as testing data set as listed in **Table 5.2**.

5.2 ANFIS prediction model

Different membership functions were used for training ANFIS to predict surface roughness. During the training the 75 Ra values (training data sets) were used to conduct 300 cycles of learning with average error as shown in **Figure 5.1-5.6**.

Table 5.1 Measured feed force and normal force (training data set)

***n* rpm**		**750**		**1000**		**1250**		**1500**		**1750**	
f	***t***	**F_x**	**F_y**	**F_x**	**F_y**	**F_x**	**F_y**	**F_x**	**F_y**	**F_x**	**F_y**
50	**0.3**	16	20	8	13	8	7	8	8	4	6
	0.5	17	36	26	16	11	10	14	14	8	9
	0.7	31	40	28	25	16	16	19	20	9	9
100	**0.3**	21	26	13	11	9	6	5	14	14	15
	0.5	31	57	34	28	15	15	20	23	29	35
	0.7	73	78	45	44	17	19	25	32	65	34
150	**0.3**	21	23	15	15	14	12	14	15	18	26
	0.5	44	69	29	41	14	18	23	29	48	51
	0.7	92	67	56	55	23	23	35	39	79	48
200	**0.3**	21	22	13	13	16	16	21	14	14	37
	0.5	43	66	41	46	21	22	24	43	66	56
	0.7	129	66	72	73	27	33	27	50	79	68
250	**0.3**	21	67	13	19	19	17	23	27	20	53
	0.5	29	51	33	52	19	21	30	45	80	71
	0.7	183	54	76	75	27	27	34	36	83	69

Table 5.2 Measured feed force and normal force (testing data set)

***n* rpm**		**875**		**1125**		**1375**		**1625**	
F	***t***	**F_x**	**F_y**	**F_x**	**F_y**	**F_x**	**F_y**	**F_x**	**F_y**
75	**0.4**	18	40	14	17	13	16	14	22
	0.6	56	53	19	31	16	17	21	35
125	**0.4**	47	55	24	32	14	19	21	40
	0.6	49	77	43	51	20	26	43	50
175	**0.4**	51	63	26	40	14	17	18	39
	0.6	89	78	48	50	23	25	48	65
225	**0.4**	69	76	20	38	26	22	30	57
	0.6	81	78	44	44	23	32	66	75

- The triangular memberships function (trimf) gives a training average error equals 0.36108.

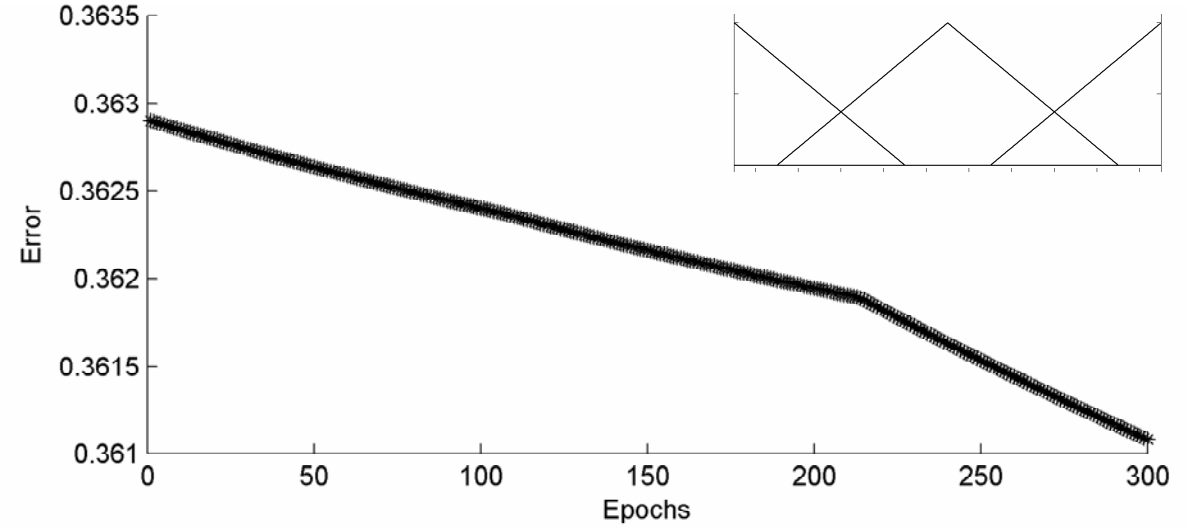

Figure 5.1 Training error curve of modeling Ra for trimf using 100 epochs.

- The trapezoidal memberships function (trapmf) gives a training average error equals 0.38564.

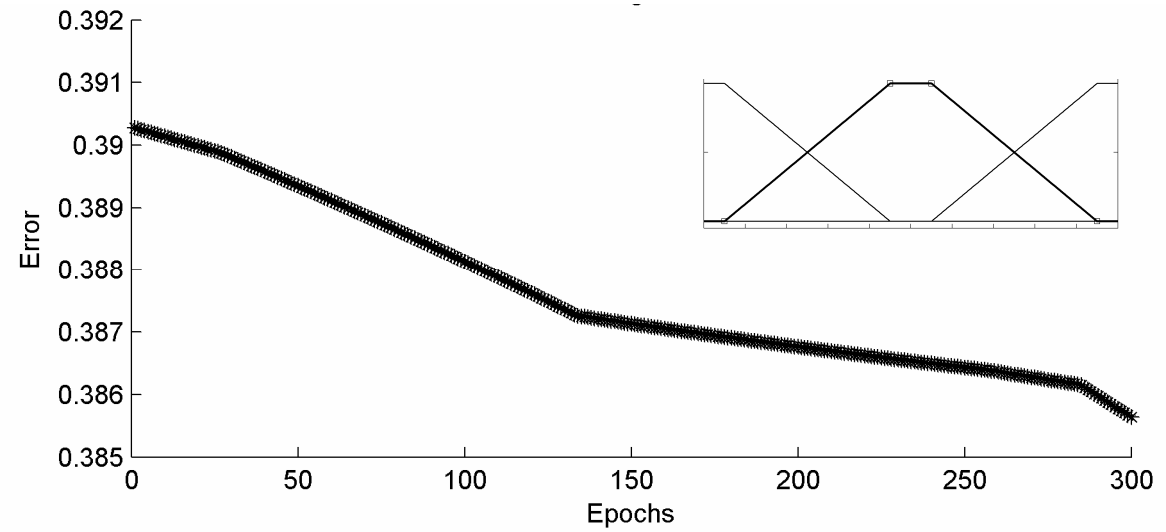

Figure 5.2 Training error curve of modeling Ra for trapmf using 100 epochs.

- The Generalized bell memberships function (gbellmf) gives a training average error equals 0.32874.

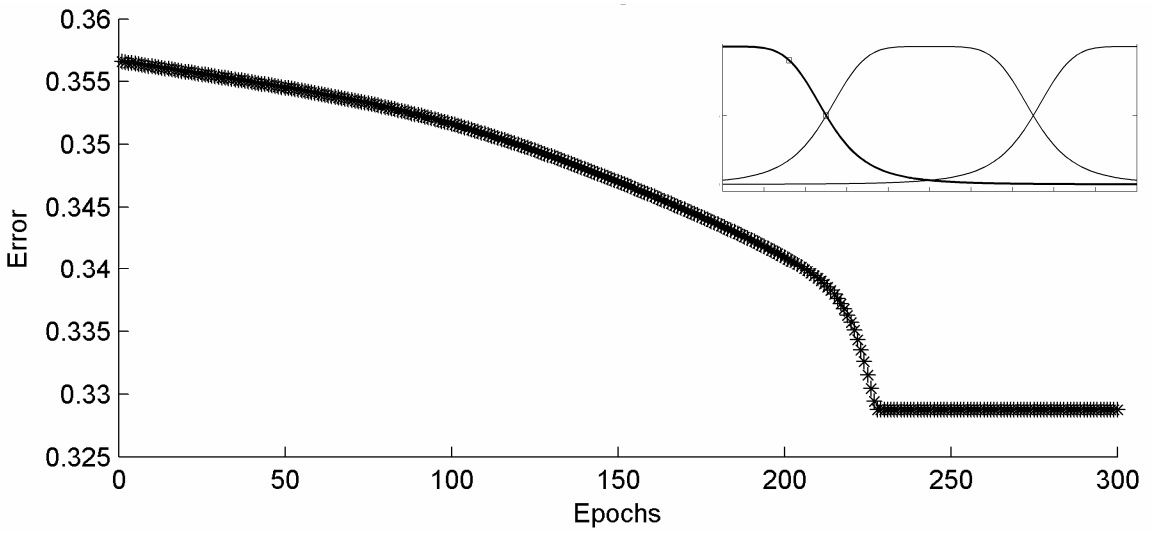

Figure 5.3 Training error curve of modeling Ra for gbellmf using 100 epochs.

- The Gaussian memberships function (gaussmf) gives a training average error equals 0.35982.

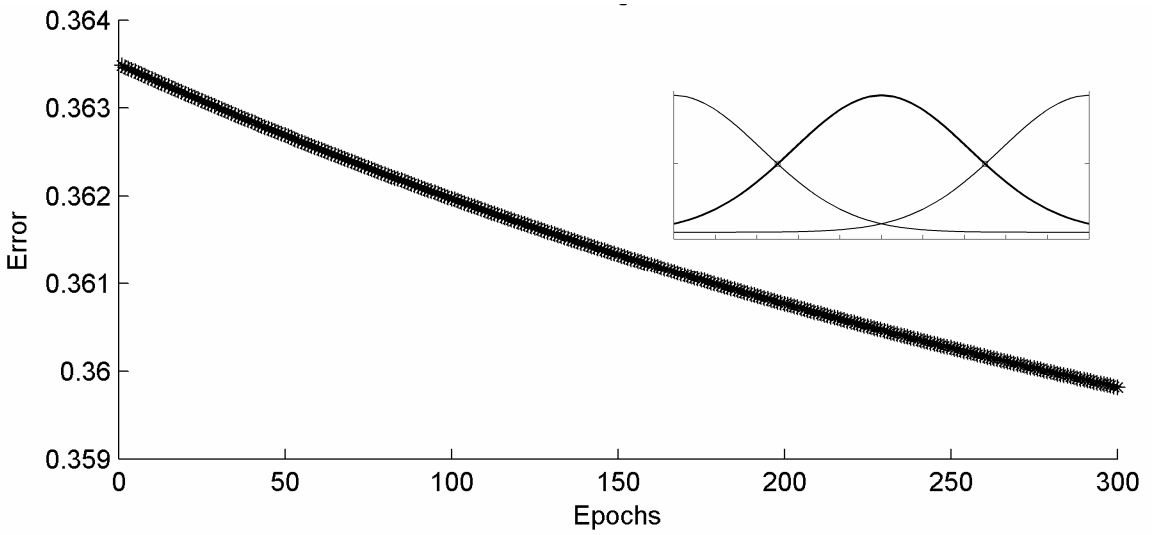

Figure 5.4 Training error curve of modeling Ra for gaussmf using 100 epochs.

- The Pi-shaped memberships function (pimf) gives a training average error equals 0.38689.

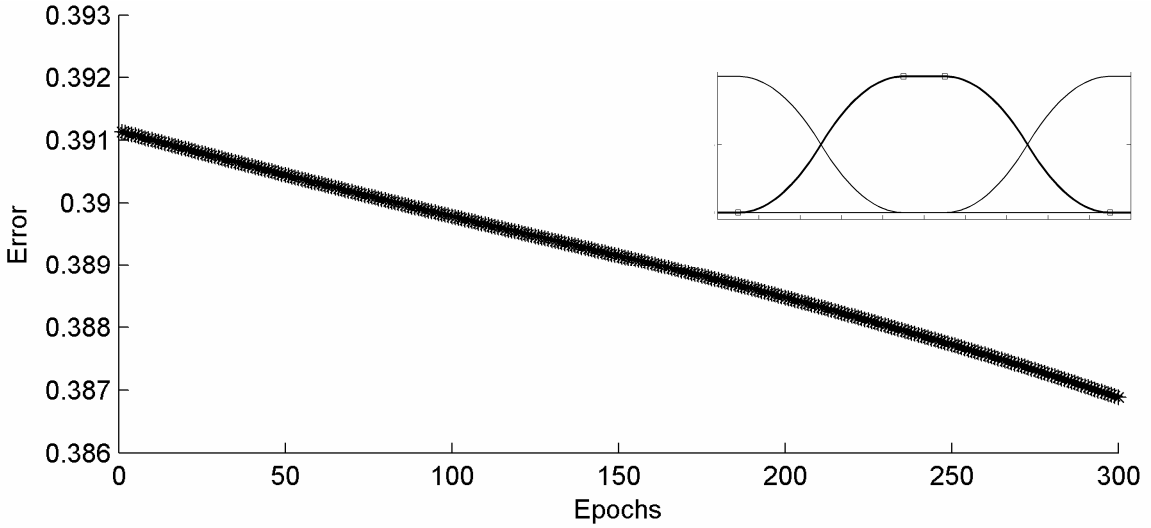

Figure 5.5 Training error curve of modeling Ra for pimf using 100 epochs.

- The difference between two sigmoidal memberships function (dsigmf) gives a training average error equals 0.34393.

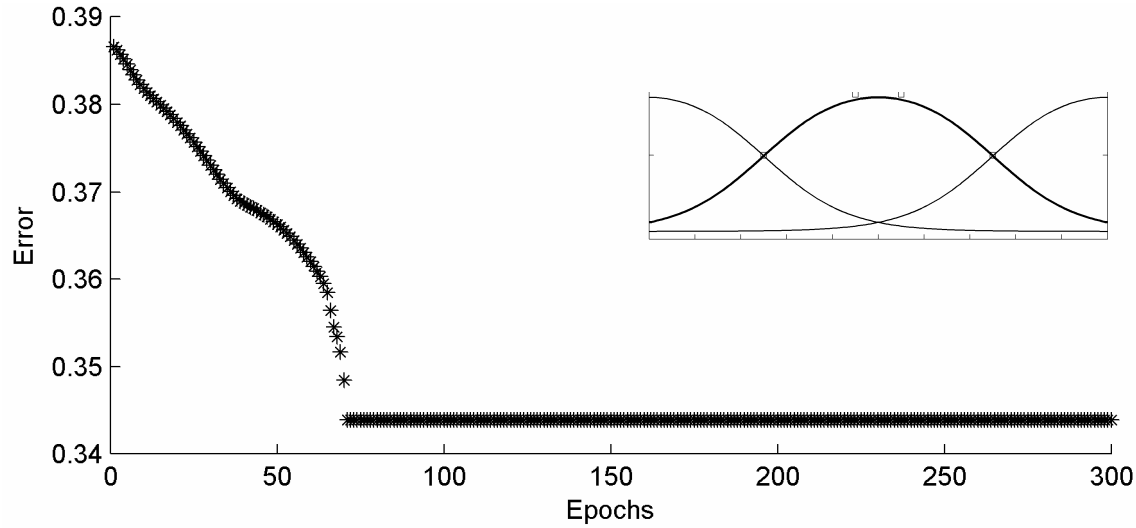

Figure 5.6 Training error curve of modeling Ra for dsigmf using 100 epochs.

It is shown that; the generalized bell memberships function (gbellmf) gives the lowest training error so it was adopted during the training process of ANFIS in this model. **Figure 5.7** shows the initial and final membership functions of the feed force. There is obviously a small change in the final membership function shape after training in the medium area, but very large change in the small and large areas. These changes indicate that the small and large values of feed force have great effect on surface roughness but the medium values have slightly effect on surface roughness.

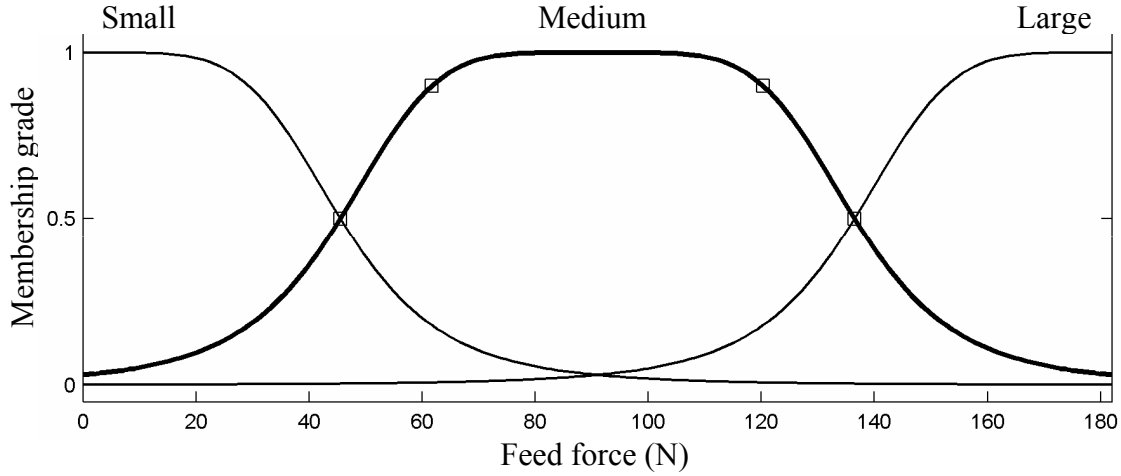

a) Initial membership functions

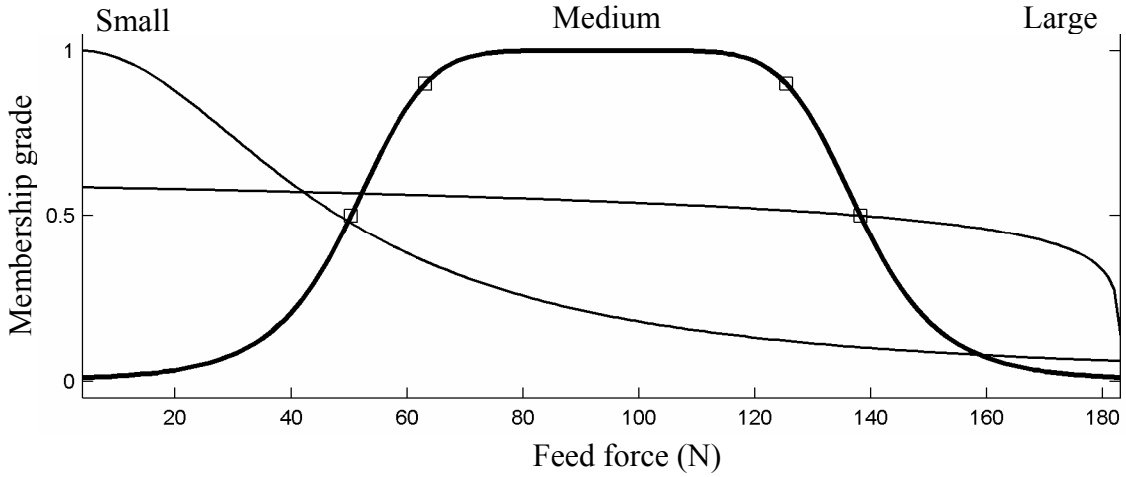

b) Final membership functions

Figure 5.7 Initial and final membership function of feed force.

Figure 5.8 shows the initial and final membership functions of the normal force. It is indicated that the final membership function after training experiences great variation in the small medium and large areas. These changes indicate that all the range of normal force has great effect on surface roughness.

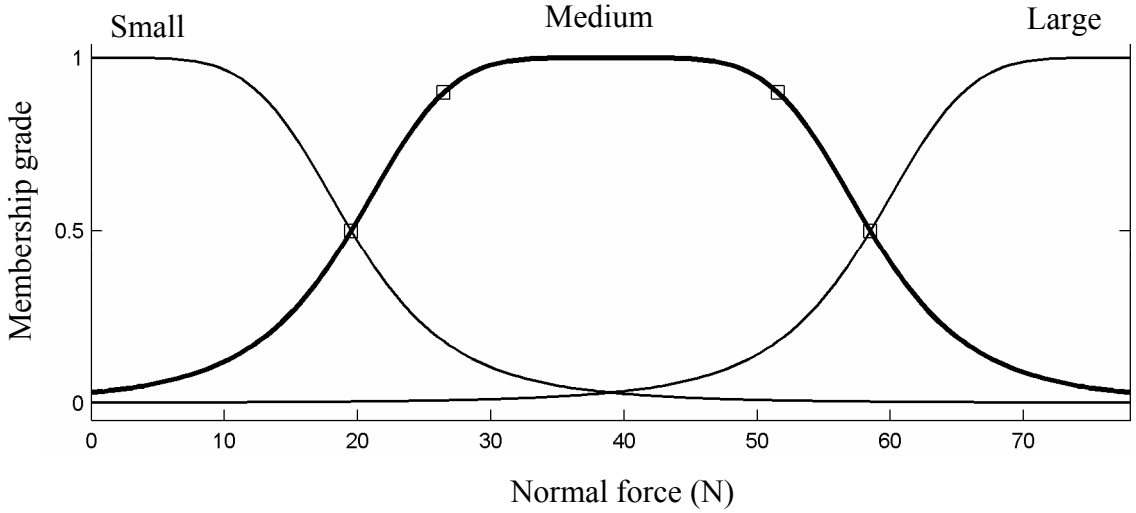

a) Initial membership functions

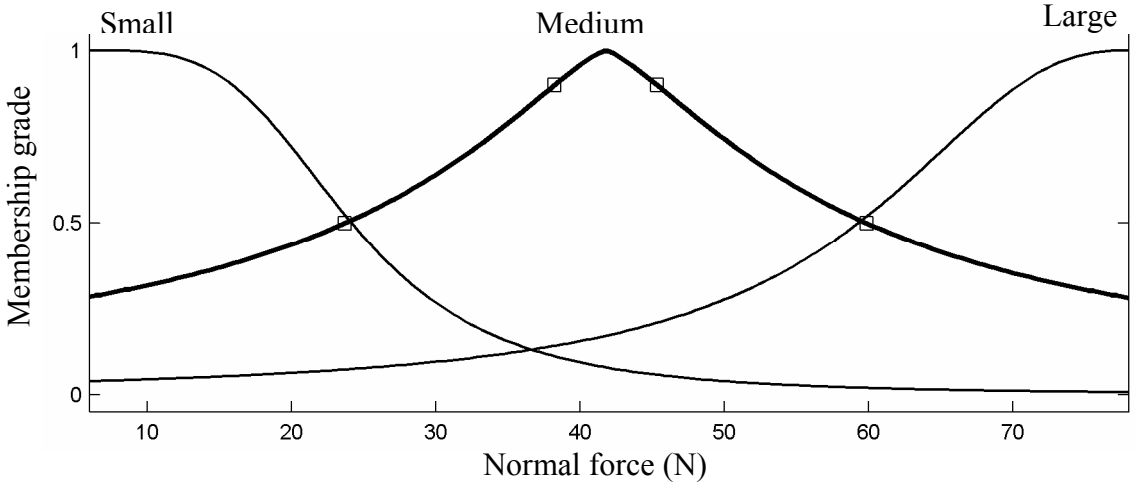

b) Final membership functions

Figure 5.8 Initial and final membership function of normal force.

The fuzzy rule architecture of ANFIS when the gbellmf function is adopted consists of 9 fuzzy rules as shown in **Figure 5.9.** From this figure we can compute the value of Ra by put any values of feed force and normal force within the range of the training data.

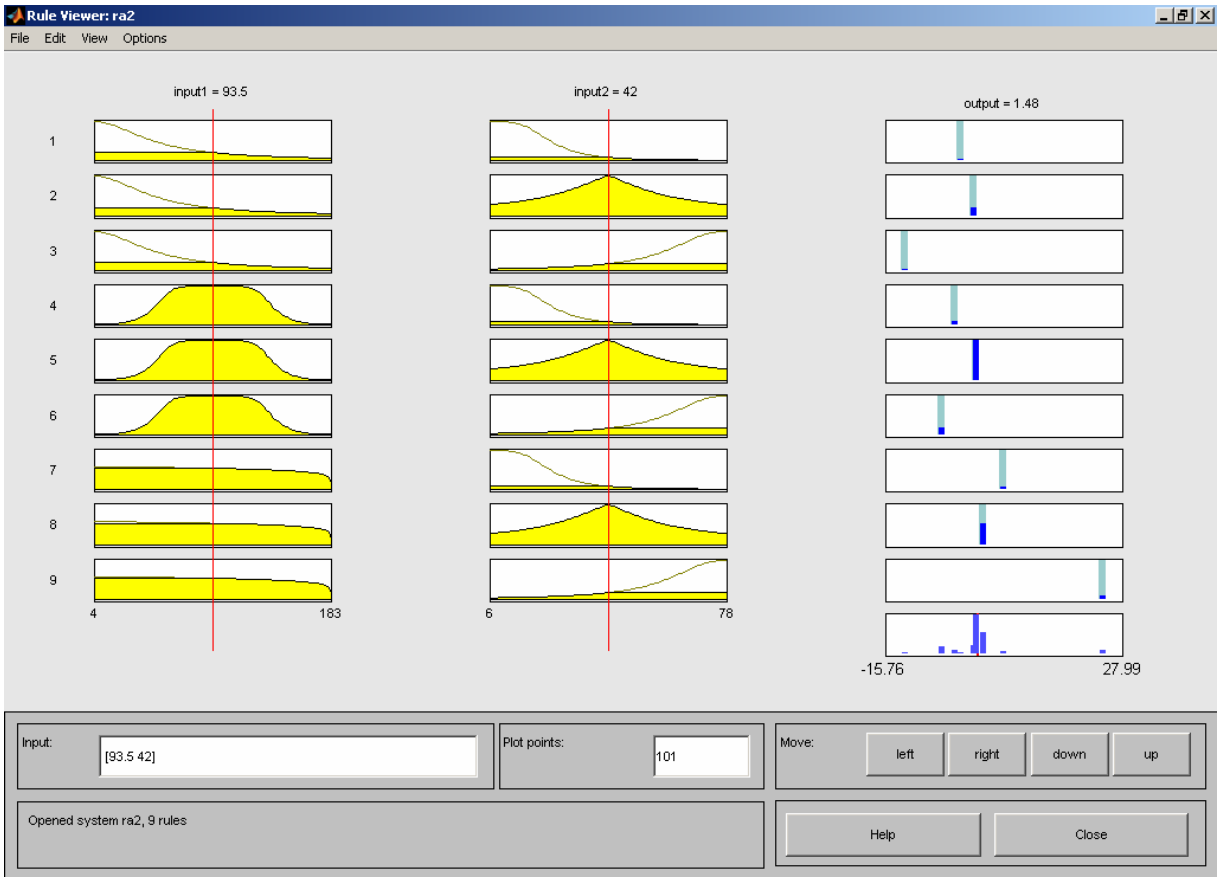

Figure 5.9 The rule viewer of fuzzy of Matlab program of modeling Ra.

CHAPTER SIX

RESULTS AND DISCUSSION

This chapter consists of two main parts.
The first part is on the investigation of cutting parameters effects.
The second part is on the interrelationships between cutting predictor variables (speed, feed rate, depth of cut and forces) and surface roughness.

6.1 Investigation of cutting parameters effects

In **Chapters 3, 4** and **5**, a detailed description of the experimental study of the cutting parameters and surface roughness were presented. Data of the surface roughness and forces during milling tests were collected. **Figures 6.1-6.45**, Show that the experimental data used to make the ANFIS models.

6.1.1 The effect of cutting parameters on the surface roughness

Figures 6.1-6.3 show the effect of the rotational speed on the surface roughness at deferent feed rates and depths of cut. These figures show that at any value of feed rate and depth of cut, the surface roughness decreases with increasing rotational speed for the range of speed from 750rpm to 1350rpm and then the

surface roughness increases with increasing rotational speed for the range of speed from 1350rpm to 1750rpm.

This phenomenon occurs at low speed where the chip parts become a stationary body of highly deformed material attached to the cutting edge. This is called a built-up edge (BUE) [52]. The growth and rapid breakage of the BUE cause a rough surface on the machined part.

Figures 6.4-6.6 show the relationship between the surface roughness and feed rate at different speed and depth of cut. These figures show that at any value of speed and depth of cut, the surface roughness increases with increased feed rate for all the range of the feed rate.

This is because the surface roughness (as defined as the machining marks on the work piece surface) is proportional to the feed rate as shown in Equations 2.1 - 2.11.

Figures 6.7-6.9 show the three dimensional plots of the surface roughness against the speed and feed rate.

Figures 6.10-6.14 show the effect of the depth of cut on the surface roughness at deferent speeds and feed rates. These figures show that at any value of speed and feed rate, the surface roughness increases slightly with increasing depth of cut for all the range of the depth of cut.

Figure 6.15 shows the three dimensional plot of the surface roughness against the speed and depth of cut.

Figures 6.1-6.15 Also show that the maximum value of surface roughness equal to 5.5µm at a speed of 750rpm, feed rate of 250mm/min and depth of cut of 0.7mm and the minimum value of surface roughness equal to 0.6µm at a speed of 1500rpm, feed of 50mm/min and depth of cut of 0.3mm.

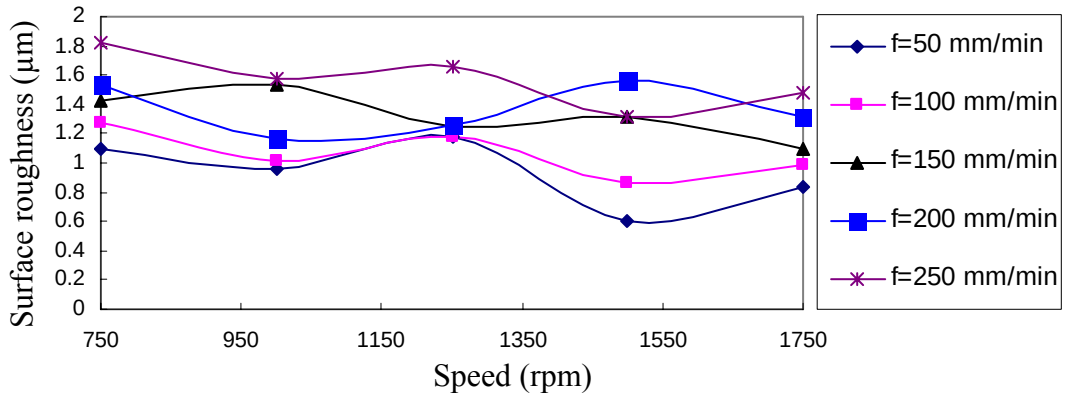

Figure 6.1 The variation of surface roughness against speed at different feed rate for depth of cut = 0.3 mm

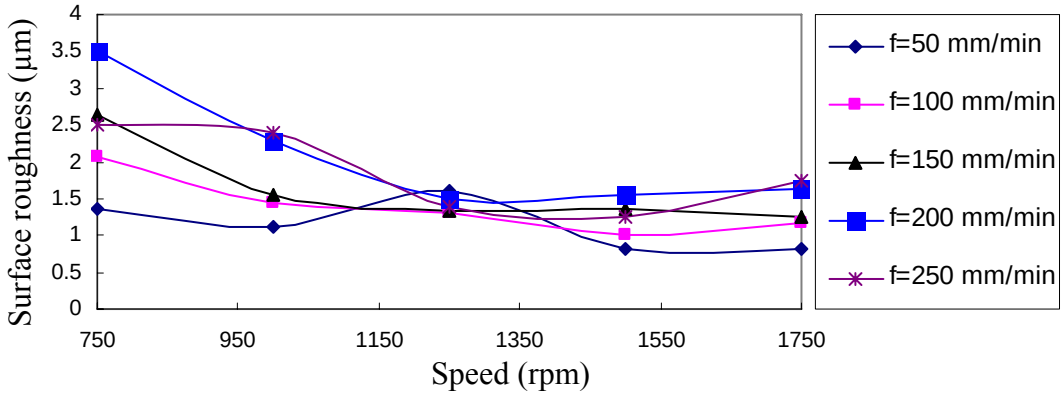

Figure 6.2 The variation of surface roughness against speed at different feed rate for depth of cut = 0.5 mm

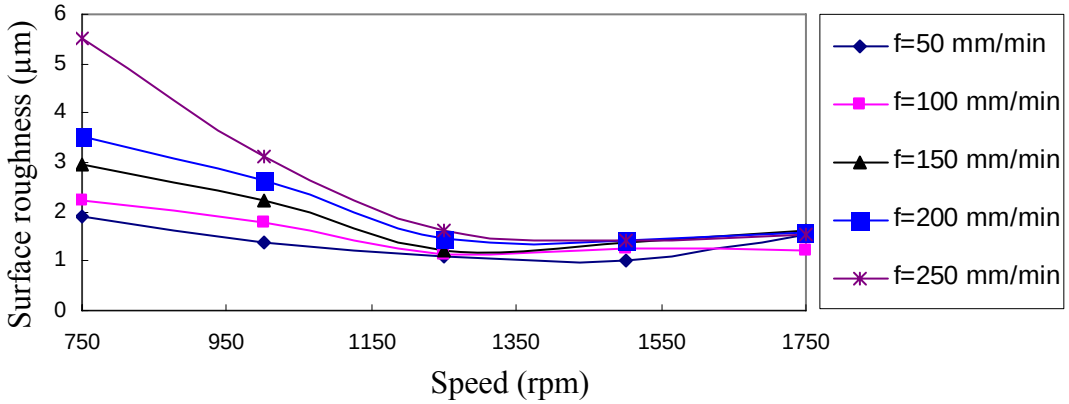

Figure 6.3 The variation of surface roughness against speed at different feed rates for depth of cut = 0.7 mm

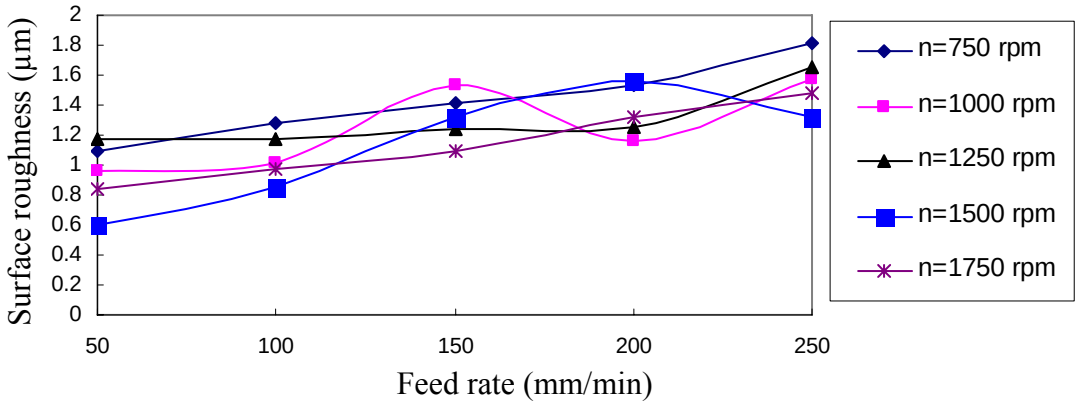

Figure 6.4 The variation of surface roughness against feed rate at different speed for depth of cut = 0.3 mm

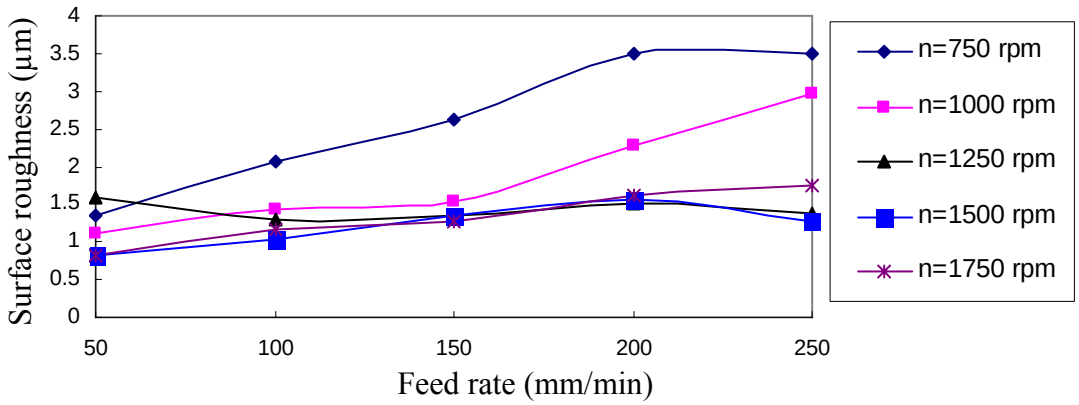

Figure 6.5 The variation of surface roughness against feed rate at different speed for depth of cut = 0.5 mm

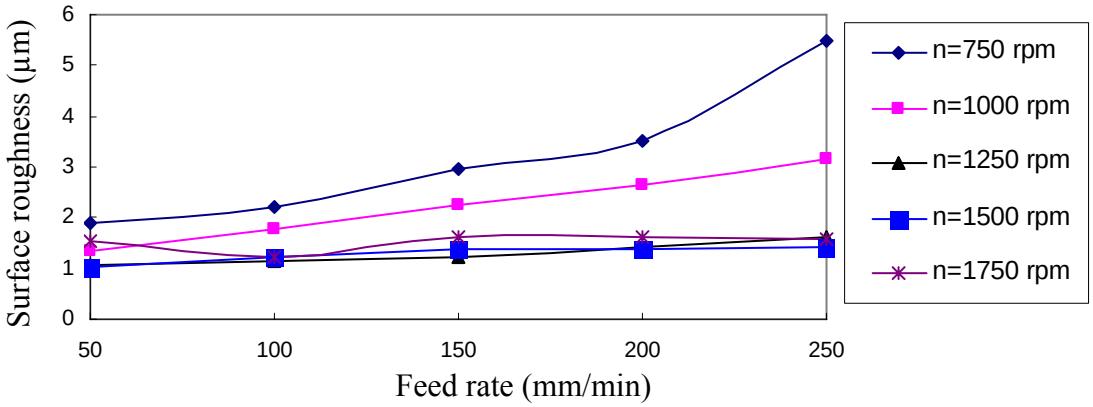

Figure 6.6 The variation of surface roughness against feed rate at different speed for depth of cut = 0.7 mm

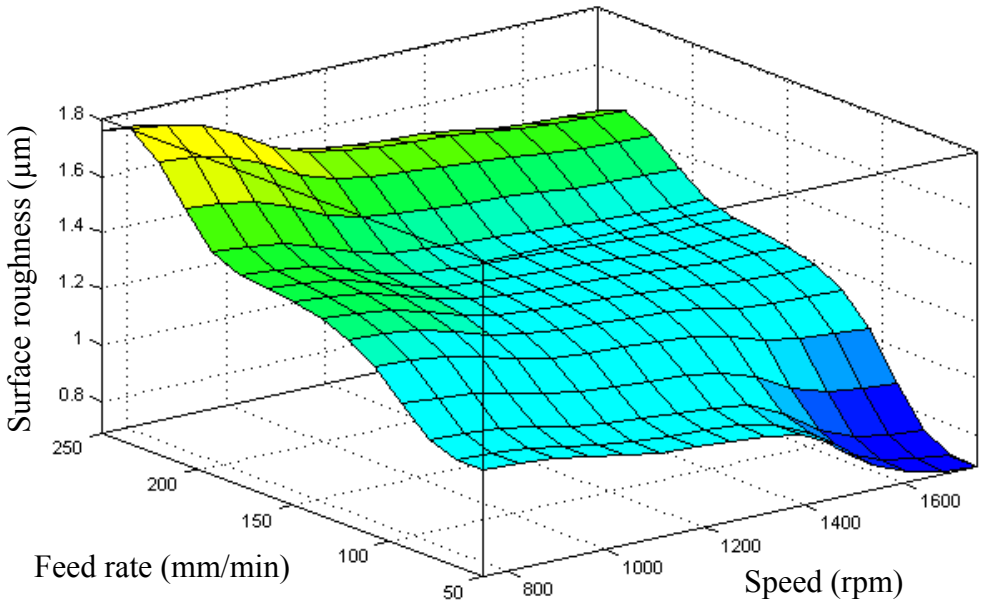

Figure 6.7 The variation of surface roughness against speed and feed rate for depth of cut = 0.3 mm

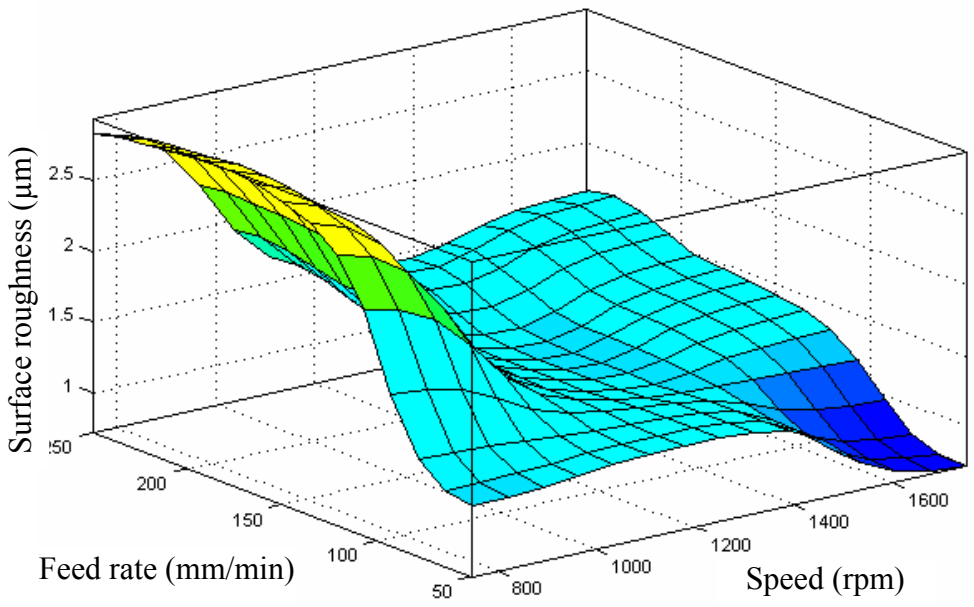

Figure 6.8 The variation of surface roughness against speed and feed rate for depth of cut = 0.5 mm

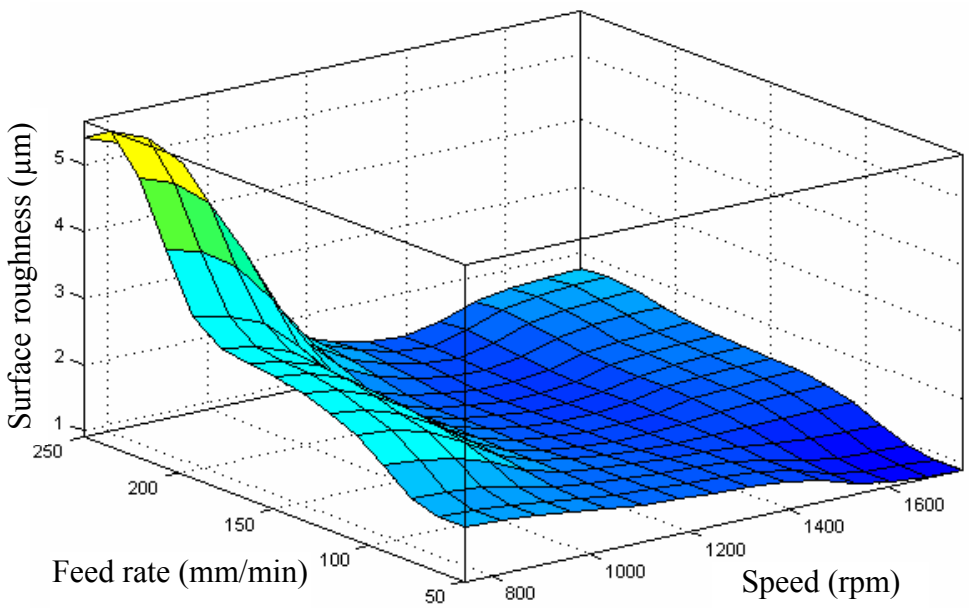

Figure 6.9 the variation of surface roughness against speed and feed rate for depth of cut = 0.7 mm

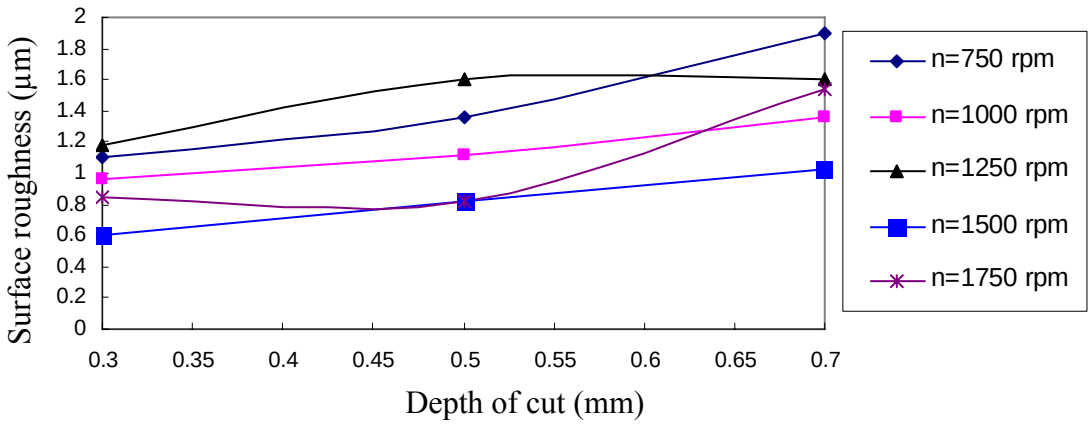

Figure 6.10 The variation of surface roughness against depth of cut at different speed for feed rate = 50 mm/min

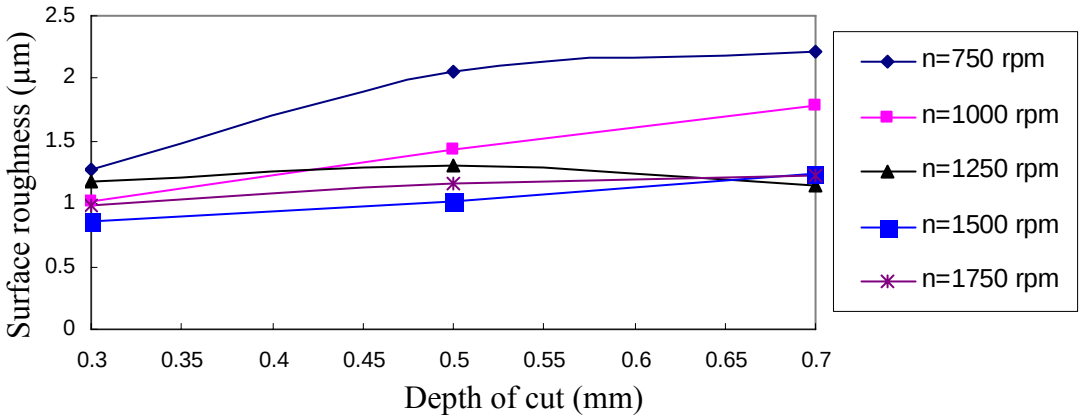

Figure 6.11 The variation of surface roughness against depth of cut at different speed for feed rate = 100 mm/min

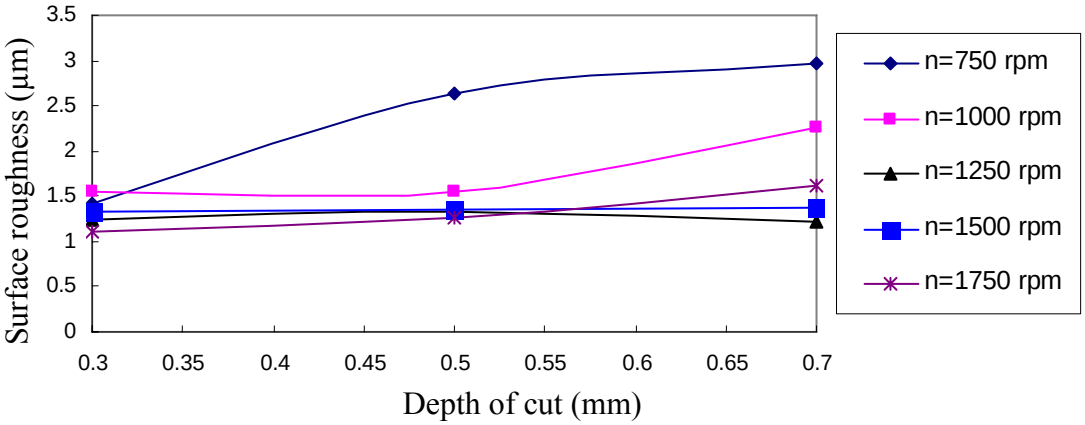

Figure 6.12 The variation of surface roughness against depth of cut at different speed for feed rate = 150 mm/min

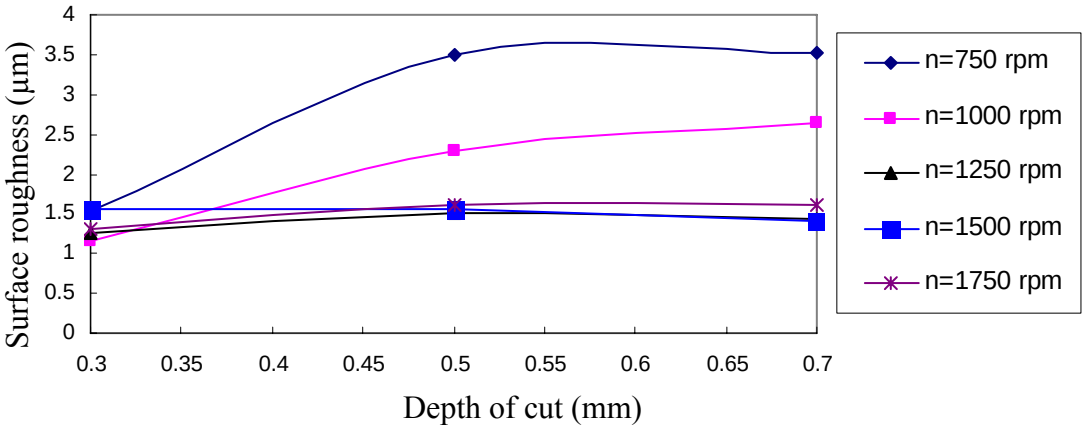

Figure 6.13 The variation of surface roughness against depth of cut at different speed for feed rate = 200 mm/min

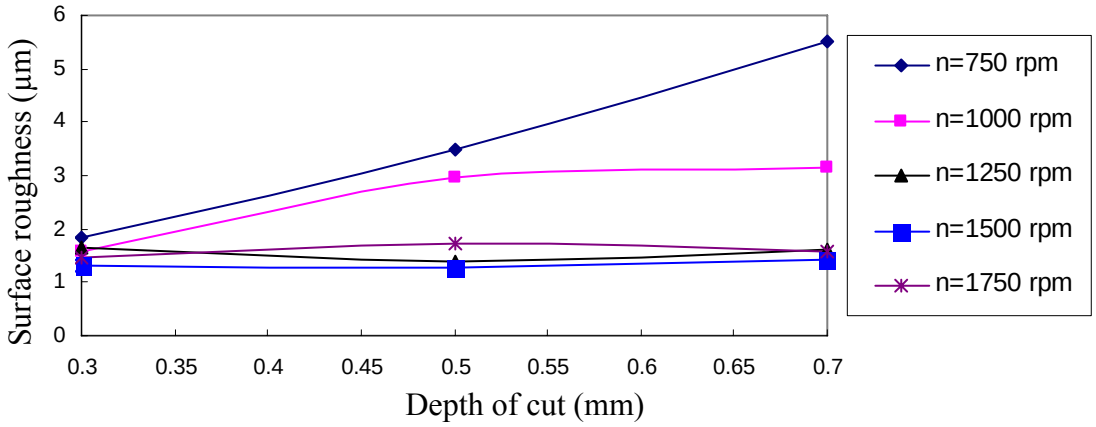

Figure 6.14 The variation of surface roughness against depth of cut at different speed for feed rate = 250 mm/min

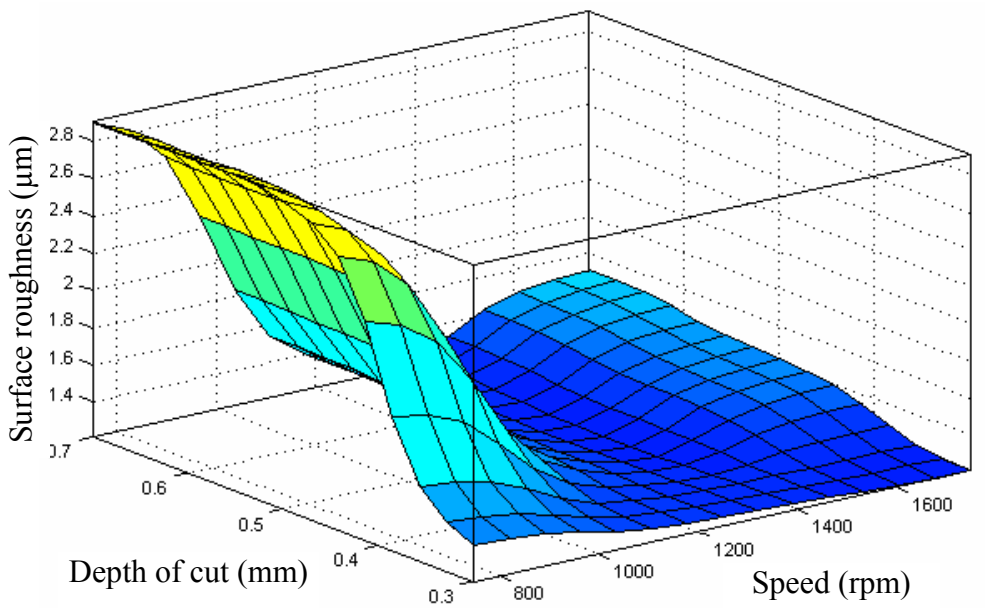

Figure 6.15 The variation of surface roughness against speed and depth of cut for feed rate = 150 mm/min

6.1.2 The effect of cutting parameters on the feed force and normal force

Figures 6.16-6.21 show the interrelation between the rotational speed and both feed force and normal force at different feed rates and depths of cut. These figures show that at any value of feed rate and depth of cut, the feed force and normal force decrease with increasing rotational speed for the range of speed from 750 rpm to 1350 rpm and then the feed force and normal force increase with increasing rotational speed for the range of speed from 1350 rpm to 1750 rpm.

There is no built-up edge at very low cutting speed (say V=0.3 m/min) since the temperature on the face of the chip is not sufficient to cause the chip surface to behave in a ductile manner. With an increase in cutting speed (say V=45 m/min) the chip metal in contact with the chip face becomes ductile and the resulting plastic flow on the chip face causes strain hardening and a further increase in the force tending to fix the chip to the tool. When the bonding force between chip and tool exceeds the shear strength of the metal in the material body of the chip, at some particularly weak point near the tool face, the BUE forms [5 and 6].

Figures 6.22-6.27 show that at any value of speed and depth of cut, the feed force and normal force increase with increasing feed rate for all the range of the feed rate.

Figures 6.28-6.33 show the three dimensional plots of the feed and normal forces against the speed and feed rate.

Figures 6.34-6.43 show that at any value of speed and feed rate, the feed and normal forces increase with increasing depth of cut for all the range of the depth of cut. **Figures 6.44** and **6.45** show the three dimensional plots of the feed and normal forces against the speed and depth of cut.

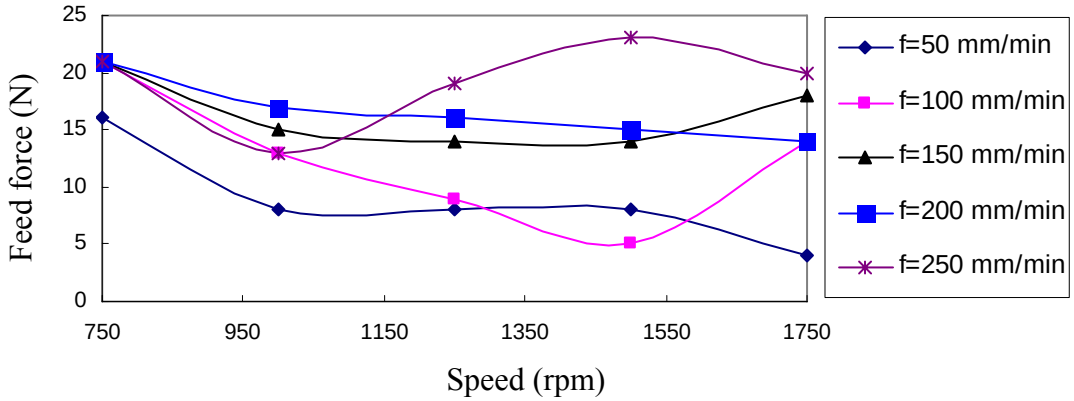

Figure 6.16 The variation of feed force against speed at different feed rate for depth of cut = 0.3 mm.

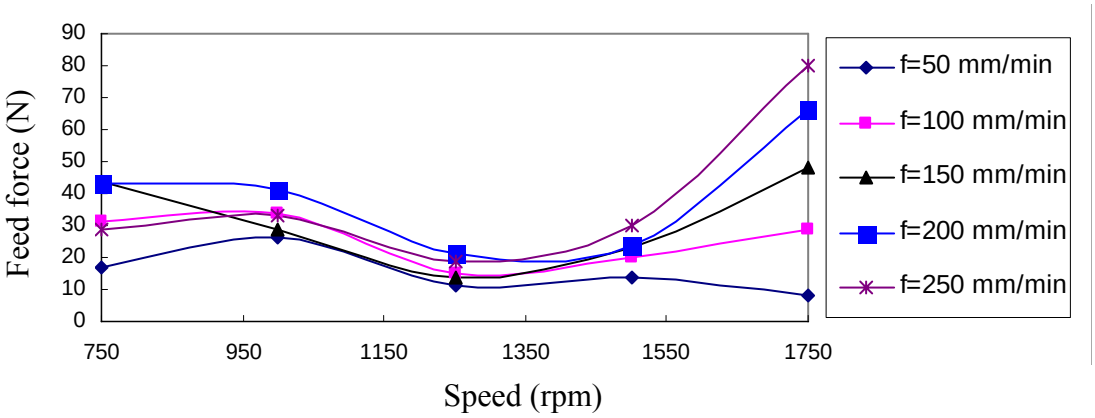

Figure 6.17 The variation of feed force against speed at different feed rate for depth of cut = 0.5 mm.

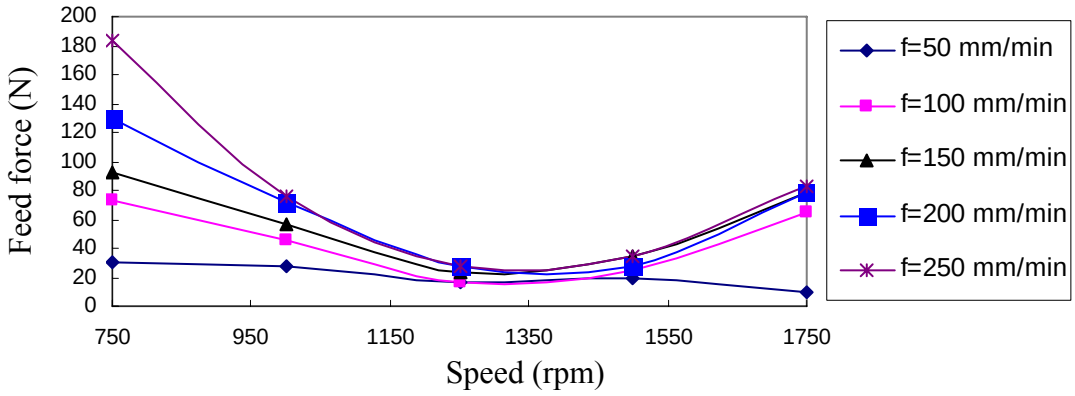

Figure 6.18 The variation of feed force against speed at different feed rate for depth of cut = 0.7 mm.

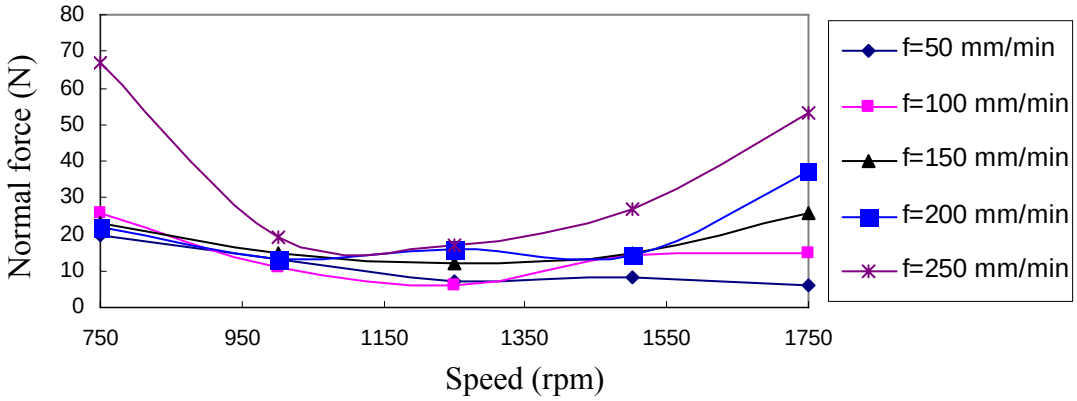

Figure 6.19 The variation of normal force against speed at different feed rate for depth of cut = 0.3 mm.

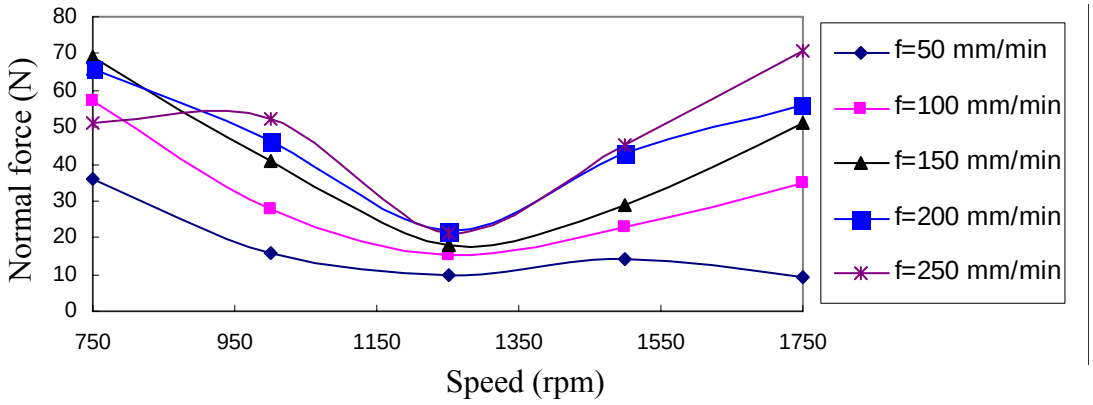

Figure 6.20 The variation of normal force against speed at different feed rate for depth of cut = 0.5 mm.

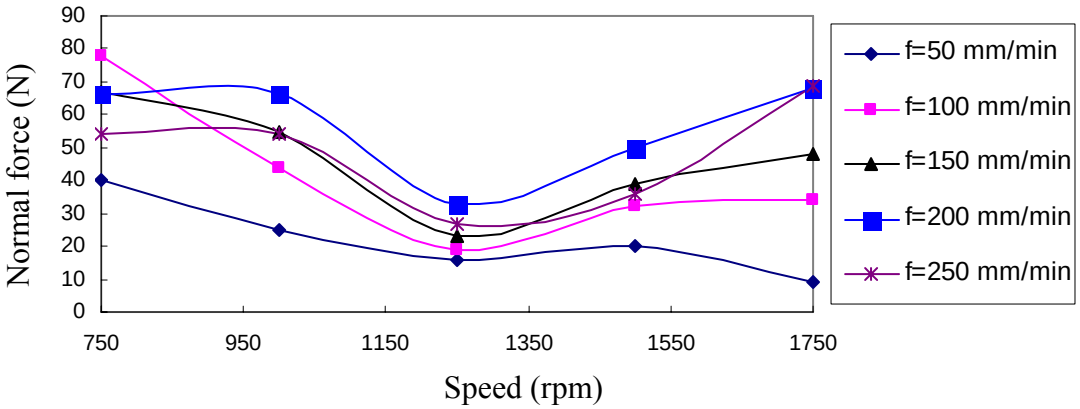

Figure 6.21 The variation of normal force against speed at different feed rate for depth of cut = 0.7 mm.

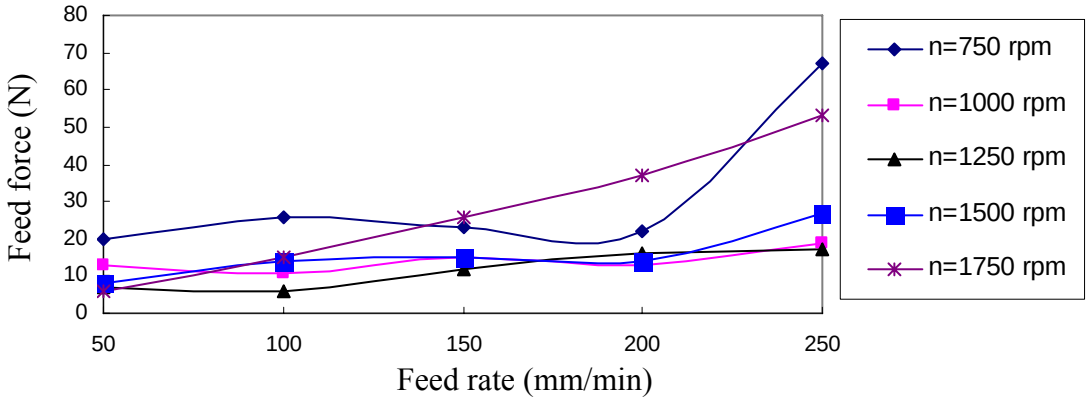

Figure 6.22 The variation of feed force against feed rate at different speed for depth of cut = 0.3 mm.

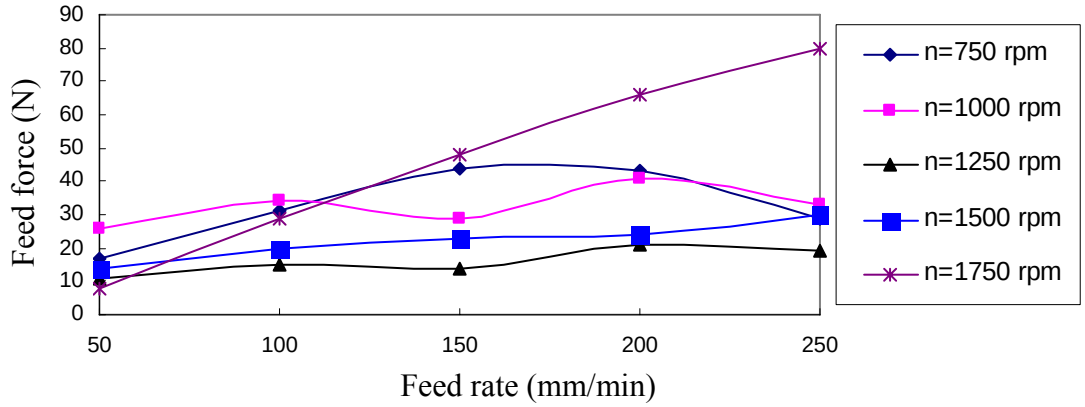

Figure 6.23 The variation of feed force against feed rate at different speed for depth of cut = 0.5 mm.

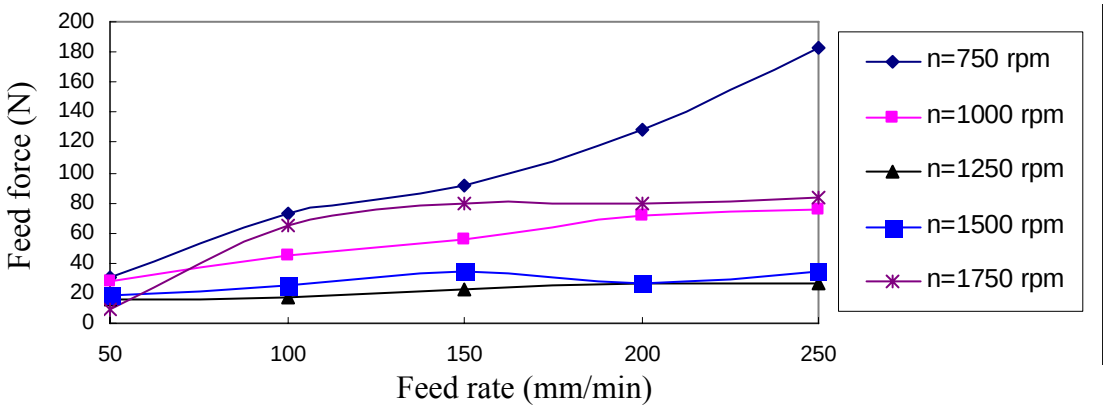

Figure 6.24 The variation of feed force against feed rate at different speed for depth of cut = 0.7 mm.

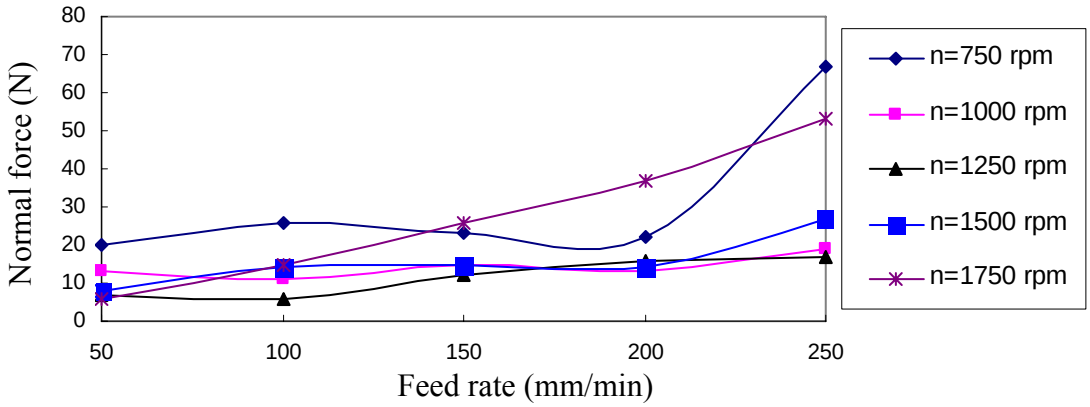

Figure 6.25 The variation of normal force against feed rate at different speed for depth of cut = 0.3 mm.

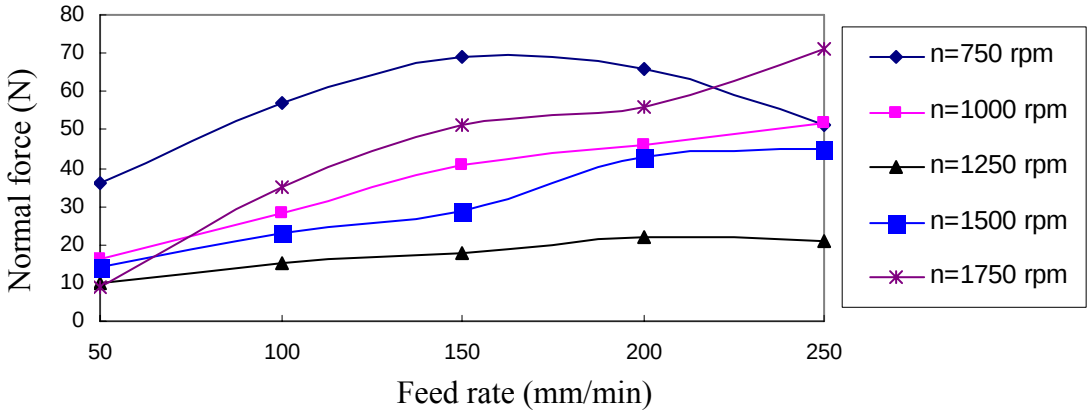

Figure 6.26 The variation of normal force against feed rate at different speed for depth of cut = 0.5 mm.

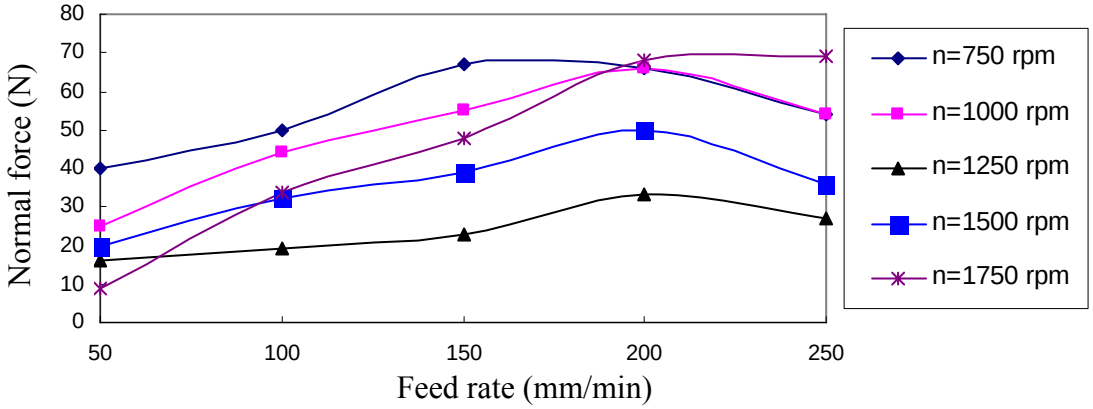

Figure 6.27 The variation of normal force against feed rate at different speed for depth of cut = 0.7 mm.

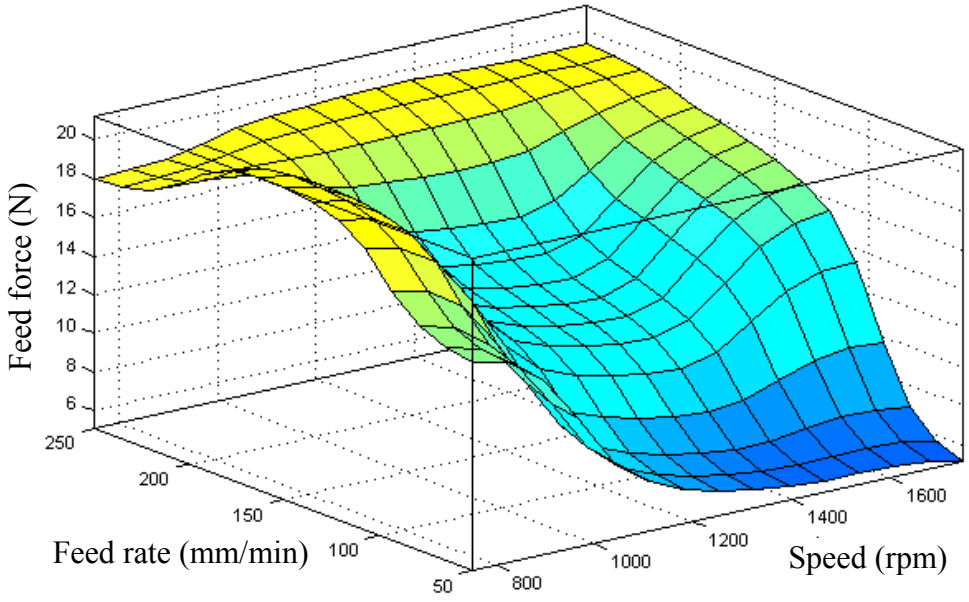

Figure 6.28 The variation of feed force against rotational speed and feed rate for depth of cut = 0.3 mm.

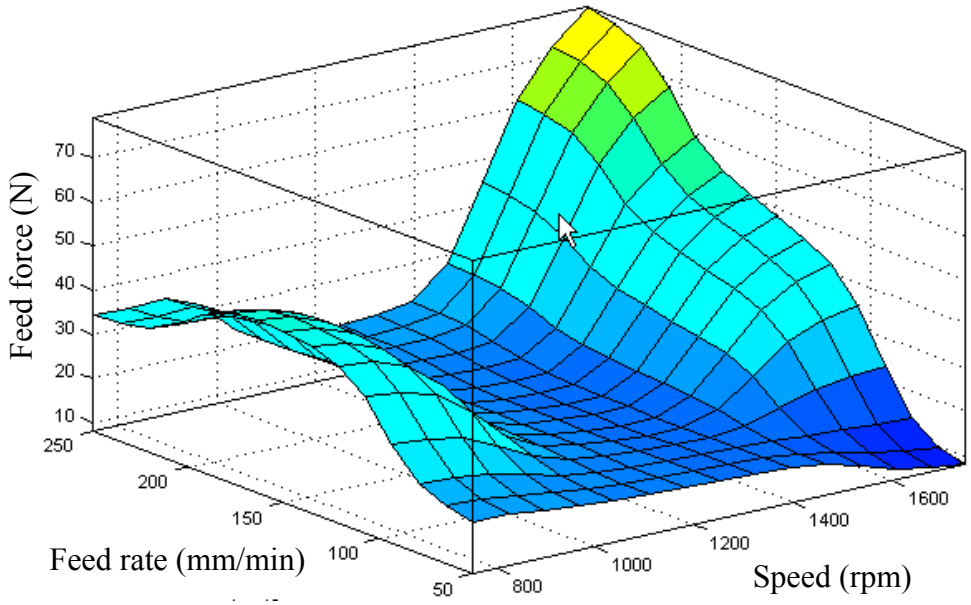

Figure 6.29 The variation of feed force against rotational speed and feed rate for depth of cut = 0.5 mm.

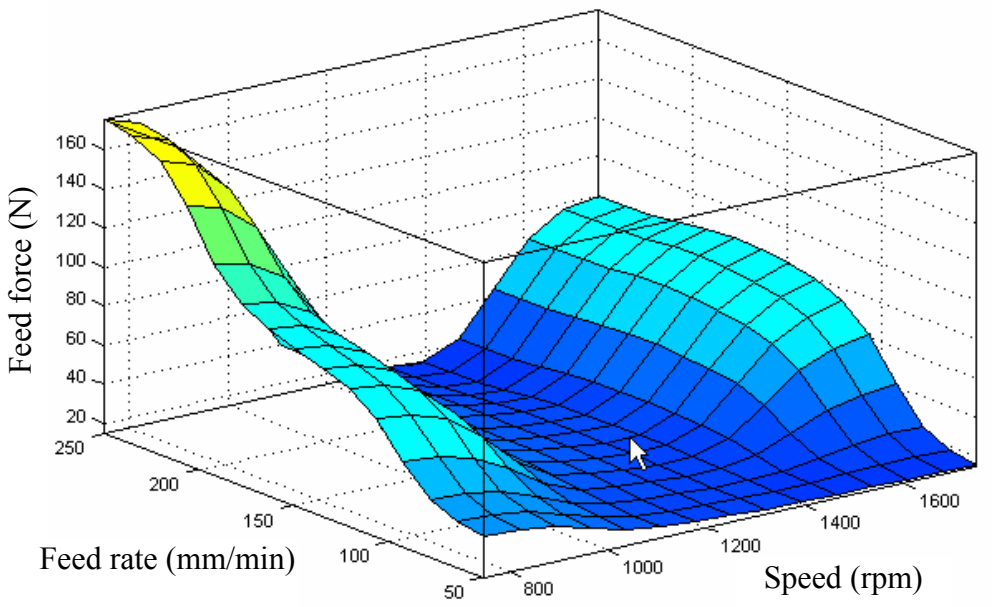

Figure 6.30 The variation of feed force against rotational speed and feed rate for depth of cut = 0.7 mm.

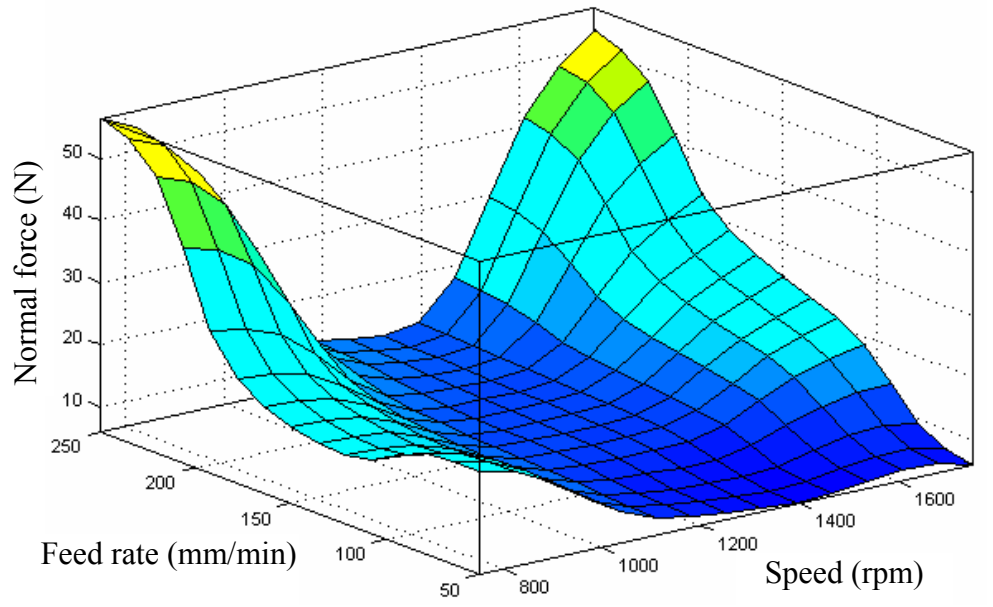

Figure 6.31 The variation of normal force against rotational speed and feed rate for depth of cut = 0.3 mm.

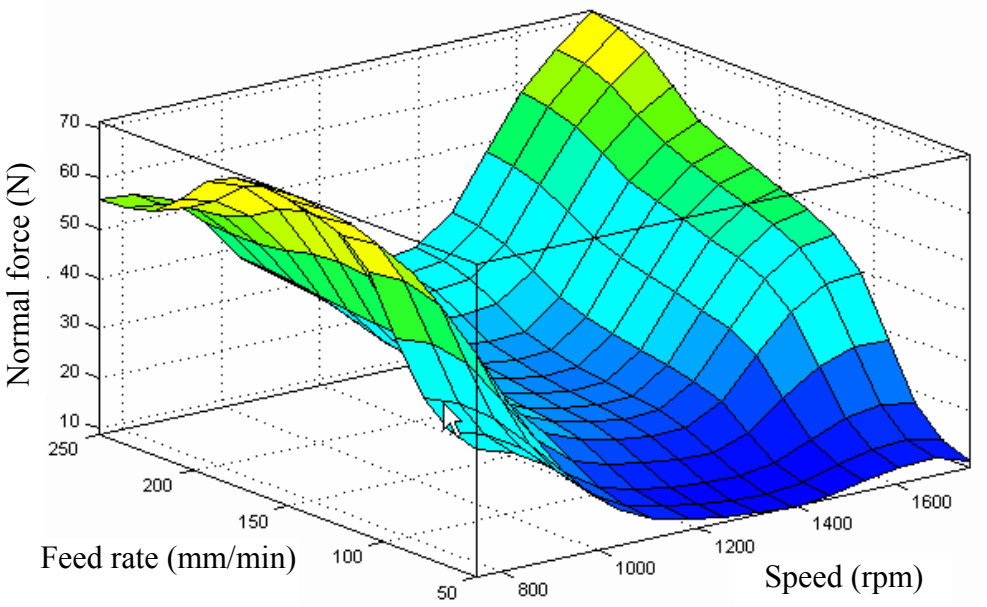

Figure 6.32 The variation of normal force against rotational speed and feed rate for depth of cut = 0.5 mm.

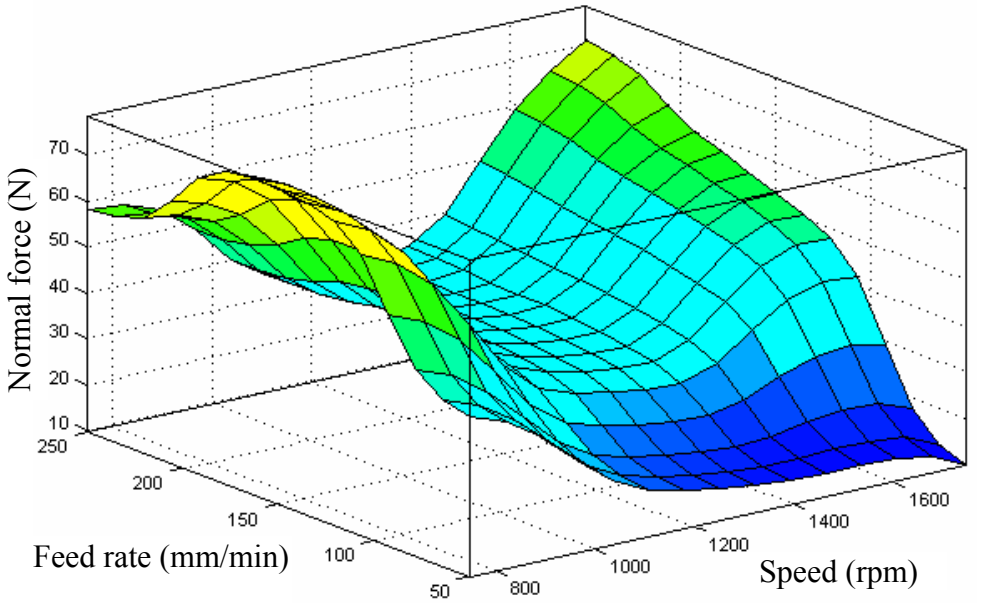

Figure 6.33 The variation of normal force against rotational speed and feed rate for depth of cut = 0.7 mm.

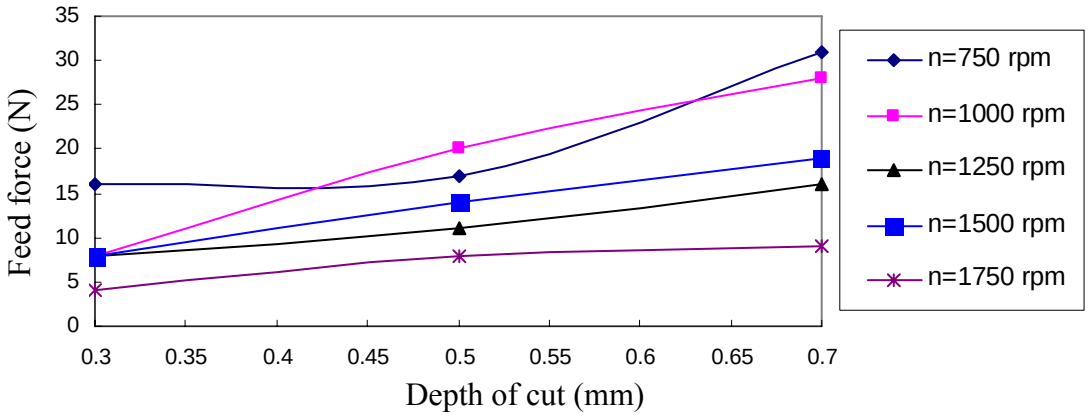

Figure 6.34 The variation of feed force against depth of cut at different speed for feed rate = 50 mm/min.

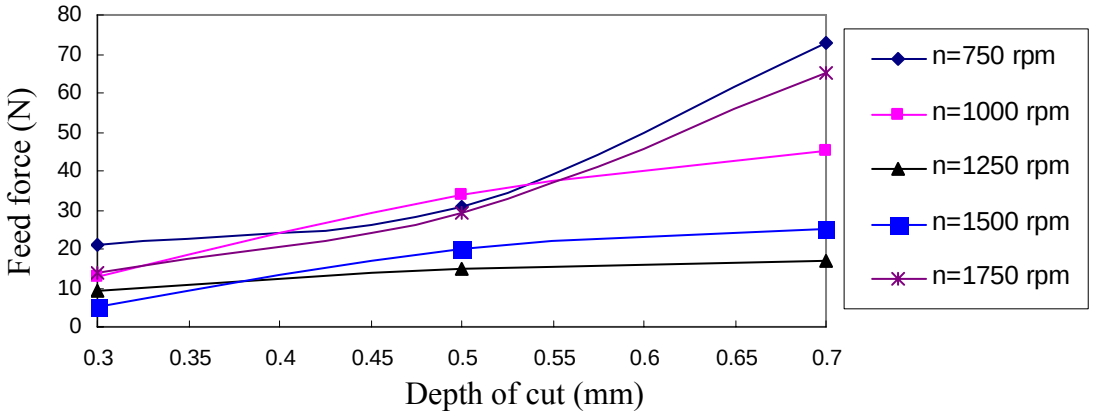

Figure 6.35 The variation of feed force against depth of cut at different speed for feed rate = 100 mm/min.

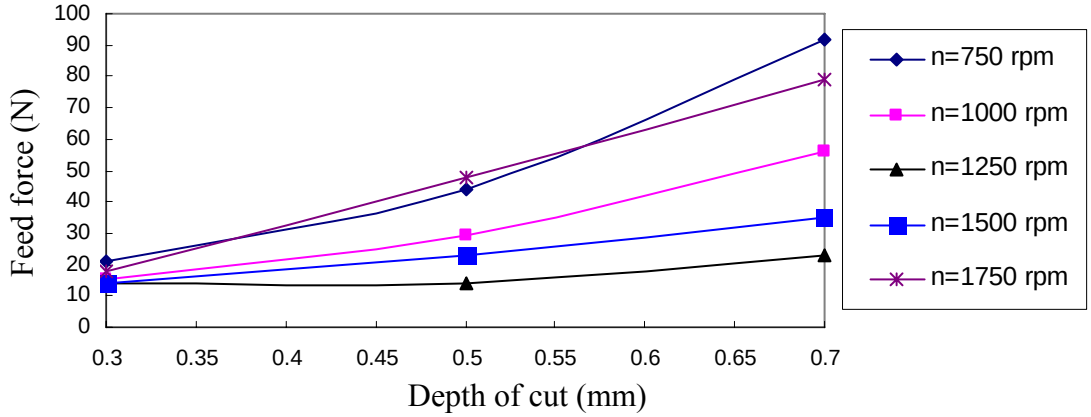

Figure 6.36 The variation of feed force against depth of cut at different speed for feed rate = 150 mm/min.

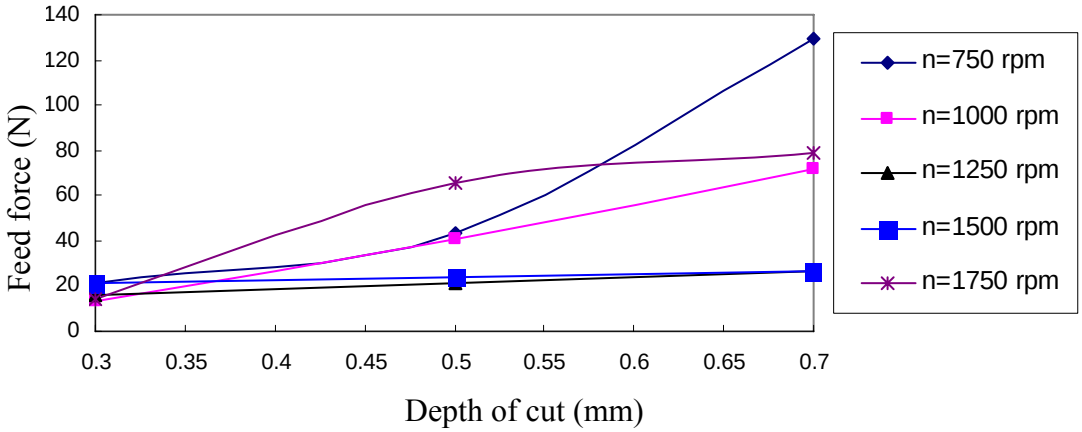

Figure 6.37 The variation of feed force against depth of cut at different speed for feed rate = 200 mm/min.

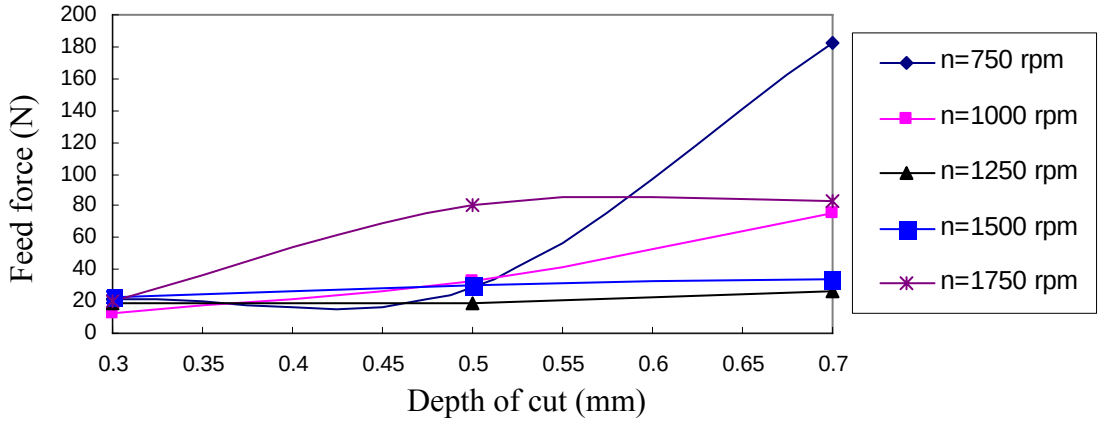

Figure 6.38 The variation of feed force against depth of cut at different speed for feed rate = 250 mm/min.

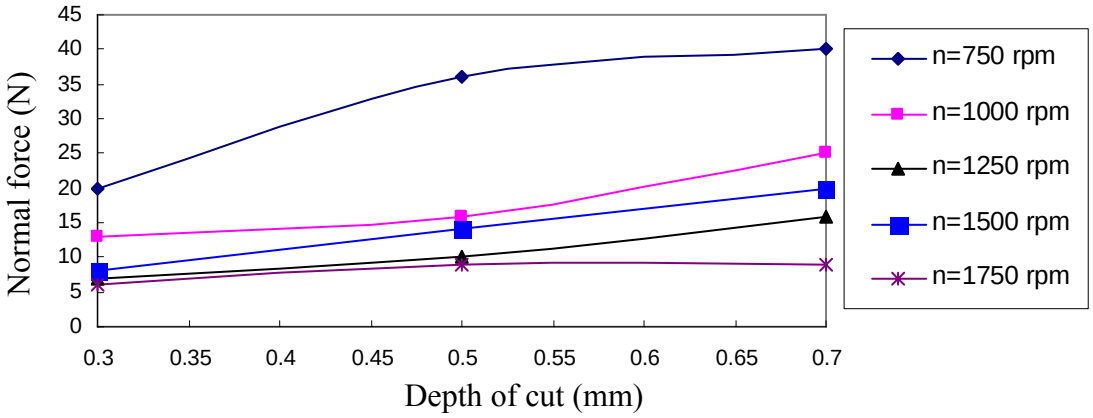

Figure 6.39 The variation of normal force against depth of cut at different speed for feed rate = 50 mm/min.

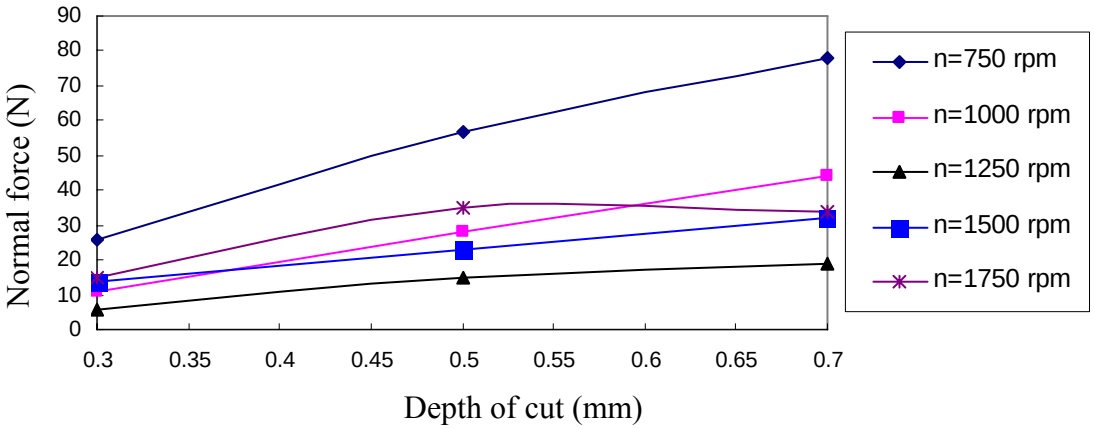

Figure 6.40 The variation of normal force against depth of cut at different speed for feed rate = 100 mm/min.

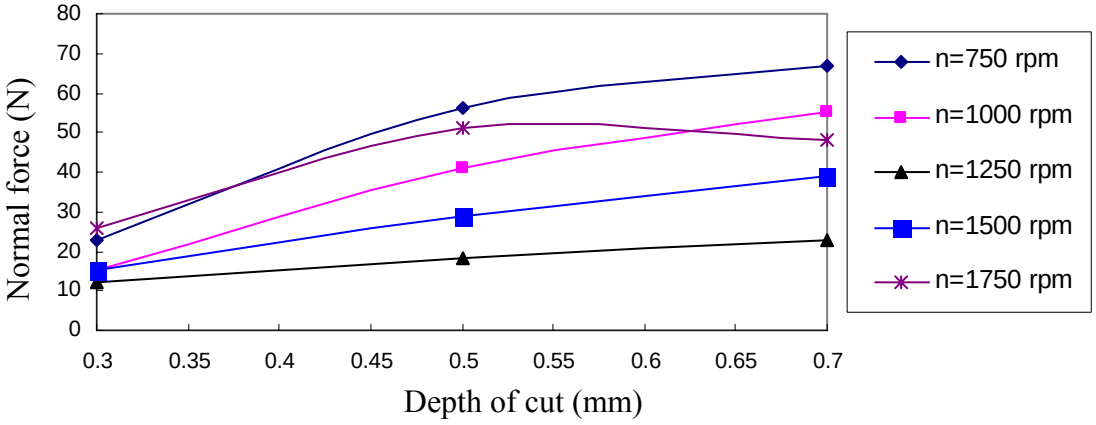

Figure 6.41 The variation of normal force against depth of cut at different speed for feed rate = 150 mm/min.

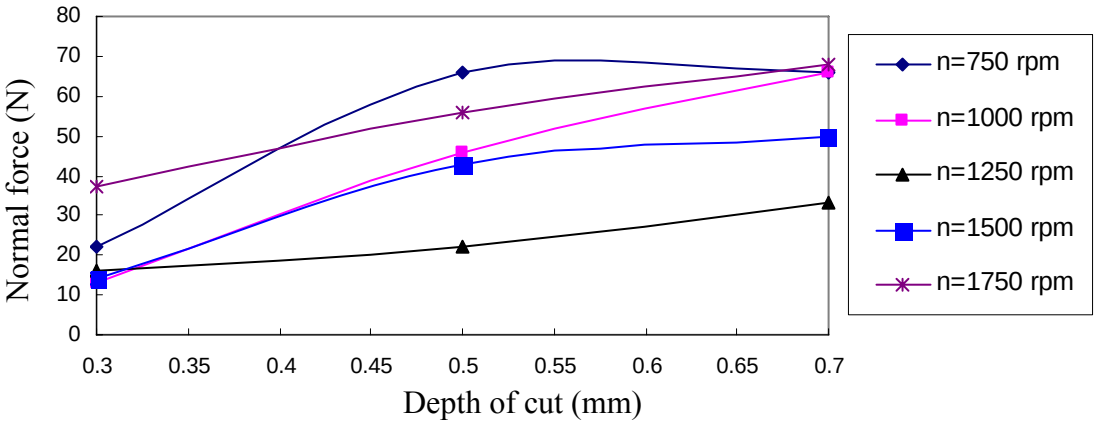

Figure 6.42 The variation of normal force against depth of cut at different speed for feed rate = 200 mm/min.

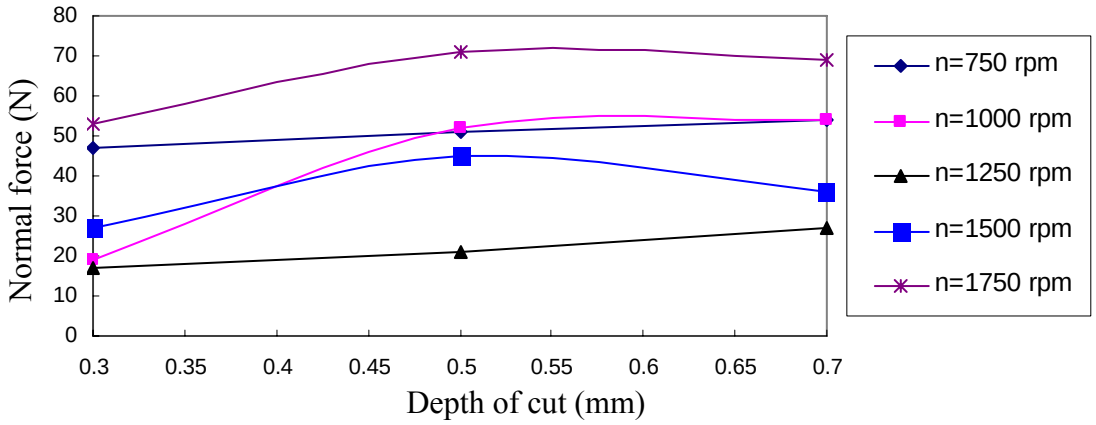

Figure 6.43 The variation of normal force against depth of cut at different speed for feed rate = 250 mm/min.

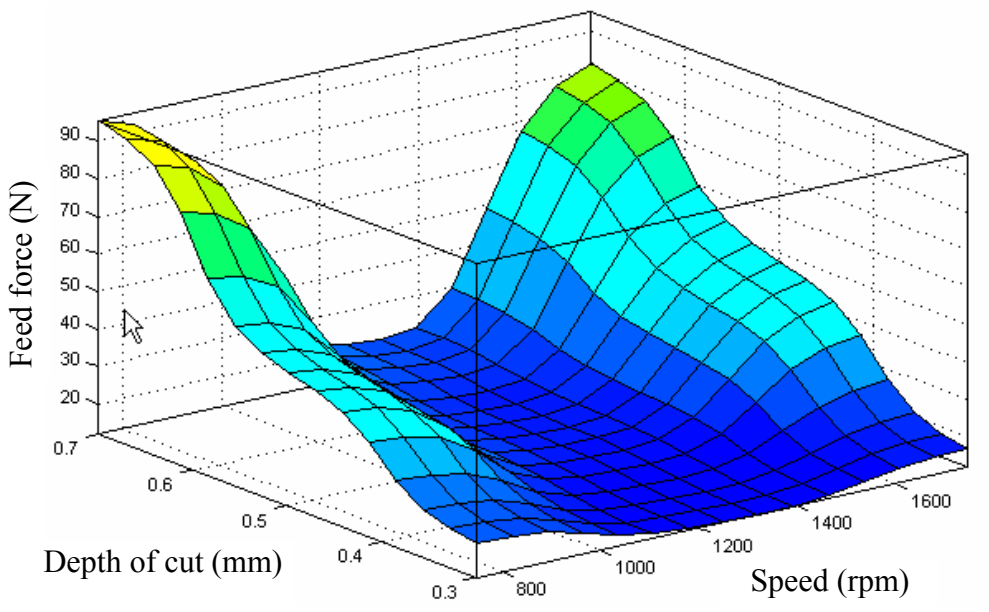

Figure 6.44 The variation of feed force against rotational speed and dept of cut for feed rate = 150 mm/min.

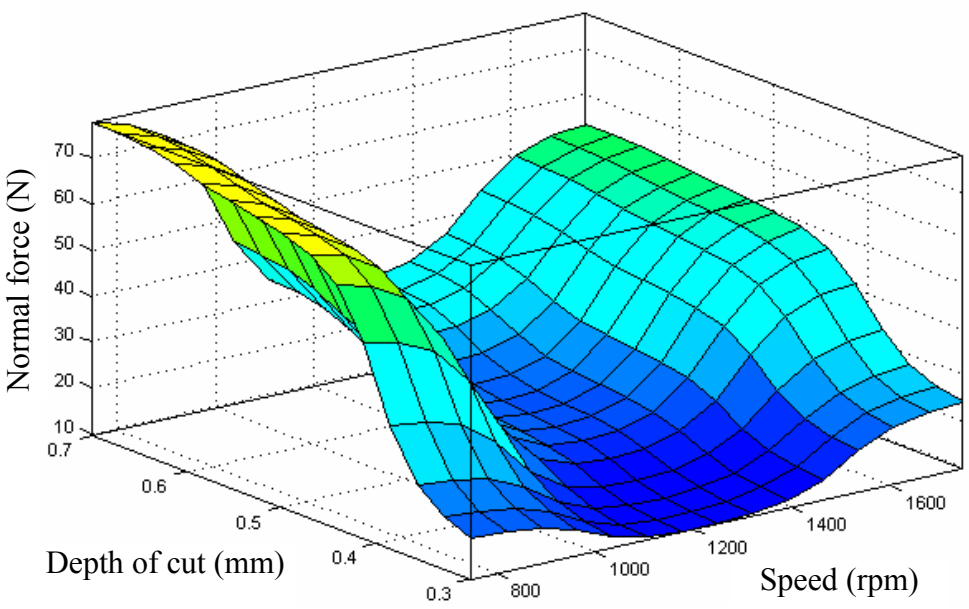

Figure 6.45 The variation of normal force against rotational speed and depth of cut for feed rate = 150 mm/min.

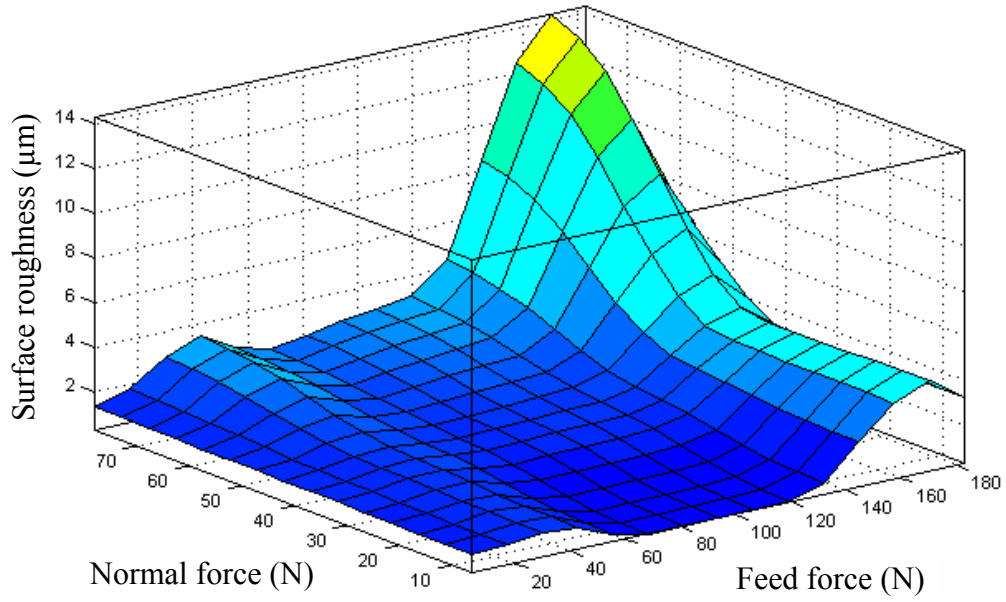

Figure 6.46 The variation of surface roughness against feed force and normal force

6.1.3 The effects of the feed force and normal force on the surface roughness

Figure 6.46 Shows the interrelation between the feed force, normal force and the surface roughness at different speed, feed rate and depth of cut. These figures show that at any value of speed, feed rate and depth of cut, the surface roughness increases with increasing the feed force and normal force for all the range of the feed force and normal force.

From the above analysis it is indicated that the feed force and normal force against the surface roughness have the same trend as the relations between the cutting parameters with the surface roughness.

6.2 Models Verification

The database with 75 end milling experiments listed in **Table 3.1**; was used to train the ANFIS using three input parameters (speed, feed rate and depth of cut) and generate **model1** as in chapter three.

The database with 75 end milling experiments listed in **Table 5.1** was used to train the ANFIS using two input parameters (feed force and normal force) and generate **model2** as in chapter five. Thirty two measured and predicted Ra values listed in **Table 6.1** were used to verify the ANFIS models.

The plot of thirty two measured Ra values versus predicted Ra using ANFIS models is shown in **Figure 6.47.** This Figure shows a comparison of the measured Ra and predicted Ra of the thirty two set of testing data following the training using ANFIS.

It is shown from the figure that the prediction values of surface roughness using two models are very close to the measured values. The average error of the prediction of surface roughness for the model1 and model 2 is equal to 8.5% and 8% respectively.

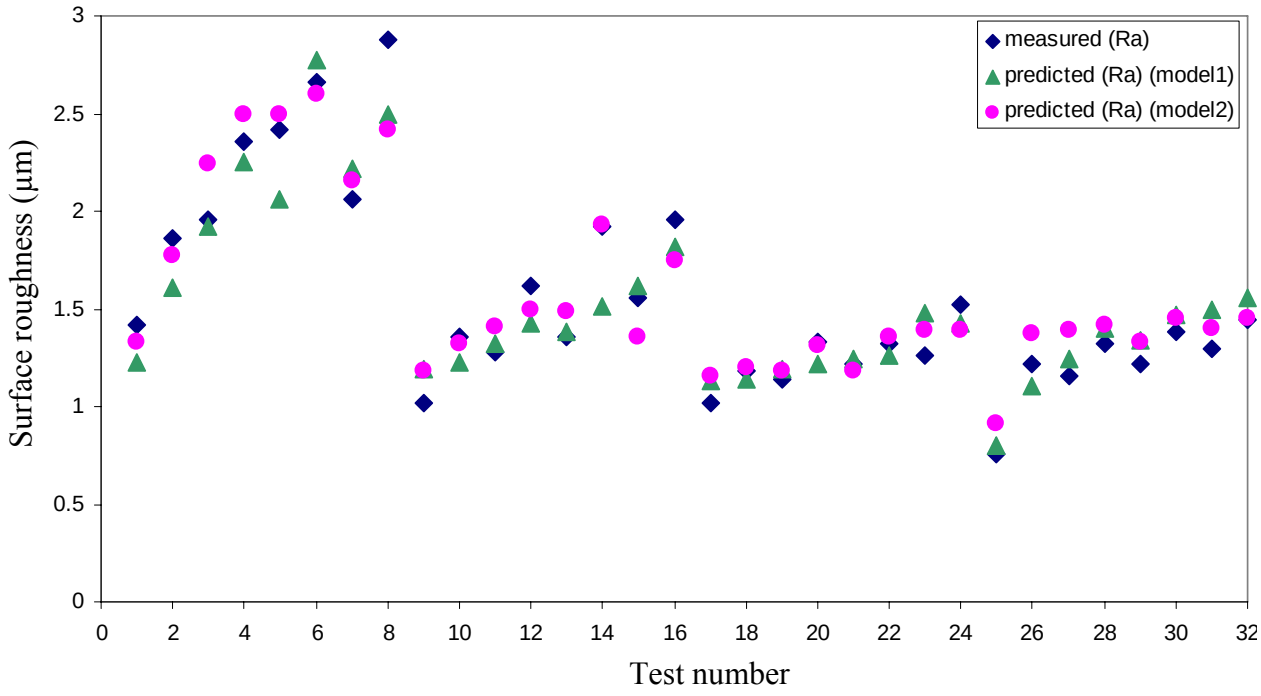

Figure 6.47 Measured Ra versus predicted Ra

Table 6.1 Comparison of measured Ra and predicted Ra.

Test No.	Parameters					Measured Ra (µm)	Model1		Model2	
	n (rpm)	*f (mm/min)*	*t (mm)*	*Fx (N)*	*Fy (N)*		Predicted Ra(µm)	Error E_i (%)	Predicted Ra(µm)	Error E_i (%)
1	875	75	0.4	18	40	1.42	1.23	13.4	1.33	6.3
2			0.6	56	53	1.86	1.61	13.4	1.77	4.8
3		125	0.4	47	55	1.96	1.92	2.0	2.24	14.3
4			0.6	49	86	2.36	2.25	4.7	2.5	5.9
5		175	0.4	51	63	2.42	2.06	14.9	2.5	3.3
6			0.6	89	90	2.66	2.77	4.1	2.6	2.3
7		225	0.4	69	82	2.06	2.22	7.8	2.16	4.9
8			0.6	81	96	2.88	2.5	13.2	2.42	16.0
9	1125	75	0.4	14	17	1.02	1.19	16.7	1.18	15.7
10			0.6	19	31	1.36	1.23	9.6	1.32	2.9
11		125	0.4	24	32	1.28	1.32	3.1	1.41	10.2
12			0.6	43	51	1.62	1.43	11.7	1.5	7.4
13		175	0.4	26	40	1.36	1.38	1.5	1.49	9.6
14			0.6	48	50	1.92	1.51	21.4	1.93	0.5
15		225	0.4	20	38	1.56	1.62	3.8	1.36	12.8
16			0.6	44	44	1.96	1.82	7.1	1.75	10.7
17	1375	75	0.4	13	16	1.02	1.13	10.8	1.16	13.7
18			0.6	16	17	1.18	1.14	3.4	1.2	1.7
19		125	0.4	14	19	1.14	1.19	4.4	1.18	3.5
20			0.6	20	26	1.33	1.22	8.3	1.31	1.5
21		175	0.4	14	17	1.22	1.24	1.6	1.18	3.3
22			0.6	23	25	1.32	1.26	4.5	1.36	3.0
23		225	0.4	26	22	1.26	1.48	17.5	1.39	10.3
24			0.6	23	32	1.52	1.43	5.9	1.39	8.6
25	1625	75	0.4	14	22	0.76	0.8	5.3	0.91	19.7
26			0.6	21	35	1.22	1.1	9.8	1.37	12.3
27		125	0.4	21	40	1.16	1.24	6.9	1.39	19.8
28			0.6	43	50	1.32	1.4	6.1	1.42	7.6
29		175	0.4	18	39	1.22	1.34	9.8	1.33	9.0
30			0.6	48	65	1.38	1.47	6.5	1.45	5.1
31		225	0.4	30	57	1.3	1.5	15.4	1.4	7.7
32			0.6	66	85	1.44	1.56	8.3	1.45	0.7
Average error E_{av} (%)								**8.5**		**8**

To evaluate the ANFIS models, the percentage error E_i and the average percentage error E_{av} defined in **Equations (6.1)** and **(6.2)** respectively were used.

$$E_i = \frac{\left| Ra_i - \hat{R}a_i \right|}{Ra_i} \times 100 \quad \text{……(6.1)}$$

Where E_i : percentage error of sample number i.

Ra_i : measured Ra of sample number. i.

$\hat{R}a_i$: predicted Ra generated by a multiple regression model or ANFIS model

$i = 1,2,3\ldots\ldots m$

Where m is the number of samples

$$E_{av} = \frac{\sum_{i=1}^{m} E_i}{m} \quad \text{……(6.2)}$$

Where E_{av} is the average percentage error of m sample data

Table 6.1 shows that the average errors of the prediction of surface roughness for model 1 and model 2 are equal to 8.5% and 8% respectively that is, the accuracy are 91.5% and 92% respectively. Therefore, model 1 is more reliable and can be used to predict the surface roughness in off line manner.

CHAPTER SEVEN

CONCLUSIONS AND FUTURE WORKS

In the present study, the investigation of the surface roughness, feed force, and normal force generated during end milling processes is summarized into four aspects: ANFIS model construction, end milling dynamometer development, cutting parameter effects, interrelationship between cutting predictor variables and surface roughness evaluation.

7.1 ANFIS models construction

1 ANFIS was used to develop an empirical model for predicting the surface roughness in end milling.

2 Spindle speed, feed rate, depth of cut, feed force and normal force were used as predictor variables. Surface roughness was used as independent variable.

3 Seventy five measured Ra values, under different cutting conditions, were used as training data set and thirty two values were used as testing data set.

3 Deferent membership's functions were adopted during the training process of ANFIS in this study.

7.2 End milling dynamometer development

1 A dynamometer design and manufacturing, Strain Gage based, two components, computer linked, were carried out to measure feed forces and normal forces in end milling.

2 This dynamometer can be used in static force measurements and also in dynamic force measurements in the two directions.

3 Strain gages bonded on the circular rings have been used for sensing of the force signals. The analogue force signals obtained from two-channels have been amplified and converted into digital signals via a data acquisition card and recorded in a computer.

4 Although the dynamometer was developed primarily for milling operations, it can be used to measure cutting forces during nearly all machining operations (turning, grinding, drilling, etc.).

5 Machining tests were performed at different cutting parameters and the results showed that the dynamometer could be used reliably to measure cutting forces.

6 The designed and constructed dynamometer is capable of measuring feed force (F_x) and normal force (F_y).

7 The measured dynamic signals reveal that the fundamental natural frequency of the dynamometer is higher than the lowest natural frequency of the milling structure.

7.3 Cutting parameter effects evaluation

1 The feed force and normal force have the same trend as surface roughness with the cutting parameters.

2 The feed force and normal force increase with increasing feed rate and depth of cut and decreasing with increasing speed.

4 The surface roughness increases with increasing feed force, normal force, feed rate and depth of cut and decreases with increasing speed.

7.4 Model Verification

1 Surface roughness was measured in off line manner using surface meter.

2 The model was verified using random 32 test data where the average error was calculated to be equal to 8.5%. The accuracy achieved by ANFIS model was 91.5%. These results indicate that ANFIS model with the (gbellmf) is accurate and can be used in the prediction of the surface roughness in end milling operation.

7.5 Future work

1 Although this work focuses on prediction of surface roughness for milling operations, the concepts introduced are general; ie., prediction of surface roughness using ANFIS can be applied to other cutting and machining processes.

2 This model can be constructed for any machine to predict any phenomenon in metal cutting using known parameters and set of data. For CNC machines this model can be included in its program.

3 This model can be used to predict the surface roughness in an on-line manner.

LIST OF REFRENCES

[1] **Insperger, T., Stepan, G., Bayly, P. V., Mann, B. P.,** "Multiple chatter frequencies in milling processes", Journal of sound and vibration, Vlo. 262(2), pp 333-345, (2003).

[2] **Paris, H., Peigne, G., Mayer, R.,** "Surface shape prediction in high speed milling", International journal of machine tools and manufacture, (2004).

[3] **Burakowski, T., Wierzchon, T.,**"Surface engineering of metals: principles, equipment, technologies", CRC Press LLC, (1999).

[4] **Lou, M. S., Chen, J. C., Li, C. M.**, "Surface roughness prediction technique for CNC end-milling", Journal of Industrial Technology Vol. 15/1, pp 1-6, (1999).

[5] **Hwang, T-W., Zhang, G. M.,**"Analysis of surface quality in machining of metals and advanced ceramics", Ph.D. Thesis, Mechanical engineering department, Engineering research center – University of Maryland, Harvard, (1992).

[6] **Bhattacharyya, A.**, "Metal cutting theory and practice", New Central Book Agency (p) Ltd., (1996).

[7] **Devries, W. R.,** "Analysis of material removal processes", Springer-Verlag, New York, (1991).

[8] **Childs, T., Maekawa, K., Obikawa, T., Yamane, Y.,** "Metal machining theory and applications", John Wiley and sons Ins., (2000).

[9] **Karnopp, B.,** "Dynamics and vibrations", CRC Press LLC, (2000).

[10] **Peigne, G., Paris, H., Brissaud, D., Gouskov, A.,** "Impact of the cutting dynamics of small radial immersion milling operations on machined surface

roughness", International journal of machine tools and manufacture, Vol. 44, pp 1133-1142, (2004)

[11] **Toh, C. K.,** "Vibration analysis in high speed rough and finish milling hardened steel", Journal of Sound and Vibration, (2003).

[12] **Sarhan, A. ,** "Force based model for automated surface quality control in milling", M. Sc. Thesis, Mechanical engineering department, faculty of engineering-Assiut University, Assiut-Egypt, (1999).

[13] **Kishawy, H.**, "Chip formation and surface integrity in high speed machining of hardened steel", Doctor of philosophy, McMaster University, (1998).

[14] **Kirby, E. D., Zhang, Z., Chen, J. C.**, "Development of an accelerometer–based surface roughness predication system in turning operations using multiple regression techniques", Journal of Industrial Technology Vol. 20/4, pp 1-8, (2004).

[15] **Chang, H. K., Kim, J. H., Kim, I. H., Jang, D. Y., Han, D. C.,** "In-process surface roughness prediction using displacement signals from spindle motion", International journal of machine tools and manufacture, (2006).

[16] **Huang, L., Chen, J. C.**, "A multiple regression model to predict in-process surface roughness in turning operation via accelerometer", Journal of Industrial Technology Vol. 17/2, pp 1-8, (2001).

[17] **Samhouri, M. S., Surgenor, B. W.**, "Surface roughness in grinding: on-line prediction with adaptive neuro-fuzzy inference system", Proceeding of thirty-third Annual North American Manufacturing Research Conference, (NAMRC 33), (2005).

[18] **Savage, M. D., Chen, J. C.**, "Effects of tool diameter variations in on-line Surface roughness recognition system", Journal of Industrial Technology Vol. 15/4, pp 1-7, (1999).

[19] **Baek, D. K., Ko, T. J., Kim, H. S.,** "Optimization of feed rate in a face milling operation using a surface roughness model", International journal of machine tools and manufacture, Vol. 41, pp 451-462, (2001).

[20] **Colak, O., Kurbanoglu, C., Kayacan, M. C.,** "Milling surface roughness prediction using evolutionary programming methods", Materials and design, Vol. 28, pp 657-666, (2007).

[21] **Senussi, G. H., Akbar, A. A., Osman, H. M.,** "Effect of machining parameters in CNC-turning on surface roughness of 304-austenitic stainless steel", Fourth International Conference on Mechanical Engineering Advanced Technology for Industrial Production (MEATIP4), Assiut – Egypt, December 12-14, pp 690-598, (2006).

[22] **Abd El-Raaouf, A. M., Osman, M. S., El-Axir, M. H., Elshanawani, A. A.**, "Applicability of fuzzy approach for the optimization and analysis of surface roughness in orthogonal cutting", Seventh international conference on production engineering, design, and control, Alexandria-Egypt, pp 1261-1272, (2001).

[23] **Feng, C. X., Wang, X. F.**, "Surface roughness predictive modeling: Neural network versus regression", IIE Transactions on Design and Manufacturing, (2002).

[24] **Ozel, T., Karpat, Y.**, "Predictive modeling of surface roughness and tool wear in hard turning using regression and neural networks", International Journal of Machine Tools & Manufacture Vol. 45, pp 467–479, (2005).

[25] **Lee, K. C., Ho, S. J., Ho, S. Y.,** "Accurate estimation of surface roughness from texture features of the surface image using an adaptive neuro-fuzzy inference system", Precision engineering, Vol. 29, pp 95-100, (2005).

[26] **Jiao, Y., Lei, S., Pei, Z. J., Lee, E. S.,** "Fuzzy adaptive networks in machining process modeling: surface roughness prediction for turning operation", International journal of machine tools and manufacture, Vol. 77, pp 1643-1651, (2004).

[27] **Ho, S.-Y., Lee, K.-C., Chen, S.-S., Ho, S.-J.**, "Accurate modeling and prediction of surface roughness by computer vision in turning operations using an adaptive neuro-fuzzy inference system", International Journal of machine tools and manufacture Vol. 42, pp 1441-1446, (2002).

[28] **Dweiri, F., Al-Jarrah, M., Al-Wedyan, H.,** "Fuzzy surface roughness modeling of CNC down milling of Alumic-79", Journal of materials processing technology, Vol. 133, pp 266-275, (2003).

[29] **Lo, S. P.**, "An adaptive-network based fuzzy inference system for prediction of workpiece surface roughness in end milling", Journal of Materials Processing Technology Vol. 142, pp 665-675, (2003).

[30] **Soltan, I. M., Eltaib, M. E. H., El-Zahry, R. M.**, "Surface Roughness Prediction in End milling using Multiple Regressions and Adaptive Neuro-Fuzzy Inference System", Fourth International Conference on Mechanical Engineering Advanced Technology for Industrial Production (MEATIP4), Assiut – Egypt, December 12-14, pp 614-620, (2006).

[31] **Soltan, I. M., Eltaib, M. E. H., El-Zahry, R. M.**, "Surface Roughness Prediction in End milling using Adaptive Neuro-Fuzzy Inference System", Fourth International Conference on Advances in Production Engineering, APE'2007, Warsaw-Poland, 14-16 June, (2007).

[32] **Kumanan, S., Jesuthanam, C. P., Ashok Kumar, R.,** "Application of multiple regression and adaptive neuro fuzzy inference system for the prediction of surface roughness", international journal of advanced manufacturing technology, Vol. 35, pp 778-788, (2008).

[33] Ho, W. H., Tsai, J. T., Lin, B. T., Chou, J. H., "Adaptive network-based fuzzy inference system for prediction of surface roughness in end milling process using hubrid Taguchi-genetic learning algorithm", Expert system with applications, pp 1-7, (2008).

[34] **Schroeder, L. D., Sjoquist, D. L., Stephan, P. E.,** "Understanding regression analysis", Sage publications, Inc., (1986).

[35] **Montgomery, D. C., Runger, G. C.**, "Applied statistics and probability for engineers", John Wiley and Sons, Inc., (2003).

[36] **Ross, T., J.,** "Fuzzy logic with engineering applecations", 2nd edition, John Wiley and Sons, Ltd, (2005).

[37] **Kasabov, N.,** "Foundations of neural networks, fuzzy systems, and knowledge engineering", MIT Press, Cambridge, Massachusetts, London, England, (1998).

[38] **Jain, L. C., Martin, N. M.,** "Fusion of neural networks, fuzzy systems and genetic algorithm: industrial applications", CRC Press LLC, (1998).

[39] **Li, H., Chen, C. L. P., Huang, H. P.,** "Fuzzy neural intelligent systems: Mathematical foundation and the applications in engineering", CRC Press LLC, (2001).

[40] **Fausett, L.**, "Fundamentals of neural networks: architectures, algorithms, and applications", Upper Saddle River, NJ07458.

[41] **Principe, J. C, Co**, "Neural and adaptive systems: Fundamentals through simulations", John Wiley and Sons, Inc., (1999).

[42] **Jang, J.-S. R., Mizutani, E., Sun, C.-T.**, "Neuro-Fuzzy and Soft Computing", Prentic Hall Upper Saddle River, (1997).

[43] **Fuller, R.**, "Neural fuzzy systems", Springer-Verlag, Berlin/Heildelberg, (1995).

[44] **Lissaman, A. J., Martin, S. J.,** "Principles of engineering production", 2nd edition, English Language Book Society/Edward Arnold, (1988).

[45] **Ranganath, B., J.,** "Metal cutting and tool design", 2nd edition, Vikas Publishing House PVT LTD, New Delhi, (1999).

[46] **Korkut, I.**, "A dynamometer design and its construction for milling operation", Materials and design, Vol. 24, pp 631-637, (2003).

[47] **Saglam, H., Unuvar, A.,** "Three-component, strain gage based milling dynamometer design and manufacturing', Society for design and process science, Vol. 5/2, pp 95-109, (2001).

[48] **Yaldiz, S., Unsacar, F., Saglam, H., Isik, H.,** "Design, development and testing of a four-component milling dynamometer for the measurement of cutting force and torque" mechanical system and signal processing, (2006).

[49] **Ford, H.,** "Advanced mechanics of materials", Spottiswoode, Ballantyne and Co. LTD, London, (1963).

[50] **Histand, M. B., Alciatore, D. G.,** "Introduction to mechatronics and measurement systems", WCB/McGraw-Hill, (1999).

[51] **Morris, A. S.,** "Measurement and instrumentation principles", Butterworth and Heinemann, (2001).

[52] **Trent, E., M.,** "Metal cutting", 2nd edition, Butler and Tanner Ltd, Frome and London, Britain, (1984).

APPENDIXES

Appendix - A

Surface Texture

The three-dimensional structure of the surface is made up of surface asperities, or peaks and valleys which are usually traces of treatment or wear. These asperities are described by parameters of roughness and waviness, as well as flaws in the geometrical structure of the surface as shown in **Figure 1**. Therefore, they should be described in all three dimensions. However, practical difficulty with their measurements causes that the problem is reduced to a two-dimensional plane on which a roughness profile is traced.

Surface roughness is a mode of unevenness with usually small distances between peaks and valleys, less than in the case of waviness **Figure 2**. Roughness is defined as a set of asperities of the real surface, conventionally described as deviations of the measured profile from a reference line within the limits of a sample length [5].

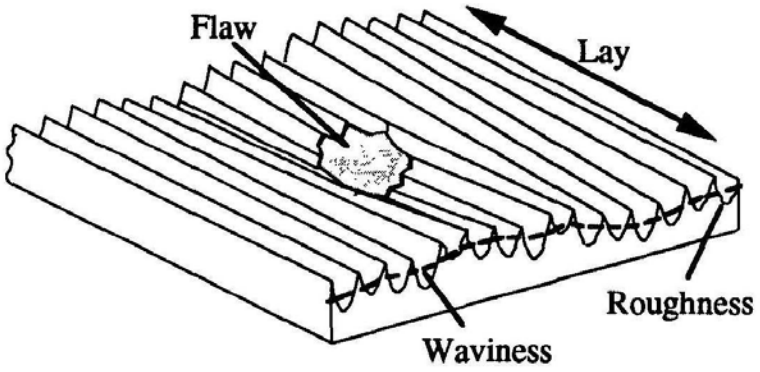

Figure 1 Surface texture to show; Roughness, Waviness, Flaws and Lay

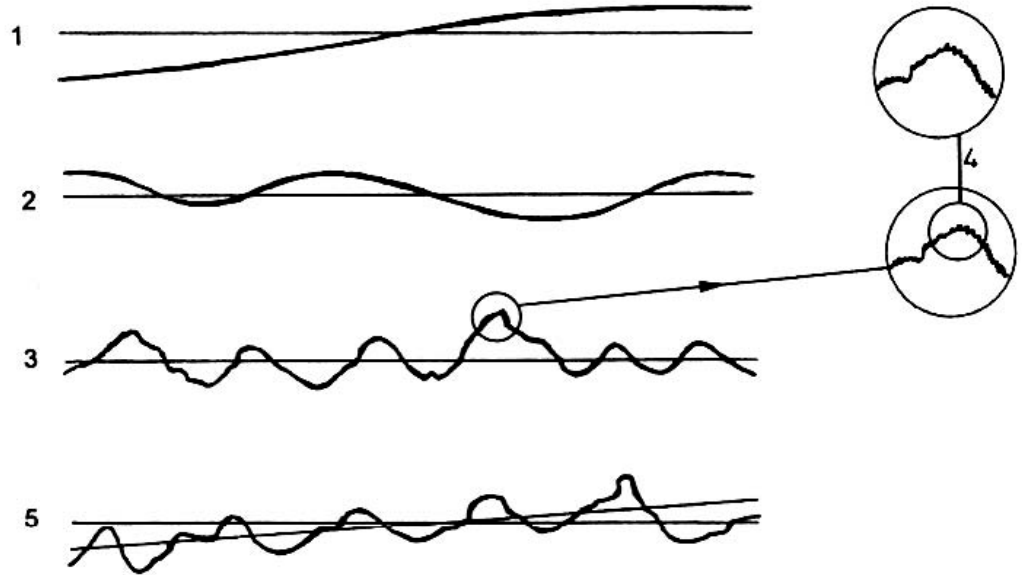

Figure 2 Elements and resultant unevenness of surface: 1 - shape flaw; 2 - waviness; 3 - roughness; 4 - submicroroughness; 5 - resultant structure of real surface.

Table 1 Surface profile parameters

Parameter	Name	Standards	Related
Height Parameters			
Ra	Roughness Average (Ra)	ASME B46.1-1995	Pa, Wa
Rq	Root Mean Square (RMS) Roughness	ASME B46.1-1995	Pq, Wq
Rt	Maximum Height of the Profile	ASME B46.1-1995	Pt, Wt
Rv, Rm	Maximum Profile Valley Depth	ASME B46.1-1995	Pv, Wv
Rp	Maximum Profile Peak Height	ASME B46.1-1995	Pp, Wp
Rpm	Average Maximum Profile Peak Height	ASME B46.1-1995	
Rz	Average Maximum Height of the Profile	ASME B46.1-1995	Pz, Wz, Rtm
Rmax	Maximum Roughness Depth	ASME B46.1-1995	Ry, Rymax, Rti,Rz
Rc	Mean Height of Profile Irregularities	ISO 4287/1-1997	Pc, Wc
Rz(iso)	Roughness Height	ISO 4287/1-1997	
Ry	Maximum Height of the Profile	ISO 4287/1-1997	
Wt, W	Waviness Height	ASME B46.1-1995	Rt,Pt
Spacing Parameters			
S	Mean Spacing of Local Peaks of the Profile	ISO 4287/1-1997	
Sm, RSm	Mean Spacing of Profile Irregularities	ASME B46.1-1995	PSm, WSm
D	Profile Peak Density	ISO 4287/1-1997	Sm
Pc	Peak Count (Peak Density)	ASME B46.1-1995	
HSC	Hight Spot Count		
λa	Average Wavelength of the Profile	ISO 4287/1-1997	
λ q	Root Mean Square (RMS) Wavelength of the Profile	ISO 4287/1-1997	
Hybrid Parameters			
Δa	Average Absolute Slope	ASME B46.1-1995	P Δ a, W Δ a
Δ q	Root Mean Square (RMS) Slope	ASME B46.1-1995	P Δ q, W Δ q
Lo	Developed Profile Length	ISO 4287/1-1997	lr
lr	Profile Length Ratio	ISO 4287/1-1997	Lo
ADF and BAC Parameters			
Rsk,Sk	Skewness	ASME B46.1-1995	Psk, Wsk
Rku	Kurtosis	ASME B46.1-1995	Pku, Wku
tp, Rmr(c)	Profile Bearing Length Ratio (Material Ratio of the Profile)	ASME B46.1-1995	Pmr(c), Wmr(c), Pmr, Rmr, Wmr
Htp, Rδc	Profile Section Height Difference	ASME B46.1-1995	
H	Swedish Height		Htp, Rt
Rk	Core Roughness Depth	ISO 13565-1996	
Rpk	Reduced Peak Height	ISO 13565-1996	Rpk*
Rvk	Reduced Valley Depth	ISO 13565-1996	Rvk*
Mr1	Material Portion	ISO 13565-1996	Rmr(c), tp
Mr2	Material Portion	ISO 13565-1996	Rmr(c), tp
Vo	"Oil-Retention" Volume		
Rpq, Rvq, Rmq	Material Probability Curve Parameters		

The terms surface finish and surface roughness are used very widely in industry and are generally used to quantify the smoothness of a surface finish. Many of the concepts of surface metrology and terminology are shown in **Table 1** and discussed as follows **[6]:**

• **Surface texture:** Surface texture is the pattern of the surface which deviates from a nominal surface. The deviations may be repetitive or random and may result from roughness, waviness, lay, and flaws.

• **Real surface:** The real surface of an object is the peripheral skin which separates it from the surrounding medium. This surface always assimilates structural deviations which are classified as form errors, waviness, and surface roughness.

• **Roughness:** Roughness consists of the finer irregularities of the surface texture, usually including those irregularities that result from the inherent action of the production process.

• **Roughness width:** Roughness width is the distance parallel to the nominal surface between successive peaks or ridges which constitute the predominant pattern of the roughness.

• **Roughness width cutoff:** Roughness width cutoff is included in the measurement of average roughness height which denotes the greatest spacing of repetitive surface irregularities.

• **Waviness:** Waviness should include all irregularities whose spacing is greater than the roughness sampling length and less than the waviness sampling length.

• **Lay:** Lay is the direction of the predominant surface pattern, normally determined by the production method.

• **Flaws:** Flaws are unintentional, unexpected, and unwanted interruptions in the topography typical of a part surface.

• **Roughness sampling length:** The roughness sampling length is the sampling length within which the roughness average is determined. This length is chosen, or specified, to separate the profile irregularities which are designated as roughness from those irregularities designated as waviness.

1 - Roughness Height Parameters

Ra - Average Roughness

Also known as Arithmetic Average (AA), Center Line Average (CLA), and Arithmetical Mean Deviation of the Profile.

The average roughness is the area between the roughness profile and its mean line, or the integral of the absolute value of the roughness profile height over the evaluation length:

$$R_a = \frac{1}{L}\int_0^L |r(x)|\,dx \quad \text{.....1}$$

Where L is the sampling length and r is the deviation from the mean line at the location along the x direction on which the trace was taken.

When evaluated from digital data, the integral is normally approximated by a trapezoidal rule:

$$R_a = \frac{1}{N}\sum_{n=1}^{N} |r_n| \quad \text{.....2}$$

Graphically, the average roughness is the area between the roughness profile and its center line divided by the evaluation length (normally five sample lengths with each sample length equal to one cutoff) as shown in **Figure 3**.

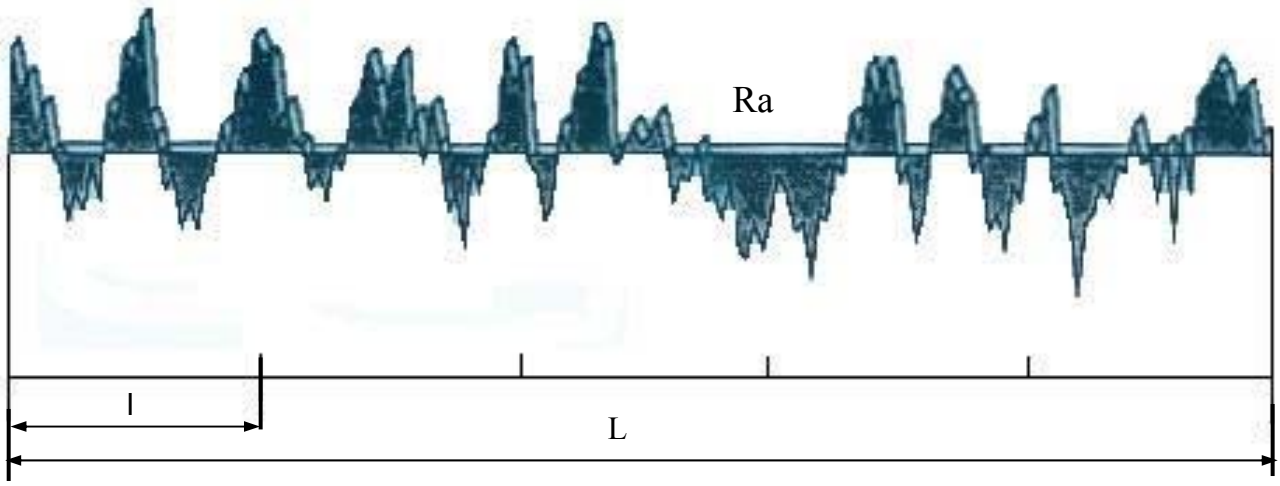

Figure 3 The average roughness, Ra.

The average roughness is by far the most commonly used parameter in surface finish measurement. The earliest analog roughness measuring instruments measured only Ra by drawing a stylus continuously back and forth over a surface and finding the average electronically. It is fairly easy to take the absolute value of a signal and to integrate a signal using only analog electronics. That is the main reason Ra has such a long history.

Ra does not tell the whole story about a surface. For example, here are three surfaces that all have the same Ra, but you need no more than your eyes to know that they are quite different surfaces, as shown in **Figure 4**. In some applications they will perform very differently as well. These three surfaces differ in the shape of the profile - the first has sharp peaks, the second deep valleys, and the third has neither.

Even if two profiles have similar shapes, they may have a different spacing between features, as shown in **Figure 5**. If we want to distinguish between surfaces that differ in shape or spacing, we need to calculate other parameters for a surface that measure peaks and valleys and profile shape and spacing. The more complicated the shape of the surface we want and the more critical the function of

the surface, the more sophisticated we need to be in measuring parameters beyond Ra.

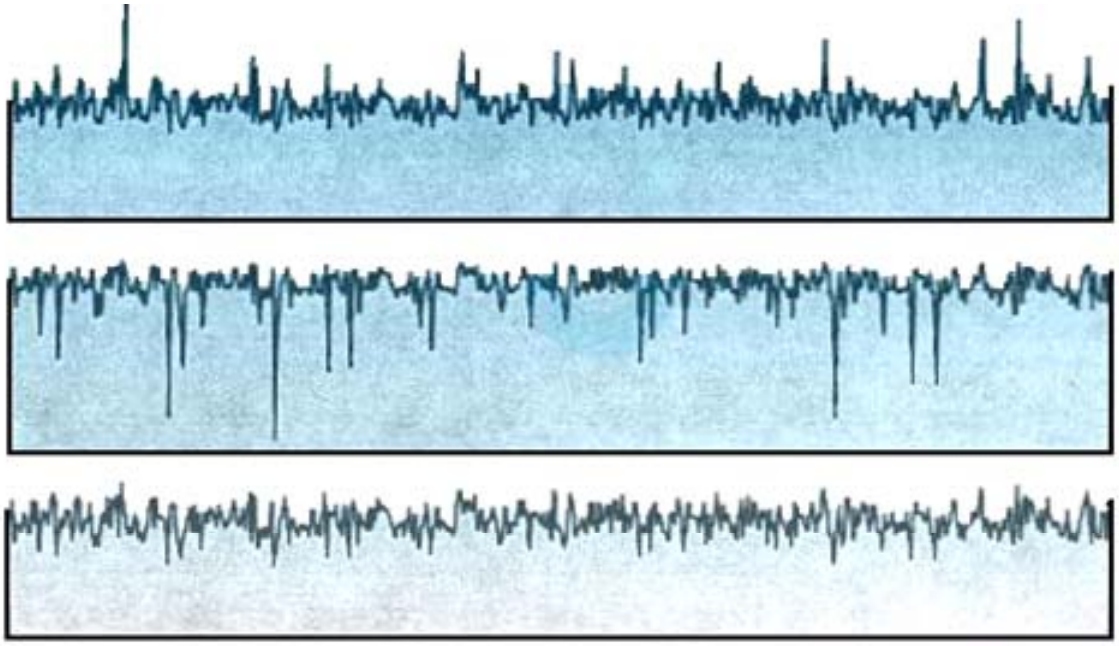

Figure 4 Three surfaces all have the same Ra but differ in the shape of the

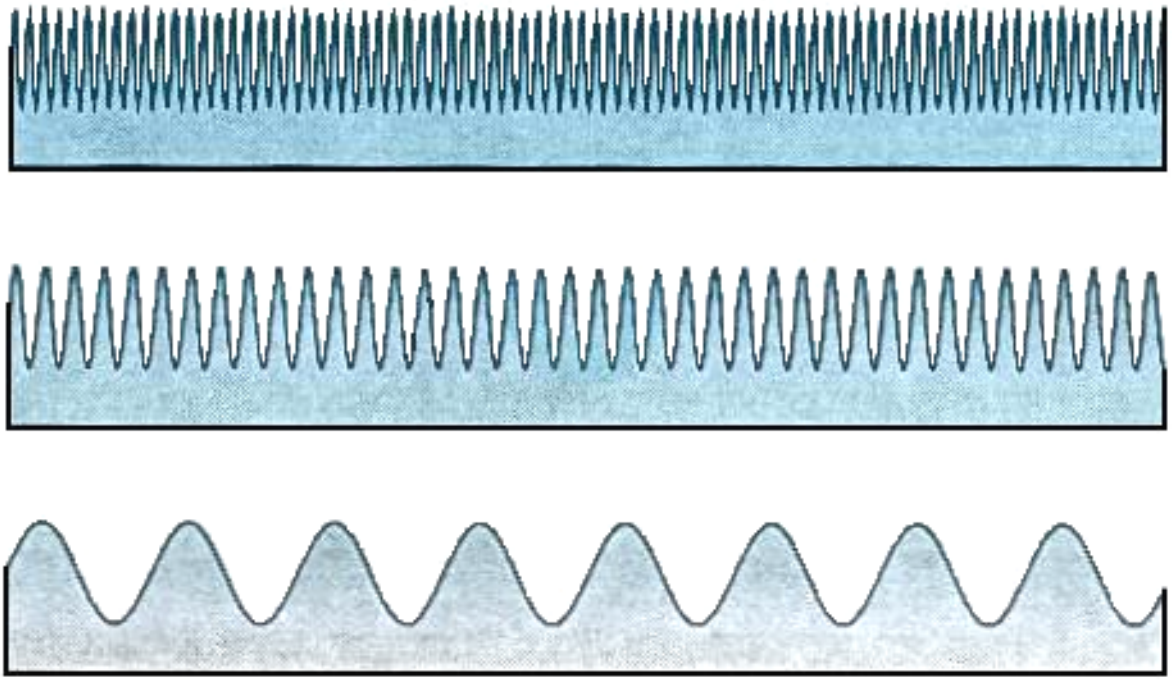

Figure 5 Three surfaces all have the same Ra and similar shapes of the profile.

Rq - Root-Mean-Square Roughness

The root-mean-square (rms) average roughness of a surface is calculated from another integral of the roughness profile:

$$R_q = \sqrt{\frac{1}{L}\int_0^L r^2(x)\mathrm{d}x} \qquad \text{……..3}$$

The digital equivalent normally used is:

$$R_q = \sqrt{\frac{1}{N}\sum_{n=1}^{N} r_n^2} \qquad \text{……..4}$$

For a pure sine wave of any wavelength and amplitude Rq is proportional to Ra; it's about 1.11 times larger. Older instruments made use of this approximation by calculating Rq with analog electronics and then multiplying by 1.11 to report Rq. However, real profiles are not simple sine waves, and the approximation often fails. Modern instruments either digitize the profile or do not report Rq.

Rq has now been almost completely replaced by Ra In metal machining specifications. Rq still has value in optical applications where it is more directly related to the optical quality of a surface.

Rt, Rp, and Rv

The peak roughness Rp is the height of the highest peak in the roughness profile over the evaluation length (p1 below). Similarly, Rv is the depth of the deepest valley in the roughness profile over the evaluation length (v1). The total roughness,

Rt, is the sum of these two, or the vertical distance from the deepest valley to the highest peak, as shown in **Figure 6**.

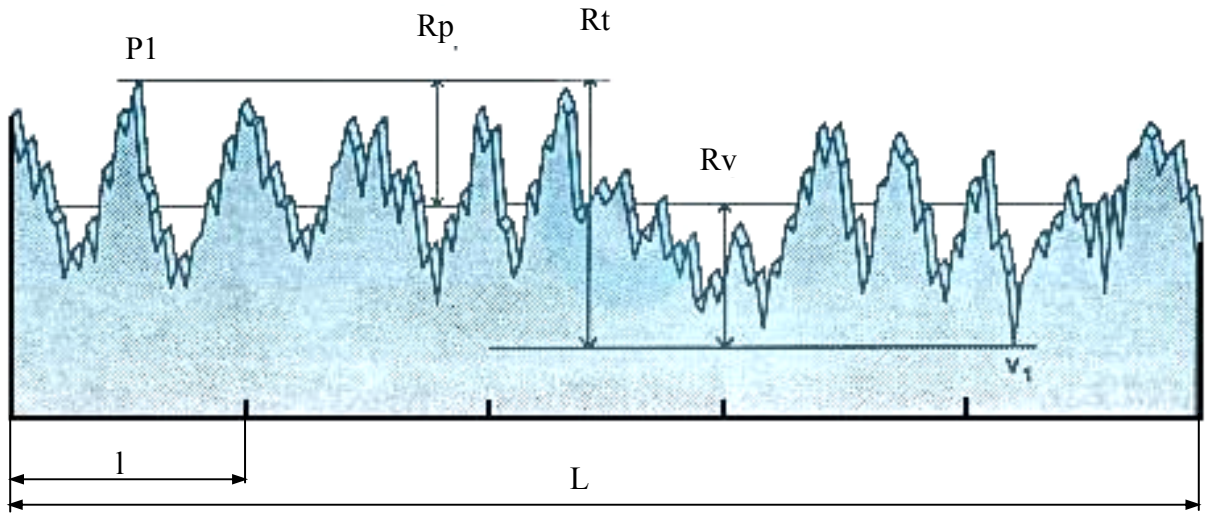

Figure 6 The maximum height of the profile, Rt

$$R_v = |\min[r(x)]|, \quad 0 < x < L \qquad \text{.....5}$$

$$R_p = |\max[r(x)]|, \quad 0 < x < L \qquad \text{.....6}$$

$$R_t = R_p + R_v \qquad \text{.....7}$$

These three extreme parameters will succeed in finding unusual conditions: a sharp spike or burr on the surface that would be detrimental to a seal for example or a crack or scratch that might be indicative of poor material or poor processing.

Rtm, Rpm and Rvm

These three parameters are mean parameters, meaning they are averages of the sample lengths. For example, define the maximum height for the i-th sample length as Rpi. Then Rpm is:

$$R_{pm} = \frac{1}{M}\sum_{i=1}^{M} R_{pi} \qquad \text{……8}$$

Similarly,

$$R_{vm} = \frac{1}{M}\sum_{i=1}^{M} R_{vi} \qquad \text{……9}$$

$$R_{tm} = \frac{1}{M}\sum_{i=1}^{M} R_{ti} = R_{pm} + R_{vm} \qquad \text{……10}$$

Where Rvi is the depth of the deepest valley in the i-th sample length and Rti is the sum of Rvi and Rpi:

$$\begin{aligned} R_{vi} &= \left|\min\left[r(x)\right]\right| \quad il < x < (i+1)l \\ R_{pi} &= \left|\max\left[r(x)\right]\right| \quad il < x < (i+1)l \\ R_{ti} &= R_{pi} + R_{vi} \end{aligned} \qquad \text{……11}$$

These three parameters have some of the same advantages as Rt, Rp, and Rv for finding extremes in the roughness, but they are not so sensitive to single unusual features.

Rymax (or Rmax) - Maximum Roughness Height within a Sample Length

Ry and Rmax are other names for Rti. Rmax is the older American name. Ry is the newer ISO and American name. For a standard five cutoff trace there are five different values of Ry. Ry is the maximum peak to lowest valley vertical distance within a single sample length.

Rymax is an ISO parameter that is the maximum of the individual or Rmax (i.e. Rti) values.

$$R_{y\max} = \max[R_{ti}] \quad 1 \le i \le M \qquad \text{……..12}$$

Serves a purpose similar to Rt, but it finds extremes from peak to valley that are nearer to each other horizontally.

Rz(DIN) -Average Maximum Height of the Profile

Rz(DIN), i.e. Rz according to the German DIN standard, is just another name for Rtm in the American nomenclature. (Over five cutoffs)

$$R_z[\mathrm{DIN}] = R_{tm} \qquad \text{……..13}$$

Rz(ISO) - Roughness Height

Rz(ISO) is the sum of the height of the highest peak plus the lowest valley depth within a sampling length, as shown in **Figure 7**.

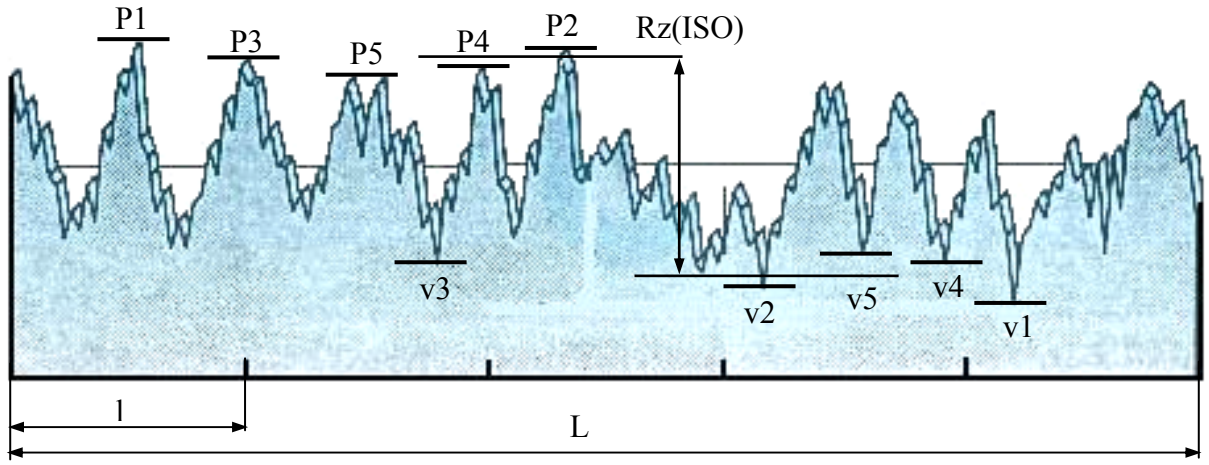

Figure 7 Roughness height, Rz(ISO)

R3zi - Third Highest Peak to Third Lowest Valley Height

The parameter R3zi is the height from the third highest peak to the third lowest valley within one sample length as shown in **Figure 8**.

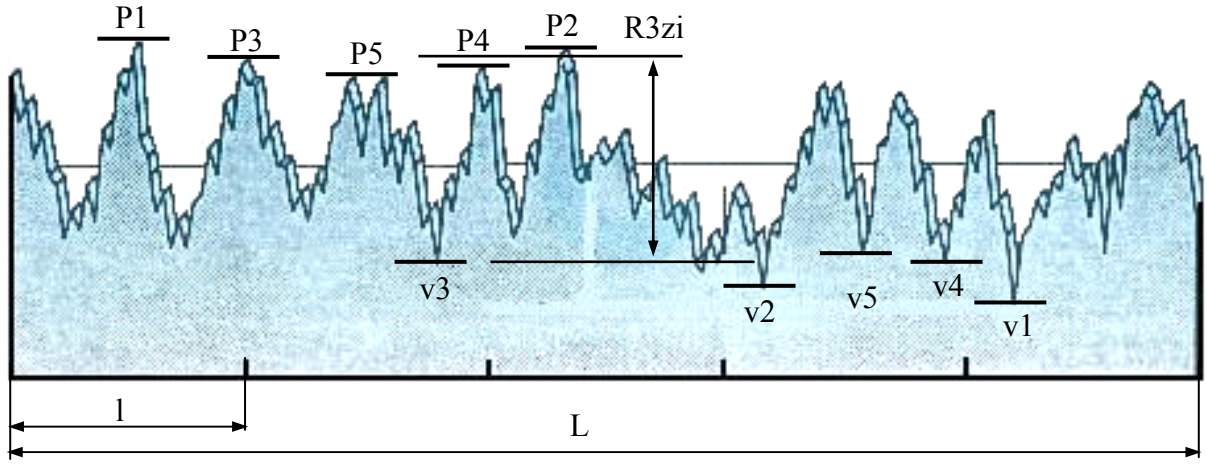

Figure 8 Third highest peaks to third lowest valley height

R3z - Average Third Highest Peak to Third Lowest Valley Height

R3z is the average of the R3zi values:

$$R_{3z} = \frac{1}{M}\sum_{i=1}^{M} R_{3zi} \quad \text{.....14}$$

R3z has much the same purpose as Rz except that less extreme peaks and valleys are being measured.

R3zmax - Maximum Third Highest Peak to Third Lowest Valley Height

R3zmax is the maximum of the individual R3zi values:

$$R_{3z\,max} = \max[R_{3zi}], \quad 1 \le i \le M \qquad \text{……15}$$

R3z and R3zmax are not defined in national standards, but they have found their way into many high-end instruments. They originated in Germany as a Daimler-Benz standard.

2 - Roughness Spacing Parameters

Pc - Peak Count

Peak count is a number giving the number of peaks per length of trace in a profile. For the purpose of calculating Pc a "peak" is defined relative to an upper and lower threshold. Usually this is a single number, the "peak count threshold", the distance from a lower threshold up to an upper threshold, centered on the mean line. A peak must cross above the upper threshold and below the lower threshold in order to be counted, as shown in **Figure 9**.

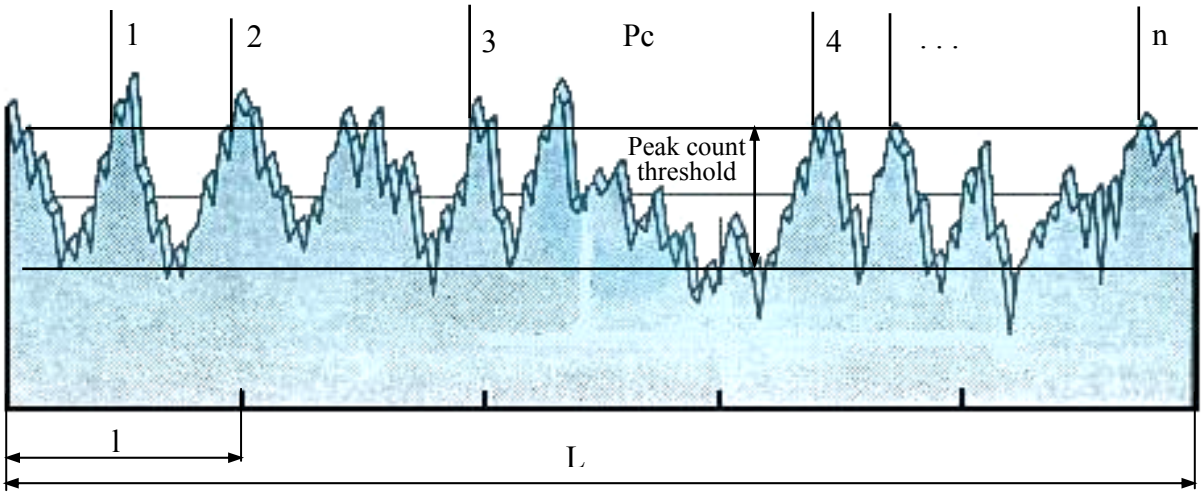

Figure 9 peak counts, Pc

Peak count is the number of peaks in the evaluation length divided by the evaluation length. (Or to be picky, by the distance from the beginning of the first peak to the end of the last peak). Pc is thus reported as [peaks/in] or [peaks/cm].

Some instruments allow the thresholds to be centered on a height that differs from the mean line. This is nonstandard but may be convenient. For example) a pair of thresholds that counts low peaks accompanied by deeper valleys may be appropriate for plateau surfaces.

The value obtained for Pc depends quite heavily on the peak count threshold for most surfaces. The figure below shows peak count versus threshold for a ground surface and a turned surface as representative samples. For the ground surface the parameter shows no stability. For the turned surface there is a bit of flattening out at a threshold of about 40 µin, but even for this surface Pc shows a wide variation with threshold, as shown in **Figure 10**.

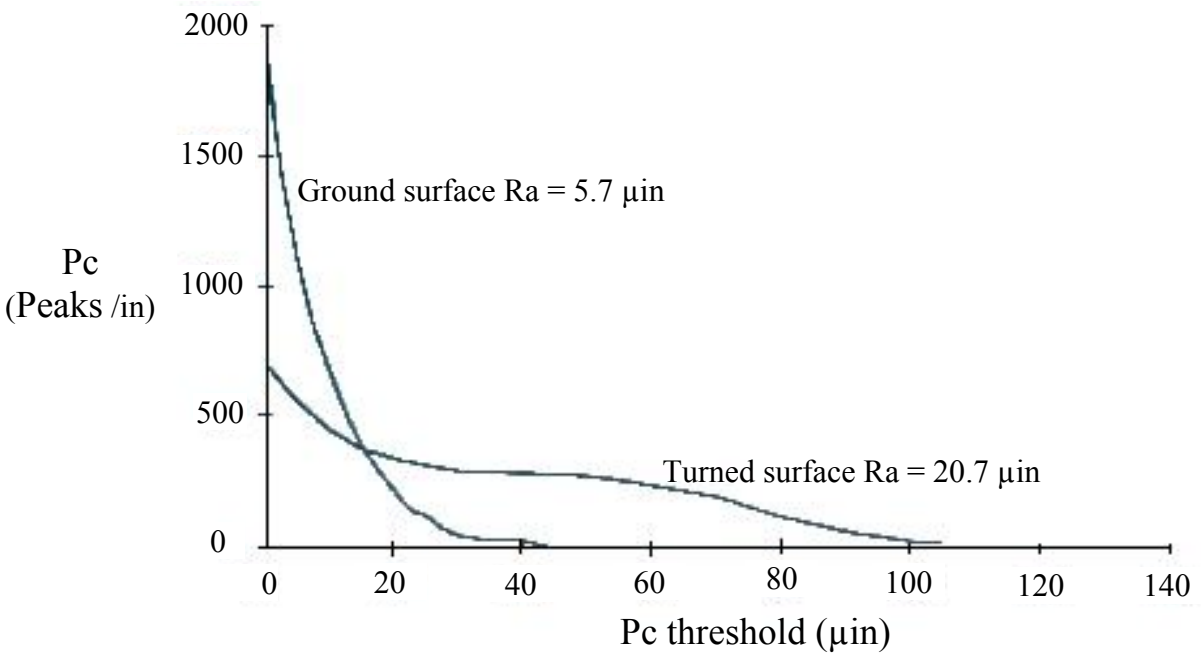

Figure 10 Peak count versus threshold for a ground surface and a turned surface

HSC - High Spot Count

High spot count, HSC, is similar to peak count except that a peak is defined relative to only one threshold. High spot count is the number of peaks per inch (or cm) that cross above a certain threshold. A "peak" must cross above the threshold and then back below it, as shown in **Figure 11**.

High spot count is commonly specified for surfaces that must be painted. A surface which has protrusions above the paint will obviously give and undesirable finish.

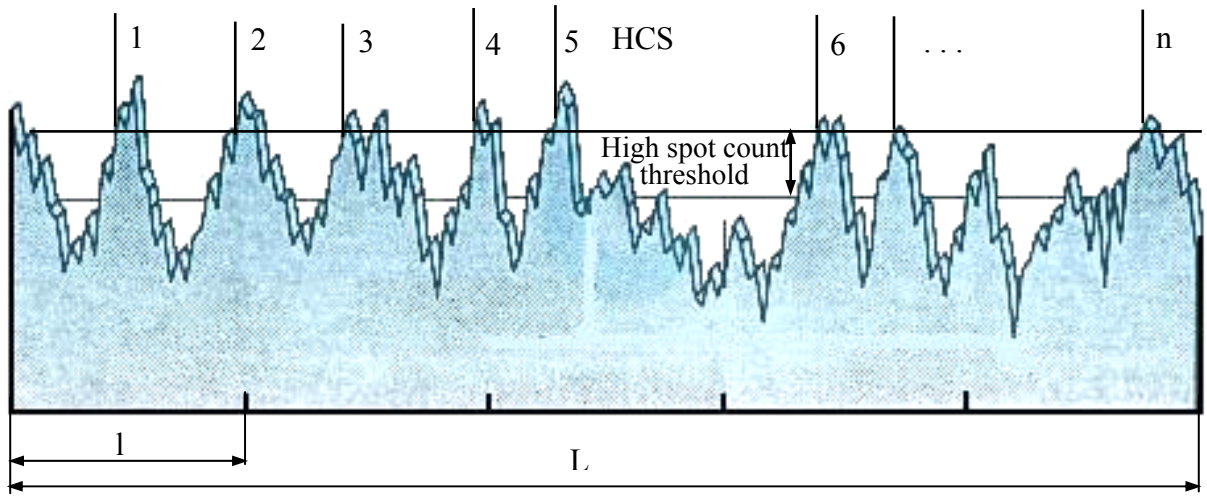

Figure 11 High spot count, HCS

Sm - Mean Spacing

Sm is the mean spacing between peaks, now with a peak defined relative to the mean line. A peak must cross above the mean line and then back below it, as shown in **Figure12**.

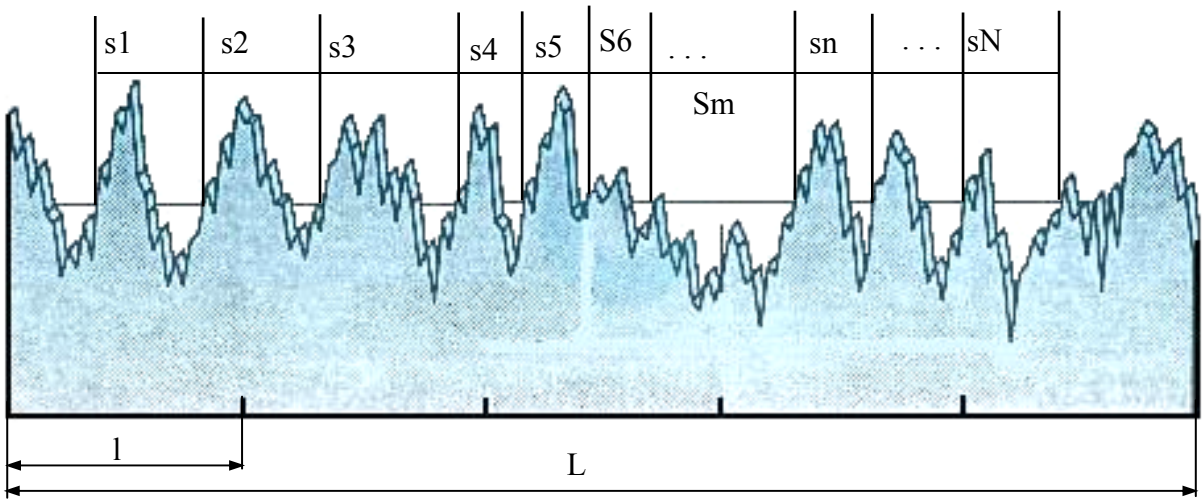

Figure 12 Mean spacing, Sm

If the width of each peak is denoted as Si, then the mean spacing is the average width of a peak over the evaluation length:

$$S_m = (1/N) \sum_{n=1}^{N} S_n \qquad \text{……16}$$

Sm is usually reported in µin or µm.

λa - Average Wavelength

The average wavelength of the surface is defined as follows:

$$\lambda_a = 2\pi \frac{R_a}{\Delta_a} \qquad \text{……17}$$

This parameter is analogous to Sm in that it measures the mean distance between features, but it is a mean that is weighted by the amplitude of the individual wavelengths, whereas Sm will find the predominant wavelength.

λq - RMS Average Wavelength

$$\lambda_q = 2\pi \frac{R_q}{\Delta_q} \qquad \text{……18}$$

λpc - Peak Count Wavelength

$$\lambda_{pc} = \frac{1}{P_c} \qquad \text{……19}$$

The above formula leaves in the reciprocal units of λpc. Therefore the value must ordinarily be converted from [in] to [λin] or from [cm] to [λm].

3 - Roughness Hybrid Parameters

Δa - Average Absolute Slope

This parameter is the average of the absolute value of the slope of the roughness profile over the evaluation length:

$$\Delta_a = \frac{1}{L}\int_0^L \left|\frac{dr(x)}{dx}\right| dx \qquad \text{……20}$$

It is not so straightforward to evaluate this parameter for digital data. Numerical differentiation is a difficult problem in any application. Some instrument manufacturers have applied advanced formulas to approximate dz/dx digitally, but the simplest approach is to apply a simple difference formula to points with a specified spacing L/N:

$$\Delta_a = \frac{1}{L}\sum_{n=1}^{N}\left|r_{n+1} - r_n\right| \quad \text{.....21}$$

If this approach is used, the value of L/N must be specified since it greatly influences the result of the approximation. Ordinarily L/N will be quite a bit larger than the raw data spacing from the instrument.

Δq - RMS Average Slope

$$\Delta_q = \sqrt{\frac{1}{L}\int_0^L \left(\frac{\mathrm{d}r(x)}{\mathrm{d}x}\right)^2 \mathrm{d}x} \quad \text{.....22}$$

$$\Delta_q = \sqrt{\frac{1}{L}\sum_{n=1}^{N}\left(r_{n+1} - r_n\right)^2} \quad \text{.....23}$$

Lo - Actual Profile Length

One way to describe how a real profile differs from a flat line is to determine how long the real profile is compared to the horizontal evaluation length. Imagine the profile as a loose string that can be stretched out to its full length.

The 2-D length of a profile comes from the following equation:

$$L_o = \int_0^L \sqrt{1 + \left(\frac{dr(x)}{dx}\right)^2}\, dx \quad \text{……24}$$

As for **Δ**a and **Δ**q, the answer in a digital evaluation depends on the spacing of the points we choose to approximate dr/dx:

$$L_o = \sum_{n=1}^{N} \sqrt{\left(\frac{L}{N}\right)^2 + (r_{n+1} - r_n)^2} \quad \text{……25}$$

Lr - Profile Length Ratio

The profile length ratio, Lr, is the profile length normalized by the evaluation length:

$$L_r = \frac{L_o}{L} \quad \text{……26}$$

The profile length ratio is a more useful measure of surface shape than Lo since it does not depend on the measurement length.

The larger the value of Lr, the sharper or crisper the surface profile appears and the larger the true surface area of the surface is. In some applications, particularly in coating, where good adhesion is needed, it may be desirable to have a large value of Lr, i.e. a large contact surface area.

For most surfaces Lr is only slightly larger than one and is difficult to determine accurately.

Statistical Analysis

The Amplitude Distribution Function

The amplitude distribution function (ADF) is a probability function that gives the probability that a profile of the surface has a certain height, z, at any position x. Ordinarily the ADF is computed for the roughness profile, although the texture or even primary profiles might be used in specialized applications.

The ADF has a characteristic bell shape like many probability distributions, as shown in **Figure 13**. The ADF tells "how much" of the profile lies at a particular height, in a histogram sense. It is the probability that a point on the profile at a randomly selected x value lies at a height within a small neighborhood of a particular value z:

$$\mathrm{Prob}(z + dz > r(x) > z) = \mathrm{ADF}(z)dz \quad \text{.....27}$$

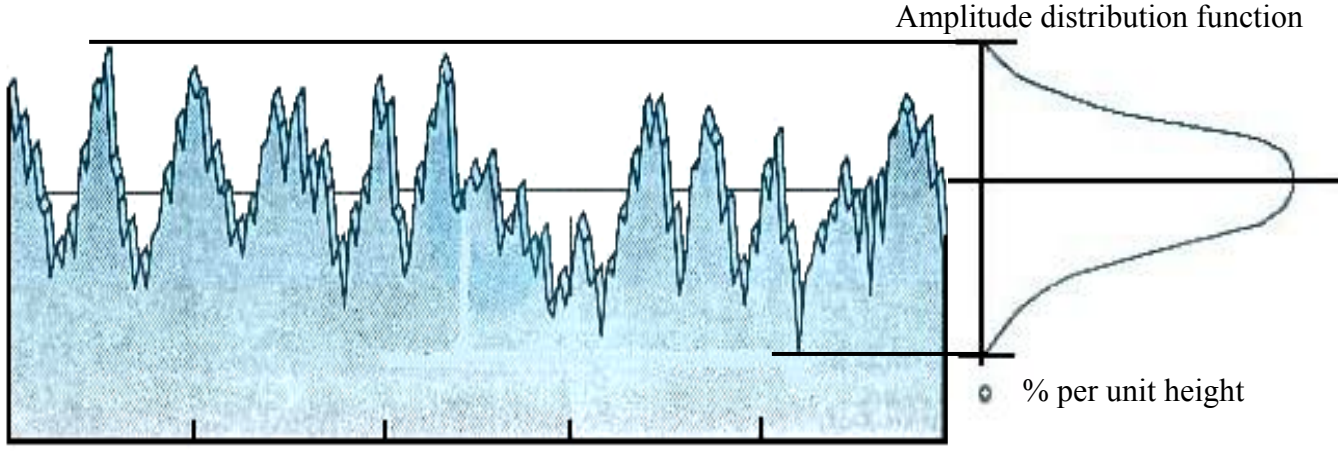

Figure 13 The amplitude distribution function

The Bearing Ratio Curve

The Bearing Ratio Curve is related to the ADF, it is the corresponding cumulative probability distribution and sees much greater use in surface finish. The bearing ratio curve is the integral (from the top down) of the ADF.

We postpone further discussion of the bearing ratio curve until a later section, after we have considered other statistical techniques that work with a profile directly or are related to the shape of the ADF.

Other names for the bearing ratio curve are the bearing area curve (this is becoming obsolete with the increase in topographical methods), the material ratio curve, or the Abbott-Firestone curve.

4 - Statistical Parameters

Rq - Root-Mean-Square Roughness

The root-mean square average roughness, Rq, was defined earlier. We note at this point, though that is the variance of the amplitude distribution function. In this sense it is a statistical parameter that measures the width of the ADF: the wider the ADF, and the rougher the surface.

Rsk – Skewness

Skewness is another parameter that describes the shape of the ADF. Skewness is a simple measure of the asymmetry of the ADF, or, equivalently, it measures the symmetry of the variation of a profile about its mean line.

$$R_{sk} = \frac{1}{LR_q^3}\int_0^L r^3(x)\mathrm{d}x \quad \text{……28}$$

Or

$$R_{sk} = \frac{1}{NR_q^3}\sum_{n=1}^{N} r_n^3 \quad \text{……29}$$

Surfaces with a positive skewness, such as turned surfaces have fairly high spikes that protrude above a flatter average. Surfaces with negative skewness, such as porous surfaces have fairly deep valleys in a smoother plateau. More random (e.g. ground) surfaces have a skew near zero, as shown in **Figure 14**.

The skewness parameter correlates with load carrying capability, porosity, and other characteristics of surfaces produced by processes other than conventional machining. A value of Rsk greater than about 1.5 in magnitude (positive or negative) indicates that the surface does not have a simple shape and a simple parameter such as Ra is probably not adequate to characterize the quality of the surface. For example, as shown in **Figure 14**, each surface has about the same Rt, but the surfaces are quite different.

Note that skewness is non-dimensional. Often the skewness is denoted as "Sk" instead of Rsk.

Surfaces with a large positive skewness can cause large measurement errors when measured with skidded instruments, particularly if there is a large spacing between the spikes of the surface.

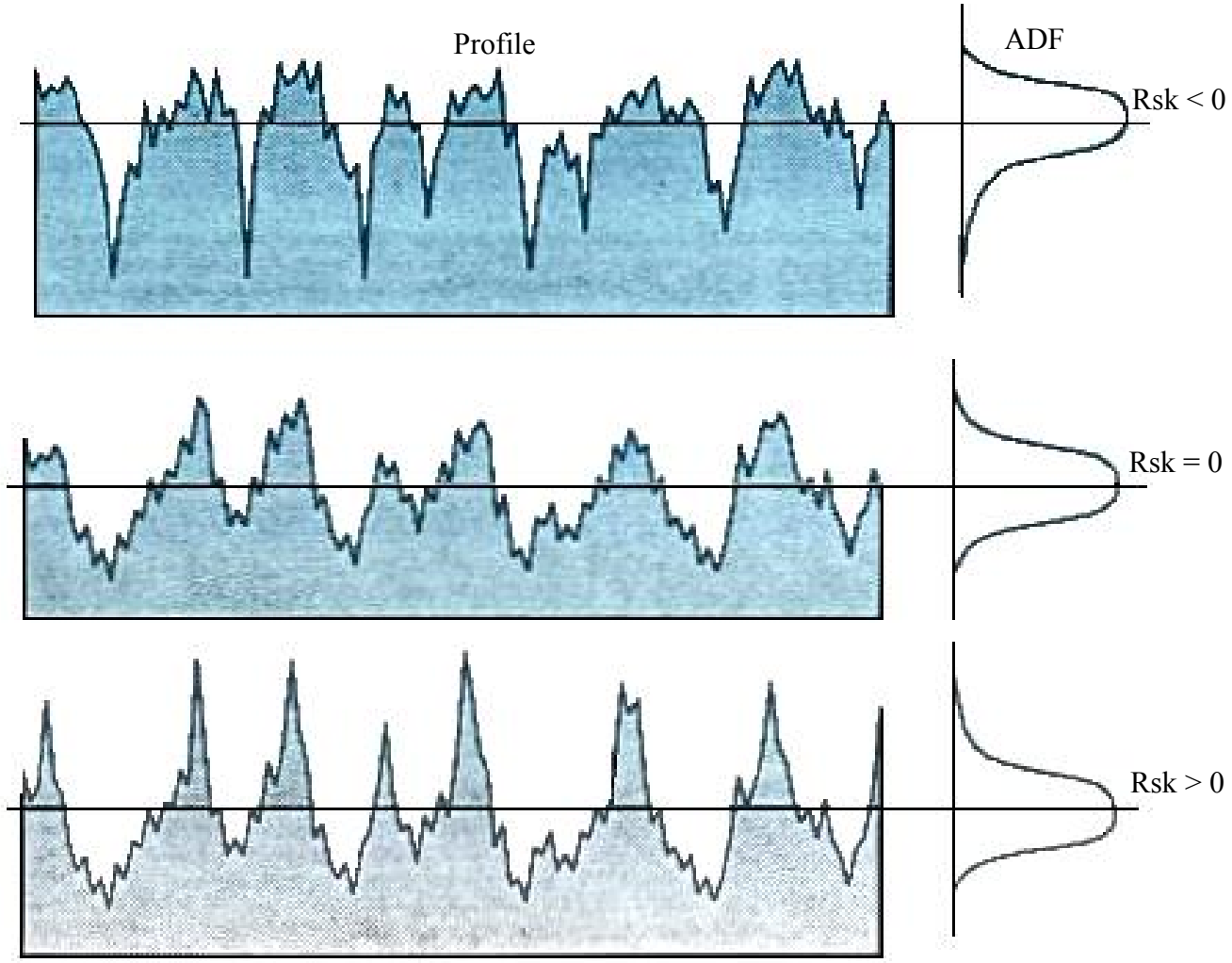

Figure 14 Skewness, Rsk

Rku – Kurtosis

Kurtosis is the last ADF shape parameter considered. Kurtosis relates to the uniformity of the ADF or, equivalently, to the spikiness of the profile.

$$R_{sk} = \frac{1}{NR_q^3}\sum_{n=1}^{N} r_n^3 \quad \text{……30}$$

Or

$$R_{ku} = \frac{1}{NR_q^4}\sum_{n=1}^{N} r_n^4 \quad \text{……31}$$

A reader familiar with statistics will recognize that Rq, Rsk, and Rku are related to moments of the ADF probability distribution.

Bearing Ratio Analysis

Physical Significance of the Bearing Ratio Curve

The bearing ratio curve mathematically is the integral of the amplitude distribution function. It is a cumulative probability distribution. Ordinarily, the integral is performed from the highest peak downward, so each point on the bearing ratio curve has the physical significance of showing what linear fraction of a profile lies above a certain height (compared to the ADF which tells how much of a surface lies at a given height) as shown in **Figure 15**.

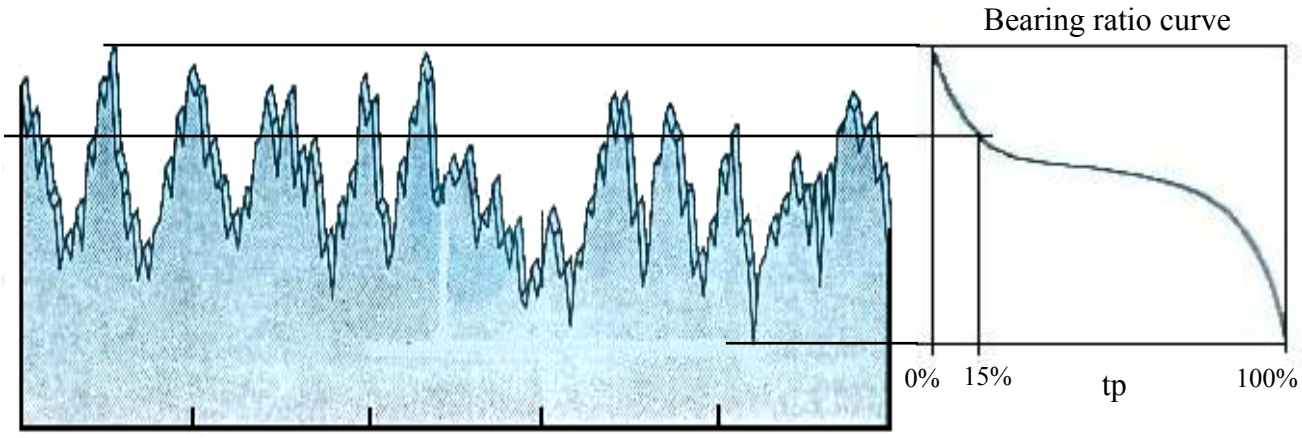

Figure 15 Physical Significance of the bearing ratio curve

Simple Bearing Ratio Parameters

tp - Bearing Ratio

The symbol tp has two meanings. First, it is used generically as the abscissa of the bearing ratio curve. It is just a percent bearing ratio. Second, tp as a parameter refers to the bearing ratio at a specified height. The most common way of specifying the height is to move over a certain percentage (the reference percent) on the bearing ratio curve and then to move down a certain depth (the slice depth). The bearing ratio at the resulting point is "tp" as shown in **Figure 16**. The purpose of the reference percent is to eliminate spurious high peaks from consideration; these will wear off in early part use. The slice depth then corresponds to an allowable roughness or to a reasonable amount of wear.

Another common way of choosing the height level for tp is as a distance up or down from the mean line of the roughness profile.

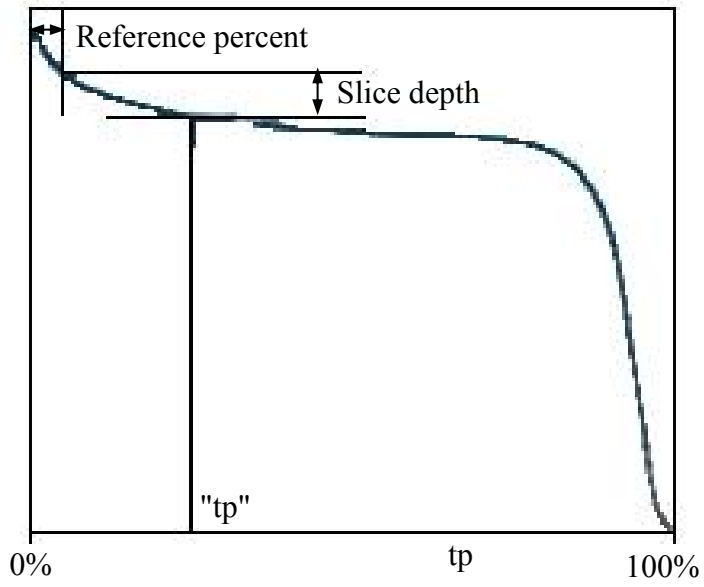

Figure 16 Bearing ratio curve (tp)

Htp - Bearing Height

The parameter tp is the bearing ratio at only one point. If we want to measure the roughness of the surface from the bearing ratio curve, it become appropriate to look at two points on the curve and look at the height difference between them as shown in **Figure 17**. The bearing height is the height between two points on the bearing ratio curve at specified values of tp, tp1 and tp2. These specified values will depend on the application.

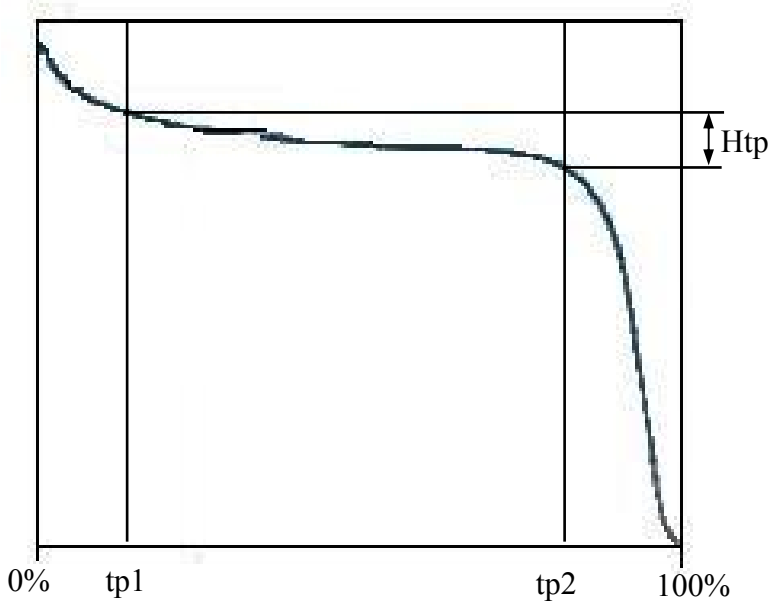

Figure 17 Bearing Height

H - Swedish Height

The Swedish height parameter, H, is just Htp with specific values for tp1, and tp2, namely 5% and 90%. H thus has a purpose similar to Rt, but is not as strongly influenced by occasional high peaks or deep valleys.

Waviness Profile Parameters

So far we have considered parameters derived from the roughness profile. This is by far the most common type of parameter measured. However, in some applications we may be concerned with surface texture deviations with longer wavelengths. Statistical parameters of the waviness profile may be evaluated just as they are for the roughness profile.

One major problem with evaluating waviness parameters is that a longer trace length is needed in order to have statistically significant results. There is no standard for how long is long enough or how to break the waviness into separate sample lengths as we do for roughness. Thus the following parameters do not have such a rigorous connection to sample length and filter cutoff. Usually they are evaluated for one sample length equal to the longest trace possible on a particular part with a particular instrument.

Wt - Total Waviness Height

Like Rt, Wt is the height from the lowest valley to the highest peak of the waviness profile.

Before digital instruments and phase-correct filtering, there was no way to compute the waviness cleanly. It was common in such a case to compute Wt by an approximation:

$$W_t \approx P_t - R_t \quad \text{.....32}$$

The worst deviation of the roughness plus the worst deviation of the waviness is approximately equal to the worst deviation of the texture or total profile. This approximation should be unnecessary with modern instruments.

Wa - Average Waviness

Another parameter used to report waviness is the arithmetic absolute average, analogous to the ubiquitous Ra.

$$W_a = \frac{1}{L}\int_0^L |w(x)|\,dx \quad \text{.....33}$$

Or

$$W_a = \frac{1}{N}\sum_{n=1}^{N} |w_n| \quad \text{.....34}$$

Advanced Statistical and Bearing Ratio Analysis

Rk Parameters

There is a significant amount of information encapsulated in the shape of the bearing ratio curve for a surface. Recent efforts in surface finish have tried to summarize that shape information in a few parameters. The Rk parameters are a simple approach where the knee-shaped BAC is approximated by a set of straight lines.

Rk Construction

The Rk construction is designed to divide the bearing ratio curve into three sections: the small peaks above the main plateaus, the plateaus themselves, and the deep valleys between plateaus.

The first step is to slide a "window" across the bearing ratio curve looking for the minimum secant slope. The window is 40% tp wide. As the window slides across the curve it intersects two points on the curve. The goal is to find the position where the slope between the two points is minimized, or since the window has constant width, where the height Htp between the two points is minimized as shown in **Figure 18**.

Once the window with minimum secant slope is found, a fairly complicated construction begins. In **Figure 19** we have found the minimum slope window and the points A and B where the window intersects the bearing ratio curve. Next draw a line through these two points to find the intercepts at 0% and 100%, points C and D. The vertical height between C and D is the first parameter, Rk. Draw a horizontal line across from C to the bearing ratio curve, point E. Find the area below the bearing ratio curve and above the line CE, shown shaded in the upper part of the figure. Next, compute Rpk as the height of triangle CEG which has the same area as the shaded area. For the valleys draw a horizontal line from D over to point F on the curve. Compute the area of the air space below line DF and above the bearing ratio curve (shown shaded in the lower part of the figure). Next compute the height, Rvk, of triangle DFH which has the same area as the shaded region.

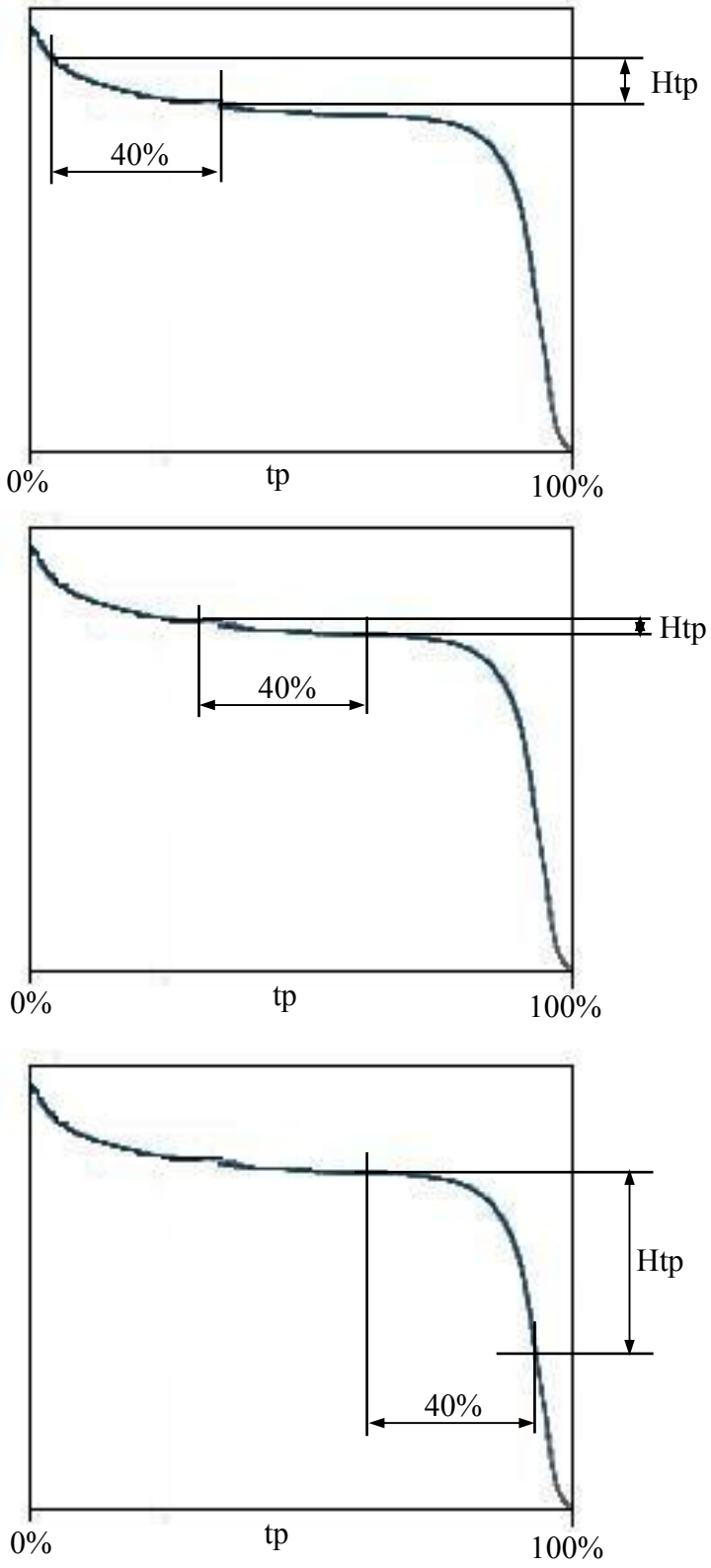

Figure 18 The bearing ratio curve divide into three sections

Rk

The parameter Rk is the vertical height between the left and right intercepts of the - line through the ends of the minimum Htp 40% window.

Rk correlates with the depth of the working part of the surface, the flat part of the bearing area curve. After the initial running in period (i.e. after the peaks represented by Rpk are worn down), this part of the surface carries the load and most closely contacts the mating surface. Sometimes this part of the surface is called the "core roughness" or the "kernel" (hence the k subscript).

Rpk

Rpk is an estimate of the small peaks above the main plateau of the surface. These peaks will typically be worn off (or down) during the run-in period for a part. Generally, it would be desired to have a fairly small Rpk.

Rvk

Rvk is an estimate of the depth of valleys which will retain lubricant in a functioning part.

MR1

MR1 is the fraction of the surface which consists of small peaks above the main plateau.

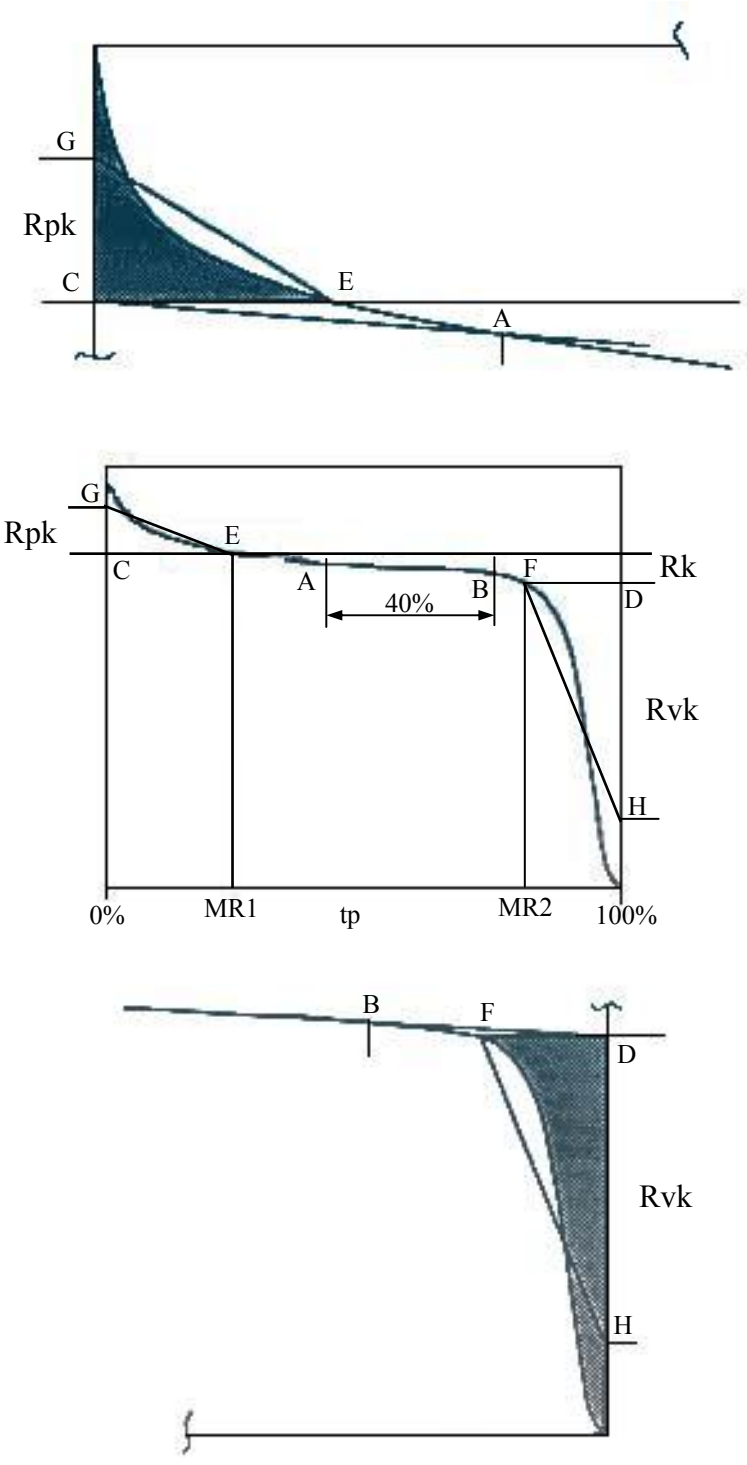

Figure 19 Rk Construction

MR2

MR2 is the fraction of the surface which will carry load during the practical lifetime of the part. Alternatively, 100%-MR2 is the fraction of the surface that consists of deeper valleys that will retain lubricant.

A1

The "area" of the peak portion of the bearing ratio curve is denoted by A1. It is related to Rpk and MR1:

$$A_1 = \frac{1}{2}\frac{R_{pk}MR_1}{100\%} \quad \text{.....35}$$

A2

The "area" of the valleys in the Rk construction is denoted by A2. It is related to Rvk and MR2:

A2 is also called Vo, the oil retention "volume" of the surface.

$$A_2 = \frac{1}{2}\frac{R_{vk}(100\% - MR_2)}{100\%} \quad \text{.....36}$$

Gaussian Probability Scale

The Gaussian probability scale linearizes the cumulative Gaussian distribution. The slope of the line is Rq as shown in **Figure 20**.

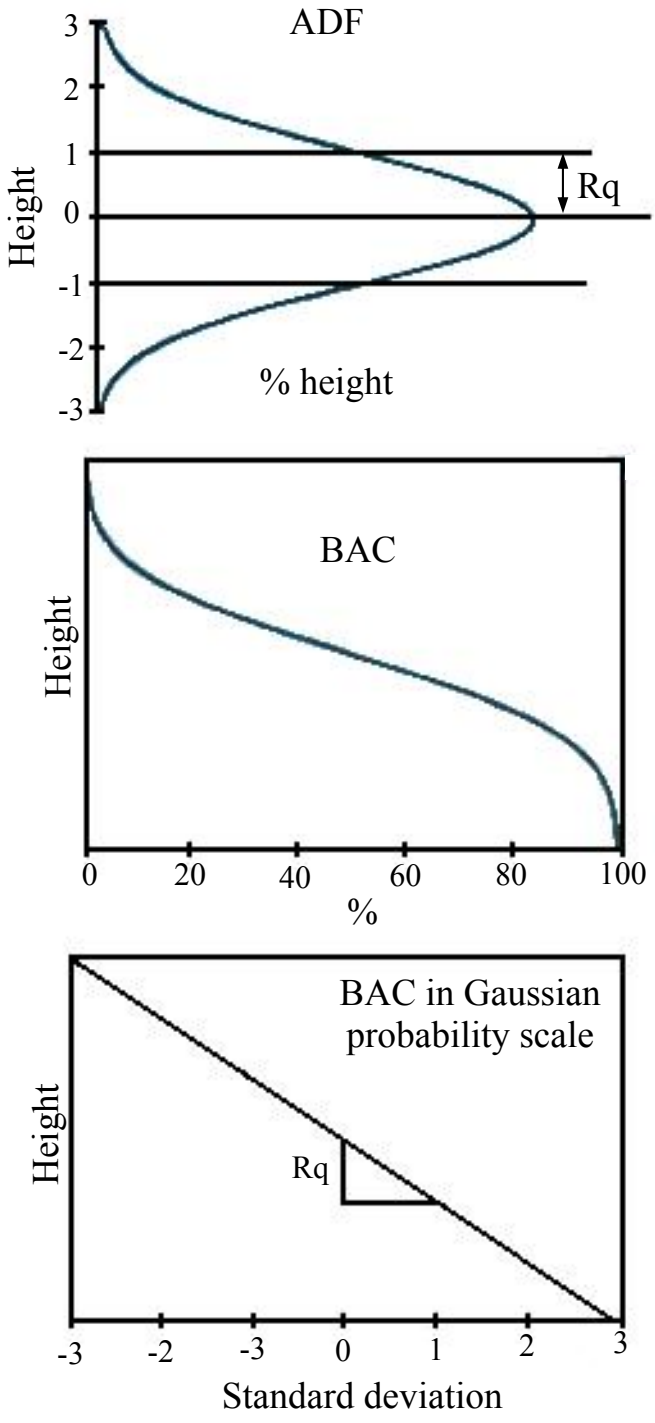

Figure 20 Gaussian probability scales

Appendix - B

Operational amplifiers (OPAMP)

The amplifier specifications as follow:

Controls: Fine gain: +/- 15% full scale – overlaps into each adjacent gain range.

Course zero: +/- 45% full scale at 10 mv input range.

Fine zero: +/- 15% full scale at 10 mv input.

Input: 8 switch-selectable ranges between 0.43 mv/v and 4.8 mv/v.

Output: 0-5 VDC.

Performance: Accuracy: </= 0.025% full scale

Operating temperature: 0^0 F to 130^0 F

Frequency response: 0-3000 Hz

Noise: 10 mv RMS maximum

Appendix - C

Data acquisition card (ADC)

The ADC specifications as follow:

Digital outputs I/O 1 to I/O 16:

Opto-coupler, open collector output: 50mA, max 30 VDC.

Minimum conversion time to set 16 output: 800µs.

Digital inputs I/O 1 to I/O 16:

Opto-coupler input: min 5V/5mA, max 20/40mA.

Minimum conversion time to read 16 inputs: 800 µs.

Analogue outputs:

8 outputs DAC1 to DAC8, resolution: 64 steps.

Minimum conversion time to set one output: 600µs.

Minimum conversion time for the eight outputs together: 2ms.

Maximum output current: 6mA

Minimum output voltage (at 2mA): 0.1V

Maximum output voltage (at 2mA): 11.5V (adjustable)

Resolution per step (from 0.1 to 11.5): 160mV ± 90mV

1 precision output DA1, resolution: 256 steps.

Conversion time to set the output: 600µs.

Maximum output current: 2mA

Minimum output voltage: 0V

Maximum output voltage (at 0.5mA): 4.5V (adjustable)

Resolution per step (from 0 to 4.5): 17.5mV

Deviation: max. 26mV

Analogue inputs:

4 analogue inputs AD1 to AD4, resolution: 256 steps.

Minimum conversion time to read one input: 1ms.

Minimum conversion time to read four inputs: 1.6ms.

Minimum input voltage: 0V

Maximum input voltage: 5V

Input impedance: ±50 Mohm

Resolution: 19.5mV

Deviation: max. 30mV

Communication protocol: I^2C bus

LED indication for each I/O

25 pin D series connector for computer (optically isolated)

25 pin D series connector for printer

Supply voltage: mains supply voltage.

PCB dimensions: 237*133 mm

NB: conversion speed is dependent on the chosen computer

Appendix - D

The Borland C program

```
#include <stdio.h>
#include <conio.h>
#include <time.h>
#include <I2C.H>
#include <I2C.C>
main()
{
int k=0;
float VX,VY;
File *cptr;
int notkeypressed = 1;
I2CbusDelay = 1;
SelectI2CprinterPort(1);
I2CBusNotBusy();
cptr=fopen("C:\data.txt","w");
fprintf(cptr,"  VX            VY\n");
do{
k=k+1;
```

```
ReadADchannel(1);
ReadADchannel(2);
VX=(AD[1])*5.0*1000/256.0;
VY=(AD[2])*5.0*1000/256.0;
fprintf(cptr,"%f\t%f\t\n",VX,VY);
if(kbhit()) notkeypressed=0;
printf("%f\t%f\t\n",VX,VY);
}
while(notkeypressed);
fprintf(cptr,"];\n");
fclose(cptr);
return 0;
};
```

Appendix - E

The CNC part program

N00 ; THIS FILLE FOR PLM-2000 MILL

N10 ; THIS PROGRAM FOR PRODUCE THE MACHINED SURFACE.

N20 G90 G71

N30 M03 S1500 F100

N40 G01 Z-20.5

N50 G01 X60

N60 G00 Z-0.5

N70 G00 X0

N80 M05

N90 M02

بسم الله الرحمن الرحيم

التنبؤ بخشونة السطح في عملية التفريز الرأسية

ملخص البحث

التنبؤ بخشونة السطح في عملية التفريز الرأسية التي تعد من عمليات القطع الرئيسية يكون لـــه اعتبار اقتصادي هام جداً حيث انه يزيد من الانتفاع بالماكينة ويعمل علي تقليل تكـــاليف الانتـــاج فـــي عملية التصنيع.

في هذا البحث يتم دراسة التنبؤ بخشونة السطح لمادة النحاس(٤٠/٦٠) بالاعتماد علي ظـــروف القطع التي تشمل سرعة القطع، معدل التغذية و عمق القطع.

تم استخدام نموزج ANFIS في التنبؤ بخشونة السطح بعد اجـــراء عمليـــة التفريـــز الراســـية. خشونة السطح استخدمت كمتغير تابع بينما سرعة القطع في المدي من ٧٥٠ الـــي ١٧٥٠ لفـــة فـــي الدقيقة، معدل التغذية في المدي من ٥٠ الي ٢٥٠ مليميتر في الدقيقة، وعمق القطع في المـــدي مـــن ٠,٣ الي ٠,٧ مليميتر، استخدموا كمتغيرات مستقلة. قوة القطع و قوة التغذيـــة اســـتخدما كمتغيـــرات مستقلة اخري وذلك لعمل نموزج اخر لمقارنتة بالنموزج الاول والتحقق من مدي كفاءة النموزج الاول. العديد من الدوال تم ضبطها خلال عملية التدريب باستخدام نموزج ANFIS.

خشونة السطح تم قياسها بعد الانتهاء من عملية القطع بجهاذ قياس الخشونة الابري. ايضا تـــم قياس قوة القطع وقوة التغذية مباشرة اثناء عملية القطع باستخدام جهاذ يعمل بمقاييس انفعال.

تم دراسة تاثير عوامل القطع (سرعة القطع، معدل التغذية و عمق القطع) علي قوة القطع وقـــوة التغذية وخشونة السطح. وتم التاكد من دقة البرنامج المستخدم في عملية التنبؤ بخشونة السطح عـــن

طريق مجموعة قراءات عملية كما استخدمت هذه القراءات لحساب ومعرفة نسبة الخطأ لهذا البرنامج. النتائج العملية اثبتت فعالية النموزج المقترح. قيم خشونة السطح المتنبأ بها تم مقارنتها مع القيم المقاسة عملياً فكانت نسبة متوسط مربع الخطأ ٨,٥% أي ان الدقة تساوي ٩١,٥%.

علي الرغم من ان هذا البحث ركز علي التنبؤ بخشونة السطح في عملية التفريز الراسية الا ان المفاهيم المستخدمة مفاهيم عامه لذلك يمكن استخدام برنامج ANFIS في التنبؤ بخشونة السطح في العديد من عمليات القطع الاخري.

التنبؤ بخشونة السطح في عملية التفريز الرأسية

رسالة ماجستير

مقدمه من المهندس

ابراهيم ماهر عبدالرحيم سلطان

قسم الهندسة الميكانيكية

كلية الهندسة – جامعة اسيوط

٢٠٠٨

اشـــــراف:

أ.د. / رفعت الشـــيخ محمد الزهري
استاذ هندسة الانتاج بهندسة اسيوط
د. / محمد الســيد حســـــني الطيب
استاذ مساعد في الهندسة الميكانيكية

لجنــة الحكـــم:

أ.د. / تـوفيـــق تـوفيـــق الميدانـــــي
استاذ هندسة الانتاج بهندسة المنصورة
أ.د. / أحمد عبدالمنعم أبـواسـماعيل
اســـــتاذ التحكـم بهنـدسـة اسـيوط
أ.د. / رفعت الشيخ محمد الزهري